Analytical Modeling and Applications of Residual Stresses Induced by Shot Peening

Julio Davis

A dissertation submitted in partial fulfillment of
the requirements for the degree of

Doctor of Philosophy

University of Washington

2012

Reading Committee:

M. Ramulu, Chair

A.S. Kobayashi

D. Stuarti

Program Authorized to Offer Degree:
Mechanical Engineering

University of Washington

Abstract

Analytical Modeling and Applications of Residual Stresses Induced by Shot Peening

Julio Davis

Chair of the Supervisory Committee:
Professor M. Ramulu
Mechanical Engineering

The complex response of metals to the shot peening process is described by many fields of study including elasticity, plasticity, contact mechanics, and fatigue. This dissertation consists of four unique contributions to the field of shot peening. All are based on the aforementioned subjects.

The first contribution is an analytical model of the residual stresses based on J2-J3 incremental plasticity. Utilizing plasticity requires a properly chosen yield criteria so that yielding at a given stress state of a particular material type can be predicted. Yielding of ductile metals can be accurately predicted with the Tresca and Von Mises yield criteria *if* loading is simple, but if a material undergoes combined loading prediction of yielding requires an alternate criteria. Edelman and Drucker formulated alternate yield criteria for materials undergoing combined loading using the second and third deviatoric stress invariants, J_2 and J_3. The residual stress is determined from the yield state and is thus influenced by the third invariant. From Hertzian theory a triaxial stress state forms directly below a single shot and is defined in terms of three principal stresses. The stress state becomes substantially more complex when a surface is repeatedly bombarded with shots. The material experiences shear, bending, and axial stresses simultaneously along with the induced residual stress. The state of stress easily falls under the category of combined loading. The residual stress

is calculated from both the elastic and elastic-plastic deviatoric stress. Incremental plasticity is used to calculate the elastic-plastic deviatoric stress that depends on both invariants J2 and J3. Better predictions of experimental residual stress data are obtained by incorporating the new form of the elastic-plastic deviatoric stress into Li's theoretical framework of the residual stress.

The second contribution is a time dependent model of the plastic strain and residual stress. A general dynamic equation of the residual displacements in the workpiece is introduced. The equation is then expressed in terms of the inelastic strain. The imposed boundary conditions lead to an elegant second order differential equation in which the plastic strain acceleration is a natural result. The time dependent model is similar ***in mathematical form*** to the Kelvin Solid model, aside from the strain acceleration term. Upon solving the ODE, expressions for the plastic strain and plastic strain rate as functions of time are immediately obtained. Comparisons with numerical results are within 10%. To the author's knowledge this approach has never been published.

The third contribution is an extension of the second. Parameterizing the plastic strain leads to a simple transformation of variables so that the temporal derivatives can be written in terms of spatial gradients. Solving the second order ODE gives a solution for the plastic strain and hence residual stress (via Hooke's law) as a function of depth, z. Comparisons made with two aluminum alloys, 7050-T7452 and 7075-T7351, are in good agreement and within 10%.

The fourth and final contribution of the dissertation applies the theory of shakedown to calculate the infinite life fatigue limit of shot peened fatigue specimens undergoing high temperature fatigue. The structure is said to shakedown when the material will respond either as perfectly elastic or with closed cycles of plastic strain (elastic shakedown and plastic shakedown respectively). Tirosh uses shakedown to predict

the infinite life fatigue limit for shot peened fatigue specimens being cyclicly loaded at room temperature. The main complication that occurs during high temperature fatigue is residual stress relaxation. At high temperatures the magnitude of the shot peening residual stress will decrease which leads to diminishing fatigue benefits. A strain quantity known as the recovery strain is directly responsible for the relaxation of the shot peened residual stress. We incorporate the recovery strain into the shakedown model and prove that shakedown is still valid even when the residual stress is time dependent because of relaxation. The reduction of the infinite life fatigue limit is calculated for shot peened Ti-6-4, Ti-5-5-3, and 403 stainless steel.

TABLE OF CONTENTS

LIST OF FIGURES

LIST OF TABLES

ACKNOWLEDGMENTS

I would like to thank Professor Ramulu for his invaluable supervision, advice and guidance. I also wish to extend thanks to him for giving me creative control of the research in this dissertation. I also thank the members of my committee for their guidance and suggestions.

DEDICATION

Dedicated to the memory of Peter, Larry, and Jennifer

NOMENCLATURE

$\sigma^r_{finite}(z)$ - Residual stress in a finite structure

$\sigma_s(z)$ - Stress source as defined by Flavenot

$\sigma_{bending}(z)$ - Bending stress

$\sigma_{axial}(z)$ - Axial stress

$\epsilon(z)$ - Strain related to stress source via Hooke's law

h_p - Plastic zone depth

h - Plate thickness

$\bar{M}$ - Bending moment

$\bar{F}$ - Axial force

σ_r - Radial stress in a spherical pressurized cavity

σ_θ - hoop stress in a spherical pressurized cavity

R - Inner radial distance of pressurized cavity edge from origin

C - Radial distance of plastic zone of pressurized cavity from origin

b - Outer radial distance of pressurized cavity edge from origin

$\underline{\sigma}(z,t)$ - Periodic time dependent stress field

$\underline{\sigma}^{el}(z,t)$ - Periodic time dependent elastic stress field

$\underline{\sigma}^{r}(z,t)$ - Periodic time dependent residual stress field

$\underline{\epsilon}(z,t)$ - Periodic time dependent strain field

$\underline{\epsilon}^{el}(z,t)$ - Periodic time dependent elastic strain field

$\underline{\epsilon}^{ine}(z,t)$ - Periodic time dependent inelastic strain field

$\underline{\epsilon}^{p}(z,t)$ - Periodic time dependent plastic strain field

R_0 - Initial radius of the yield surface

ΔR - Incremental increase in the yield surface. A result of isotropic hardening.

$\underline{M}$ - Compliance matrix

$\underline{\epsilon}^{Hertz}$ - Hertzian strain field

σ_{ii}^{Hertz} and σ_{ii}^{e} - Hertzian principal stresses in the ii direction

ϵ_{ii}^{e} - Hertzian principal strains in the ii direction

ϵ_{m}^{e} - Mean Hertzian principal strain

f - Yield function also referred to as yield surface

$\underline{S}$ - Elastic deviatoric stress field

$\underline{\alpha}$ - Plastic internal variable also called a "backstress" representing a translation of the yield surface in stress space

E - Youngs Modulus of target

ν - Poisson's ratio of target

ν_s - Poisson's ratio of shot

$\underline{C}$ - Hardening modulus

$\underline{\tilde{\alpha}}$ - modified tensorial internal variable

S_{eq}^{el} - Von Mises equivalent elastic stress

$\Delta\epsilon^{p}(z)$ - Change in plastic strain

$\Delta\epsilon_{eq}^{p}(z)$ - Change in equivalent plastic strain

a_e - Elastic indentation radius

R^* - Shot radius

k - An impact efficiency coefficient

ρ - Shot density

V - Shot velocity

E_0 - Equivalent modulus of shot and target

s_{ii}^{e} - Elastic deviatoric stress in the ii direction

σ_{i}^{e} - Von Mises equivalent stress

ϵ_{i}^{e} - Von Mises equivalent strain

e_{ii}^{e} - Strain deviator in the ii direction

α - Ratio of plastic indentation diameter to elastic indentation diameter

D_p - Plastic indentation diameter

ϵ_i^p and ϵ_e^p - Effective elastic plastic strain

ϵ_s - Yield strain

ϵ_b - True strain corresponding to the ultimate tensile strain on an engineering stress strain curve

σ_i^p and σ_e^p - Effective elastic plastic stress

σ_s - Yield stress

S_b - True stress corresponding to the ultimate tensile stress on an engineering stress strain curve

F - Static load

k_1 and k_2 - Hardening coefficients for different linear stages of plastic deformation

e_{ij}^p - Elastic plastic deviatoric strain tensor

s_{ij}^p - Elastic plastic deviatoric stress tensor

σ_{ij}^r - Residual stress tensor

$\Delta\sigma_i^e$ - Change in Von Mises equivalent elastic stress

$\Delta\sigma_i^p$ - Change in effective elastic plastic stress

$\Delta\epsilon_i^e$ - Change in Von Mises equivalent elastic strain

$\Delta\epsilon_i^p$ - Change in effective elastic plastic strain

M - Shot mass

a_p - Plastic indentation radius

$\bar{p}$ - Pressure distribution acting to rebound the shot from the surface

$\bar{z}$ - Indentation depth

J_1, J_2, J_3 - First, second and third invariants of the deviatoric stress tensor respectively. Recall the first invariant is associated with hydrostatic stresses which sum to zero because there is no change in volume during plastic deformation. The second invariant is related to the energy of distortion (a change in shape). There is no convenient physical relation for the third invariant. This quantity acts as a weighting factor for shear stresses.

$d\lambda$ - Constant of proportionality for incremental plastic strain tensor $d\epsilon_{ij}^{p}$

$\bar{G}$ - Scalar function of stress, strain and loading history

H_p - Plastic hardening modulus

k^*, m^*, n^*, A, B, C - Empirical constants of Eq. 5.8

γ, μ, S - Empirical constants of Eq. 5.9 with units $kPa - sec^2$, $kPa - sec$ and kPa respectively

Chapter 1
INTRODUCTION

1.1 A Brief History

The act of strengthening metals by hitting it with blunt objects is an extremely old practice. Some of the earliest peened armor date back to 2700 BC Cary [1]. Indeed, black smiths and sword makers were aware of the benefits of peening long before shot peening became a modern practice. However, modernization accompanied with a fundamental understanding of the technique took thousands of years to accomplish. The theory of contact mechanics provides the tools necessary to derive the stress field in colliding objects. The earliest work done in contact mechanics was by Herts [2]. Hertz was the first scientist to develop the laws governing static contact between two spheres. He developed his theory over Christmas break of 1880 while studying Newton's optical interference fringes between glass lenses Johnson [3]. When Hertz pressed the two lenses together he became intrigued at how the elastic deformation might interfere with the patterns. Hertz's theory holds only for the elastic deformation of colliding bodies but it was the first satisfactory work done in calculating the associated stresses. The complexities that arise in Hertz's theory are due to the geometrical intricacies involved in the calculations; however Hooke's law is the primary ingredient in the theory Leroy [4]. Hertz attempted to develop a theory of hardness but this proved too difficult without a theory for plasticity.

Shot peening dynamically transfers a small amount of energy to the surface of a target work piece via small metallic, glass, or ceramic shots. In effect, the energy transferred to the work piece creates a small indentation. This permanent indentation indicates that plastic deformation has occurred and a residual stress at and under the

surface of the target material has formed. Plasticity theory is an integral part of modeling the residual stress. The theory of plasticity has been in development over the last 100 years. As a result, shot peening has received considerable theoretical attention only during the last 40 years. Plasticity theory provides the necessary tools to predict when yielding in the material will occur. Several yield criterion have been proposed and employed to model plastic flow in a large variety of materials. Some of the more commonly known theories include Von Mises (strain-energy) criterion and Tresca's maximum shear stress criterion. The Von Mises criterion is widely used to solve the residual stresses induced from shot peening. In some of the present work, a more general yield criterion is explored for modeling the residual stress.

1.2 Practical Importance

A strong understanding of shot peening is necessary because of its remarkable ability to increase fatigue resistance, extend fatigue life McClung [5], increase corrosion resistance Campbell [6], lubrication and tribological applications M. Matsui [7], and surface nanocrystallization M. Umemoto [8] to name only a few. Shot Peening is an important design process in the automotive, aerospace, nuclear, medical, pressure vessel, and petroleum industries. It is primarily used to prevent fatigue induced failures via two mechanisms: 1.) a compressive residual stress that prevents crack growth and 2.) an increase in material hardness that prevents crack initiation. A compressive residual stress is a stress that remains in a material, at equilibrium, after all external loads have been removed. This compressive stress prevents a crack from growing by negating the tensile loading from the cyclic stress amplitude of fatigue. Shot peening induces a compressive stress near 60% of the materials UTS McClung [5]. A crack cannot grow through the compressive stress field hence the fatigue life increases. The fatigue benefits have been well documented. For example, shot peening has been shown to improve the fatigue strength of high strength aluminum alloys by as much as 25-35%. With shot peening's important purpose and extensive use, a strong the-

oretical understanding is necessary so that design engineers have reliable models to help approximate the benefits. Because of all these applications shot peening is a valuable surface treatment process for many different industries.

1.3 Most Influential Research

Research and development for shot peening is focused on two areas. The first area is devoted to researching the affect coverage, saturation, and intensity have on the fatigue behavior of a shot peened structure. The second is prediction and measurement of the residual stress via analytical, numerical or experimental research. Coverage is simply the fraction of area peened during a specified time. Saturation is reached when doubling the shot peening time does not result in more than 10% increase in arc height (deflection of a metal strip). The intensity is directly related to the energy of the shot stream. An intensity measurement corresponds to how much a standard metal strip, known as an Almen strip, will deflect depending on chosen parameters such as pressure and shot size. All three of these quantities are of paramount importance in understanding what the most important parameters are for process optimization and control. Different materials have a different response to shot peening. The time to 100% coverage for aluminum is not the same as for steel. Similarly, the shot peening conditions to optimize fatigue benefits for aluminum and steel are different. The material dependent response to shot peening means that each of the three parameters will have unique values for different materials. Coverage, saturation and intensity are easily measured either by experiment or with analytical modeling.

All three of the parameters are related to the residual stress and plastic strain in one way or another. For example, the deflection of an Almen strip can be correlated to the plastically deformed layer, which is, of course, related to the residual stress via the theories of elasticity and plasticity. The reason for studying the three aforementioned parameters is because they are easily measured, and convenience is extremely valuable for design engineers. The residual stress, however, is not easily

measured. *But theoretical models have the potential to provide inexpensive, reliable predictions.* Analytical modeling of the residual stresses can be divided into two categories. The first is prediction of the residual stress. The second is quantifying the fatigue enhancements of a shot peened structure. The difficulties associated with the two research areas extend from the complicated process and the complex interaction of the shots impacting the surface. However, several researchers have overcome the difficulties and have developed reliable models.

J. F. Flavenot [9] provided the first theoretical analysis of the residual stress by introducing the concept of a stress source. The stress source balances the bending and axial stresses produced by a plate. The summation of all three stresses gives the residual stress in a finite structure. Al-Hassani [10] apply Flavenots concept of a stress source to a spherical cavity model representing the impact crater. Several authors, most notably Guechichi [11], analyze shot peening with a cyclic loading solution. He incorporates the cyclic limit of elasticity into his solution of the residual stress because of the cyclic nature of shot peening. J.K. Li [12] utilizes a mechanical approach to calculate the residual stresses from Iliushin's theory of J2 deformation plasticity. Tirosh [13] devises a technique to quantify the improvement in the fatigue limit of a shot peened structure. His work is based on Melan's lower bound shakedown theorem for approximating the allowable safe stress amplitude of a cyclicly loaded structure that otherwise might fail from plastic strain accumulation (ratchetting). All of the authors provide several techniques to model shot peening and their work laid the foundation for this dissertation.

As previously mentioned, the two most important theoretical research topics are:

1. Develop reliable analytical tools to predict the most important aspects of the residual stress; the value at the surface and the maximum that occurs beneath the surface.

2. Model enhanced fatigue properties such as increased fatigue limits

The proposed research takes aim at each of the listed topics by building on the work of Li and Tirosh. Furthermore, a concurrent goal is to develop and verify an entirely new analytical model that is also capable of approximating the residual stress. The boundary conditions outlined by Guechichi motivated the new techniques, and are based on the time dependent response of the impact. The thesis is organized in the following manner:

1.4 Structure of the Thesis

A brief description of the salient points of shot peening are introduced in chapter 1. Chapter 2 discusses important material required to read the thesis. An in depth review of the theoretical, numerical and experimental concepts of shot peening are presented. The sections devoted to theoretical work describe all prior research that the thesis is built on. Details of numerical simulations of several authors [14–16] are discussed to highlight important material response that cannot be observed from experiments, specifically, the time dependent plastic strain and strain rate.

A review of the experimental fatigue behavior of common aluminum, steel and titanium alloys is also given, followed by the research scope and objectives in chapter 3. In Chapter 4, an analytical model of the residual stress is constructed by evaluating the elastic-plastic deviatoric stresses using J2-J3 plasticity. All prior analytical modeling of the residual stresses utilize the Von Mises plasticity criterion. The Von Mises criterion predicts yielding adequately for simple loading. But one may ask the simple but fundamental question: Can the loading response of shot peening be classified as simple? We know that structures undergoing simple loading experience only one mode of loading, i.e. either axial stresses or bending stresses for example. Combined loading occurs when a structure undergoes multiple modes of loading, i.e. axial, bending, torsion, etc. simultaneously. Combined loading experiments reveal [17] that the Von Mises Criterion cannot predict yielding for combined loading as accurately as simple loading. An original contribution of the thesis is to extend Li's

residual stress model to incorporate a yield criterion that is capable of predicting yielding under conditions of combined loading more accurately.

Chapter 5 starts with a brief introduction to a semi-analytical model of time dependent plastic strains induced during shot peening. Research presented in this dissertation also investigates the time dependent material response to a high speed shot impact. There is an absence of analytical work but a handful of researchers have made numerical contributions to this topic. Meguid [16] and Al-Hassani [14] used the finite element method to show the loading and unloading history is exceptionally fast, on the order of $10^5 \frac{1}{s}$. We choose to model the shot impacting the metal surface, assumed to be semi-infinite, as an impulse because of the short time scales involved. The equations developed are strikingly similar to the Kelvin solid model used to model the time dependent behavior of viscoelasticity. The model is further developed to calculate the residual stress as a function of depth.

Chapter 6 is an extension of the work in chapter 5. The plastic strain is parameterized using time. By envisaging the plastic strain to be parameterized with time, a parametric transformation leads to a strain gradient based model of the residual stress. In chapter 7, the concept of shakedown is used to calculated the fatigue life extension after residual stress relaxation via the recovery strain. The approach used to model the high temperature fatigue behavior of shot peened structures is adopted from Tirosh. Tirosh quantifies the improvement in the fatigue limit of shot peened structures at room temperature. At elevated temperatures the residual stress becomes time dependent and will respond by decreasing in magnitude. Therefore, we first verify that shakedown still applies when thermal relaxation creates a recovery strain causing a time varying residual stress. After proving shakedown remains valid, the fatigue benefits are calculated based upon the relaxed values of the residual stress. Chapter 8 is the final chapter of the dissertation. A brief summary and conclusion is provided along with future research directions and recommendations.

Chapter 2

BACKGROUND AND LITERATURE REVIEW

2.1 Introduction

A general discussion of the analytical, numerical and experimental research of shot peening is presented in this chapter. The reader needs a thorough comprehension of all three areas to fully understand the analytical models developed throughout the dissertation. Section 2.1 presents general concepts of shot peening. The history of shot peening is considered and the various peening techniques (automated vs. manual peening) are discussed and compared. Important measurement parameters including coverage, arc height, and saturation are described because these quantities are unique to the field. A review of the analytical approaches are outlined in section 2.3. The theoretical work of Flavenot and Nikulari is derived. We show that their "stress source" method provides the groundwork for all later modeling efforts. Developing a theoretical model is indeed a non trivial task. A thorough model must consider a wide variety of phenomenon including dynamic elastic and plastic loading as well as strain rate, strain hardening, shake down, kinematic and isotropic hardening Al-Hassani [10].

The residual stress distribution is responsible for many benefits. The last thirty years has seen a large increase in the amount of research in the area of shot peening residual stress modeling, largely due to the marked increase in numerical capabilities, giving way to numerical solutions of the residual stress fields produced from single and multiple shot impacts. Six different types of finite element models have been created to numerically simulate shot peening. These are outlined in section 2.4. Each model has different degrees of freedom and surface symmetries. Symmetric surface

geometries make for a more computationally efficient model. Section 2.5 covers a comparatively small amount of the experimental research available in the literature but thorough enough to gain understanding of the fatigue behavior of shot peened structures. Fatigue is the largest research field and hundreds if not thousands of experimental studies have been conducted.

2.2 Shot Peening Process and Parameters

Shot peening is a surface treatment process whereby tiny spherically shaped media is propelled at a workpiece several tens of thousands of times with enough energy to create a uniform plastic layer in the surface and subsurface region of the material. The induced plastic layer is approximately a few hundred micrometers in thickness. A layer of hardened material protects against many harmful mechanical phenomenon such as crack initiation and growth caused by fatigue and corrosion. Fig. 2.1 is an illustration of a typical shot peening air nozzle with relevant parameters. For this type of shot peening machine shots are accelerated by a prescribed pressure and expelled from the nozzle at some diverging angle and impact velocity.

The history of shot peening is interesting. Shot peening was actually an accidental discovery that originated from sand blasting. Not long after sand blasting was found to increase the fatigue life and strength of metal in the 1920s, people realized the potential of shot peening and quickly integrated it alongside other metal working processes. The first rudimentary shot peening machine was developed in 1927 by E.G. Herbert called the Cloudburst Machine, which dropped steel balls from a given height on a target surface Cary [1]. The Cloudburst machine along with hardness testers developed around the same time provided the first reliable information about cold work hardening a target surface by the multiple bombardments of spherical indenters. From this point on there was an immense amount of research and development produced for work hardening of materials by repeated impact of a spherical object. Effort to develop shot peening was further fueled by a desire for stronger materials

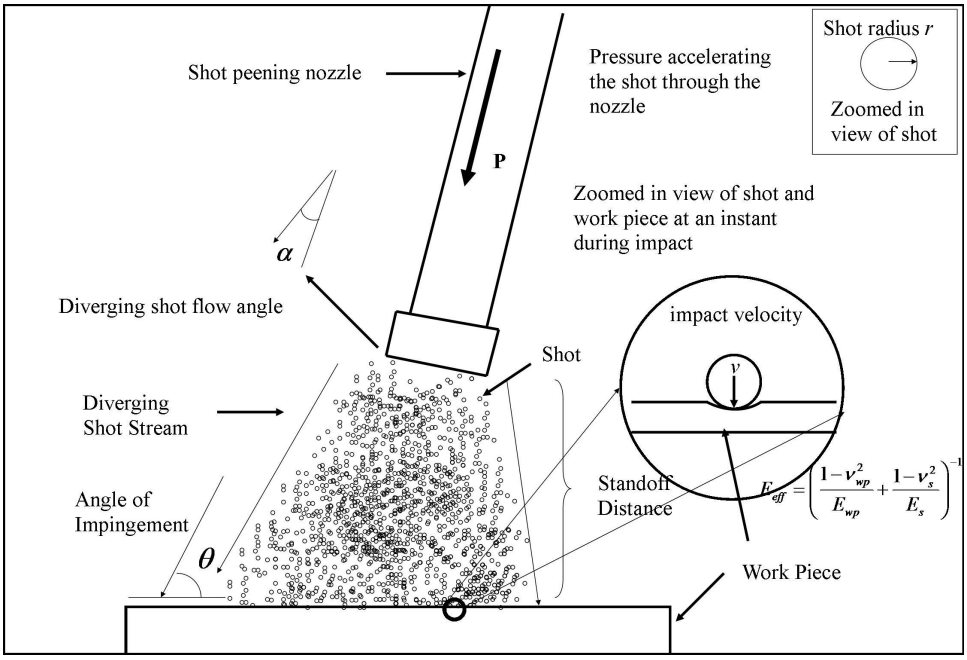

Figure 2.1: Schematic diagram of shot peening air nozzle with relevant parameters

to use during World War II.

Over the following decades shot peening was substantially developed both experimentally and analytically. The Almen strip and gage were invented in 1943 by J.O. Almen. These are the main tools to help control and standardize the shot peening process. Almen strips are thin strips of steel with varying thickness used to indirectly characterize the amount of peening a work piece has undergone. Almen strips that are smaller in thickness (0.81 - 0.76mm) called N type strips, are used for lower intensities and thicker strips (2.41 - 2.36mm) known as C type strips, are used for higher intensity levels. An intermediate intensity is used with A type strips of thickness 1.27 - 1.32mm. The Almen gage is a tool that measures the amount of curvature (almen height, mm) that has been induced in the Almen strip by the shot induced compressive layer. Despite the simplicity of the tools, more than half a century later they are still the most commonly used measuring devices. The tool's basic function,

easy application, and convenience are a desirable asset for measuring shot peened components. Along with tools to measure properties such as arc height of peened Almen strips, experimental techniques both destructive and non-destructive have been developed to obtain compressive residual stress measurements.

In 1945 E.W. Milburn developed an X-ray diffraction technique to measure the compressive stresses in the work piece Milburn [18]. X-ray diffraction is both expensive and destructive, so the utility is somewhat limited. Ultrasonic techniques have been developed to measure the residual stress distribution in a variety of objects. Measurements made with ultrasonic devices are non destructive in nature. In fact, some instruments are portable so that measurements can conveniently be made on real structures and laboratory samples P.J. Withers [19]. The use of eddy currents has also been employed in the efforts to calculate the residual stress distribution in a shot peened surface. The technique also has the benefit of being non destructive.

A large variety of peening machines have also been developed since the conception of shot peening. The two main types of shot peening machines used in the industry are categorized by the way the shots are propelled from the machine. One type of machine, referred to as centrifugal wheel machines, rotates a wheel head at large angular speeds while shots are fed into the center of the wheel. The motion creates a large centripetal acceleration and the shots are then propelled from the rotating wheels by paddles that are attached to the wheel head. The second type of machine uses a pressurized air nozzle to accelerate the shot. Suction, gravity air, and direct pressure are the three categories of air nozzle machines Biggs [20]. Suction machines are somewhat limited because the shot size requirement is on the order of 1.2mm which makes them more appropriate for use where other types of machines are not available. The second variation of air nozzle machine is called a gravity air machine. Gravity air machines use gravity to feed the shots into an air inlet so that the shots can be accelerated by air pressure. Air nozzle machines utilize air pressure directly to accelerate the shot media. This type of shot peening machine is probably the

most versatile. Pressure builds in a chamber and when it reaches the desired level it accelerates the shots through a hose and out a nozzle.

The following sections provide a thorough explanation of coverage, intensity, arc height and saturation which are important to understanding the experimental, numerical and theoretical aspects of shot peening.

2.2.1 Coverage

Coverage is defined as the percent of area of the work piece that has been deformed by shots. In other words, coverage is the ratio of peened area to the sum of peened and unpeened area. Of course the sum of peened and unpeened area is nothing more than the total area of inspection. The peened area can further be considered as the sum of all the dimpled areas created from the shot stream. In many industrial applications of shot peening coverage must be within 100 - 200%. Within this range the residual stress is uniform and the surface is not damaged by shot peening. Coverage provides a direct way to tell if a component has been peened the necessary amount, not too little and not too much. When a component is excessively peened the surface develops detrimental stress raisers such as folding sites and an excessively rough surface. These unacceptable surface characteristics create crack nucleation sites and can lead to premature failure of the component and therefore render shot peening a harmful surface treatment process. Conversely, when a component is under peened the beneficial compressive stress in the material is not developed enough to optimize the full benefits of peening and inhibits maximization of the lifetime of a given part. It has also been observed that single impact sites of an under peened surface can act as nucleation sites as well.

The most common technique of calculating coverage is done by visual inspection. Visual inspection is performed using a microscope or magnifying glass. A microscopic photograph of the surface can also be taken by image analysis software that is capable of accurately calculating the percent of peened area. This is the preferred way of

obtaining coverage measurements but this process can be time consuming and is limited. It is also difficult to obtain accurate coverage measurements with the naked eye. Characterization of coverage that exceeds 100% is impossible to do visually since the surface has already been completely bombarded so empirical or analytical techniques are applied.

Coverage is described analytically using a simple mathematical model that approximates the random indentations impacting the surface over time as a statistical distribution known as the Avrami equation [21]. This type of distribution is used to describe many physical phenomenon including chemical reactions, a charging capacitor, or even a plane flying with increasing altitude. All these processes, including coverage, can be described quite accurately with the Avrami equation. Kirk [22] used this equation to describe coverage which has the form:

$$C = 100\left[1 - exp\left(-\frac{3\dot{m}ta^2}{4A_{spread}\rho_s r^3}\right)\right] \tag{2.1}$$

Where t is the exposure time, $\dot{m}$ is the mass flow rate, a is the indentation radius, r is the shot radius, ρ_s is the shot density and A_{spread} is the total area undergoing peening. The present author Davis [23] developed coverage models based on Hertzian theory, Brinell hardness and contact mechanics which relate coverage to pressure, impingement angle, modulus of elasticity, yield strength and surface hardness. These alternate models were derived from energy relations and have the form

$$C = 100\left[1 - exp\left(-\frac{3\beta 0.05\dot{m}C_d PD(sin\theta)^2}{2.8\rho_s(tan\alpha)^2 d^2 Y\pi a^2}\right)\right] \tag{2.2}$$

$$C = 100\left[1 - exp\left(-\frac{180\beta 0.05\dot{m}C_d PD(sin\theta)^2}{\rho_s(tan\alpha)^2 d^2 Y\pi a^2\left(13 + 20ln\left(\frac{Ea}{Yr}\right)\right)}\right)\right] \tag{2.3}$$

$$C = 100\left[1 - exp\left(-\frac{1.5\beta a^2\dot{m}C_d PD(sin\theta)^2}{2r\rho_s(tan\alpha)^2 d^2\pi HB\left(2ra^2 - \frac{1}{6}((2r)^3 - ((2r)^2 - 4a^2)^{1.5})\right)}\right)\right] \tag{2.4}$$

β is found by normalizing each expression in the exponent of Eqn.'s 2.2-2.4 to a single experiment and kept constant henceforth for all remaining experimental conditions, C_d is the drag coefficient, P is pressure, D is the nozzle length, Y is the yield strength of the target, E is the modulus of elasticity of the target, d is the standoff distance, α is the divergence angle of the shot stream and HB is the Brinell hardness of the surface.

2.2.2 Intensity, Arc Height and Saturation

The Almen strip and Almen gage are tools used to measure the intensity of the incident shot stream. Intensity is an indirect way of measuring the amount of energy transferred to the surface of the Almen strip from the shot stream. The intensity (or energy) is a function of mass flow rate, shot velocity, and shot characteristics such as diameter and density. Specifically, an intensity plot, with the intensity measured on the vertical axis, gives a plot of the deflection of an Almen strip versus time. Clearly, when the incident energy of the impacting shots vary, so too will the measure of deflection and required peening time. There are three types of Almen strips used to measure intensity each have the same length and width but vary in thickness. All three strips are made from cold rolled spring steel tempered to 44 - 50 Rc and hot pressed for two hours to remove any residual stresses that may be present. The strips are given the letter designation N, A, and C with corresponding thicknesses 0.787mm, 1.30mm, and 2.38mm respectively. The symbol designation does not stand for anything. The length and width of the strips are 76.2mm and 18.92mm - 19.05mm respectively Kirk [24]. Once mounted in a fixture the Almen strip is shot peened at specified conditions. When a test strip is shot peened the strip will bow and a measurable arc develops, i.e. the strip will deflect *into* the shot stream. The deflection of the strip into the shot stream occurs because the surface area of the peened side is increasing. As peening progresses the height of the arc increases; however the arc height increases in an exponential manner because plastic deformation does not con-

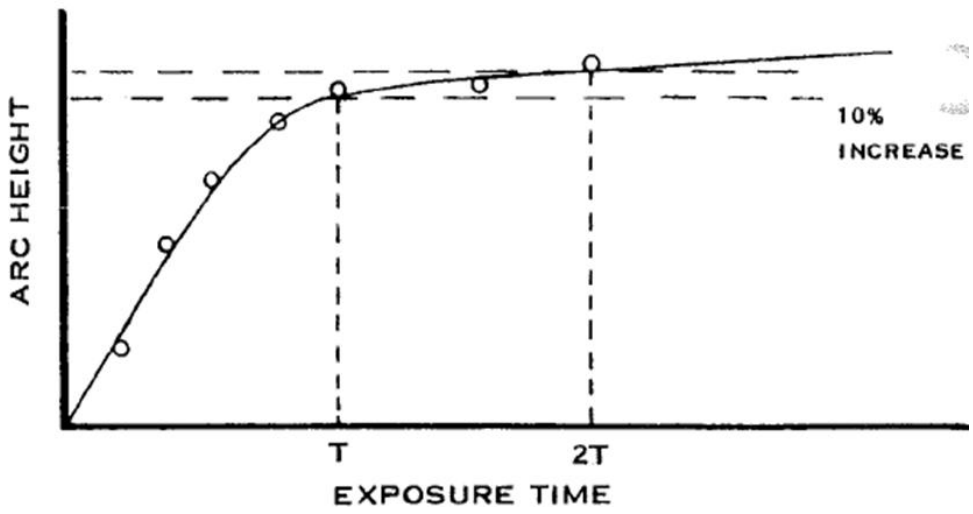

Figure 2.2: A typical intensity plot along with time to obtain saturation

tinue indefinitely. Shakedown of the structure will prevent accumulated deformation. The rate of change of the arc height approaches zero for increasingly larger peening times. The rate of development is dependent upon the peening conditions and time. If the intensity of the peening conditions is relatively large then the rate at which the Almen strip arc develops will be large as well. Therefore the time necessary to reach a particular arc height will be shorter. Thus intensity is defined as the height of the arc of the Almen strip, produced from a given set of peening conditions, after a given time of peening. Fig. 2.2 shows a typical intensity plot produced from multiple measurements of arc height development using an Almen gage. Notice how the rate at which the arc development slows with time. Arc height development is not quite an exponential phenomenon but does display a rapid decrease in arc height development for longer peening times. An intensity plot is produced by shot peening several strips for increasingly longer times at the same intensity. Measurements of the arc height of each strip are taken with the Almen gage at different times and plotted. A single point in the figure represents an average arc height measurement taken from multiple strips exposed the same amount of time [25]. This is to assure accurate data points.

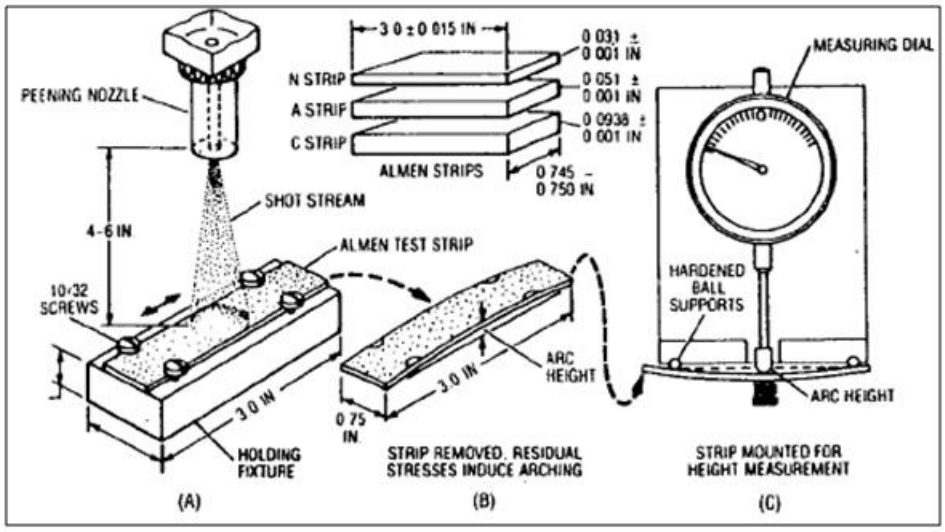

Figure 2.3: The arc height measurement process. (A) shows the peening of a test strip mounted in a fixture. (B) shows the bowing induced in the Almen strip as a result of the residual stresses in the metal. Test strips N, A, and C are also displayed along with dimensions. (C) depicts an Almen test strip mounted in an Almen gage

Two important points on the plot, located at times T and 2T on Fig. 2.5, correspond to an important parameter known as saturation. This parameter is used to characterize how arc height develops throughout the process. Saturation refers to the time to produce an arc height that has increased by no more than 10 percent if the time of peening is doubled Kirk [24]. Saturation is obtained from a plot of the intensity. On the plot in Fig. 2.5 time T is the minimum amount of time that meets the specification. The time 2T corresponds to a time when the arc height increases by no more than 10%, from time T. Fig. 2.3 provides a visual depiction of how arc height measurements are obtained.

2.3 Analytical Modeling

Analytical research of shot peening residual stresses span the last 4 decades; however, a fraction of research has been done compared to the other areas. Beginning with

section 2.3.1, a detailed description of each landmark model is given. Dating back to 1977, J. F. Flavenot [9] developed the "stress source" technique for calculating the residual stresses. Al-Hassani [10] and Al-Obaid [26] apply this concept of a stress source to a spherical cavity model. Other formulations during this time period include that of Guechichi [11] in 1986. They calculate the shot peening residual stresses by treating it as a cyclic loading phenomenon. Guechichi [11] found for materials with a definite yield stress, such as titanium and plain carbon steels, incorporating isotropic hardening and linear kinematic hardening provided good comparison with experimental residual stress values. M.T. Khabou [27] again uses a cyclic behavior law but also develops a simple rheological model to calculate the residual stress fields for materials lacking a well defined yield stress. In 1991, another landmark article published by J.K. Li [12] outlines a simple mechanical approach to calculate the residual stress fields. J.K. Li [12] uses Iliushins elastic plastic theory to calculate the elastic plastic stress deviator. The work of J.K. Li [12] has been utilized by many researchers during the last 20 years.

2.3.1 Flavenot and Niku lari

The earliest analytical technique for solving the residual stresses induced by shot peening was based on Flavenots concept of a stress source J. F. Flavenot [9]. This source of stress is introduced to the material from the peening process. Take for example an Almen strip confined by a holder, see Fig. 2.3(A). After peening, the holder exerts an axial force and bending moment on the strip to prevent it from elongating and deflecting. But once removed the strip is free to bend and elongate therefore an axial and bending stress is induced within the specimen. The stress source is ***not equilibrated*** and is considered to be the residual stress that develops in a semi infinite surface such as a very thick plate and is governed by the laws of elasticity. From the principle of superposition the stress source is summed with the axial stress and bending stress to allow for equilibrium to occur. The following

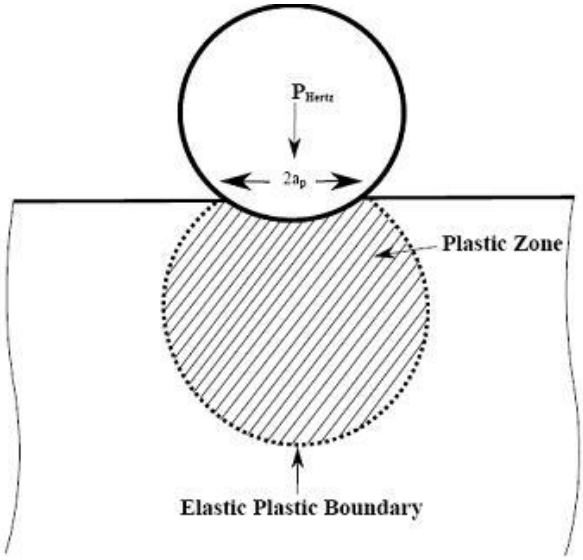

Figure 2.4: Shot impacting a semi infinite surface with elastic plastic boundary separating the elastic and plastic zone

equation is proposed by J. F. Flavenot [9]

$$\sigma^{r}_{finite}(z) = \sigma_s(z) + \sigma_{bending}(z) + \sigma_{axial}(z) \tag{2.5}$$

J. F. Flavenot [9] consider the stress source, σ_s, to be elastic and therefore governed by Hooke's law $\sigma_s(z) = -E\epsilon(z)$. Since experimental measurements of the residual stress distribution in a thick target, which is taken to be the stress source σ_s, have the form of a cosine function the following strain is proposed

$$\epsilon(z) = \epsilon_m cos\left(\frac{\pi z}{2h_p}\right) \tag{2.6}$$

However, this is not based on anything physical and no theoretical argument is offered for proposing a sinusoidal form for the stress source. h_p is the plastic zone depth and ϵ_m is the maximum strain beneath the surface. In order for this function to accurately represent the true material behavior the authors shifted the cosine function so that the max strain occurs beneath the surface a distance αh_p.

$$\epsilon(z) = \epsilon_m cos\pi \left(\frac{z - \alpha h_p}{2(1-\alpha)h_p} \right) \tag{2.7}$$

Note this expression is only valid up to $z = h_p$. From Hooke's law we now have for the stress source

$$\sigma_s(z) = E\epsilon_m cos \left(\pi \frac{z - \alpha h_p}{2(1-\alpha)h_p} \right) \tag{2.8}$$

With the source stress defined we have from simple beam theory the axial stress and bending stress

$$\begin{aligned} \sigma_{bending} &= \frac{12\bar{M}}{bh^3} \left(\frac{h}{2} - z \right) \\ \sigma_{axial} &= \frac{\bar{F}}{bh} \end{aligned} \tag{2.9}$$

The moment $\bar{M}$ and force $\bar{F}$ are

$$\begin{aligned} \bar{M} &= \int_0^k \sigma_s(z) \left(\frac{h}{2} - z \right) b dz \\ \bar{F} &= \int_0^k \sigma_s(z) b dz \end{aligned} \tag{2.10}$$

Upon integrating from $z = 0$ to $z = h_p$ and substituting into Eq. 2.5 yields the complete residual stress through a finite plate. This is given as

$$\sigma^r_{finite}(z) = E\epsilon_m \left[\frac{12}{h\pi}(1-\alpha) \left(\frac{h}{2} - z \right) C_1 + \frac{2\lambda}{\pi}(1-\alpha)C_2 - \frac{\epsilon(z)}{\epsilon_m} \right] \tag{2.11}$$

with

$$\begin{aligned} C_1 &= 1 - 2\lambda + \frac{4\lambda}{\pi}(1-\alpha)cos \left(\frac{\pi\alpha}{2(1-\alpha)} \right) + sin \left(\frac{\pi\alpha}{2(1-\alpha)} \right) \\ C_2 &= 1 + sin \left(\frac{\pi\alpha}{2(1-\alpha)} \right) \\ \lambda &= \frac{h_p}{h} \end{aligned} \tag{2.12}$$

The value of ϵ_m is obtained from the assumption that plane sections of a beam of length L bent into an arc of height δ remain plane after deformation and with the curvature expressed as $\frac{\bar{M}}{EI}$ yields

$$\epsilon_m = \frac{2}{3}\frac{\pi h\delta}{\lambda^2 L^2 h_p(1-\alpha)C_1} \tag{2.13}$$

After measuring both the Almen strip deflection and the depth of the plastically deformed layer Flavanot and Niku-lari use the formulas developed to calculate the maximum stress and surface stresses with good approximation.

2.3.2 Al-Hassani and Al Obaid

Al-Hassani [10] and Al-Obaid [26] argue that assuming plane sections of the Almen strip remain plane is not realistic and so develop a model based on a spherically pressurized cavity. They assume that the stress field below the indentation can be interpreted as a spherical cavity undergoing elastic plastic deformation as shown in Fig 2.5. The equations of the radial and hoop stress in a spherical pressurized cavity have the form

$$\begin{aligned}
&\frac{\sigma_r}{Y} = -2ln\left(\frac{C}{r}\right) - \frac{2}{3}\left(1-\frac{C^3}{b^3}\right) = \frac{\sigma_\theta}{Y} - 1 \quad \text{for } R{\leq}r{\leq}C \\
&\frac{\sigma_r}{Y} = -\frac{2}{3}\frac{C^3}{b^3}\left(\frac{b^3}{r^3}-1\right) \qquad\qquad \text{for } C{<}r{\leq}b \\
&\frac{\sigma_\theta}{Y} = \frac{2}{3}\frac{C}{b^3}\left(\frac{b^3}{2r^3}+1\right)
\end{aligned} \tag{2.14}$$

Of these equations σ_θ is the one chosen to represent the stress source because it has a peak below the surface a distance h_p for the region $R{\leq}r{\leq}C$ which is the plastic zone. See Fig. 2.5. Y is the yield strength and the parameters R, C and b represent the radial distances of the edges of the cavity, plastic zone and sphere from the origin respectively. Therefore, the plastic layer has a radial thickness $C-R$ and the elastic layer has a thickness $b-C$. With this representation the plastic depth is

given as $h_p = C - R$. Al-Hassani transforms the stress distribution to that of the plate configuration from the following coordinate change: $h = b - R$, $z = r - R$ and $h_p = C - R$. This coordinate change is applied just so the radial coordinates of the cavity, elastic and plastic layer match the geometry of the material below the shot of the plate configuration. For instance, the hollow sphere has a thickness of b - R and an Almen strip has a thickness h, therefore h = b - R. Also, to represent a radial position either in the elastic or plastic layer of the material we use r - R, with r acting as our variable parameter, for the position in a plate this is the variable parameter z. The plastic layer in the plate, hp, is equivalent to C - R for a hollow sphere. Upon substitution the hoop stress in the elastic and plastic regime Eq. 2.14 now become

$$\begin{aligned} \frac{\sigma_\theta}{Y} = \frac{\sigma_s(z)}{Y} &= 1 - 2ln\left(\frac{h_p + R}{z + R}\right) - 2\left(1 - \frac{(h_p + R)^3}{(h + R)^3}\right) && \text{for } 0 \leq z \leq h_p \\ \frac{\sigma_\theta}{Y} = \frac{\sigma_s(z)}{Y} &= \frac{2}{3}\frac{(h_p + R)^3}{(z + R)^3}\left(\frac{1}{2}\frac{(h + R)^3}{(z + R)^3} + 1\right) && \text{for } h_p < z \leq h \end{aligned} \tag{2.15}$$

This model assumes that each indentation unloads independent of each other which will result in a compressive residual stress field similar to that found in a spherical shell Al-Hassani [10]. Al Hassani and Al Obaid further develop this model by combining their solution of $\sigma_s(z)$ with Flavanots residual stress form given as the superposition of the source stress with the axial and bending stress. Therefore, unloading is assumed to takes place throughout the whole plate. Upon substituting $\sigma_s(z)$ into equations for $\bar{F}$ and $\bar{M}$

$$\begin{aligned} \frac{\bar{M}}{Y} = h_p\left(\frac{h}{2} + R\right) - R(h + R)ln\left(1 + \frac{h_p}{R}\right) + \frac{h_p}{3}(h - h_p)\left(1 - \left(\frac{h_p + R}{h + R}\right)^3\right) \\ -\frac{1}{12}\left[\left(\frac{h_p + R}{h + R}\right)^3\left[(h + R)(3h + 2R) - 4h_p(h - h_p)\right] + (h - 2R - 4h_p)^2\right] \end{aligned}$$

$$\frac{\bar{F}}{Y} = 2Rln\left(1 + \frac{h_p}{R}\right) - \frac{4}{3}h_p + \frac{1}{6}\left(\frac{h_p + R}{h + R}\right)^3(3h - R) + \frac{1}{6}(h_p + R)$$

These expressions can be simplified by assuming the plastic layer, h_p, is much less than the plate thickness h. This condition yields

$$\frac{\bar{M}}{Y} = \frac{5}{6}h_p h - hRln\left(1 + \frac{h_p}{R}\right) - \frac{(h_p + R)^3}{3h}$$

$$\frac{\bar{F}}{Y} = \frac{1}{6}(h_p + R) - \frac{4}{3}h_p + 2Rln\left(1 + \frac{h_p}{R}\right) + \frac{(h_p + R)^3}{2h^2}$$

After using these equations to solve the axial and bending stresses, superposition with the stress source, found from the spherical cavity model, will allow us to find the residual stress in a finite plate. Al Hassani simply modified the results of a separate application to obtain the residual stress from shot peening.

2.3.3 Guechichi et al.

The shot peening process has also been envisaged as a cyclic loading problem. S. Slim [28] estimates that any one point on an Almen strip can be impacted by a shot up to 15 times for 100% coverage. This is 15 cycles of high stress loading and unloading. Guechichi [11] developed a computational model of the residual stresses by assuming the shot impacting is periodic and attains a stable cyclic state. His technique is based on the method proposed by J. Zarka [29]. Guechichi [11] assumes a periodic time dependent stress field $\underline{\sigma}(x,t)$ that is a linear combination of the elastic stress field and residual stress field. Written out in shorthand notation where underline denotes a tensor quantity

$$\underline{\sigma}(z,t) = \underline{\sigma}^{el}(z,t) + \underline{\sigma}^{r}(z,t) \tag{2.16}$$

The time dependent form of the stress is now written in terms of a scalar function of time $\lambda(t)$

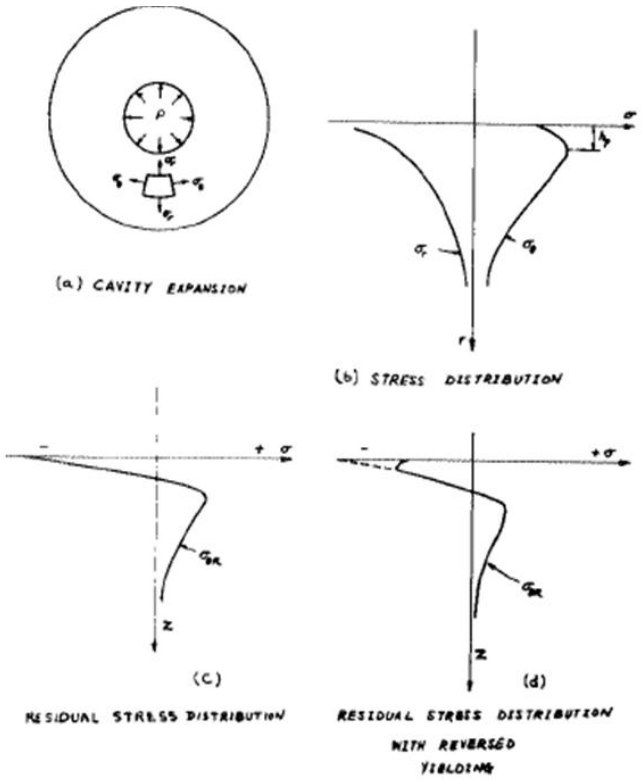

Figure 2.5: a) Pressurized cavity model b) Radial and hoop stress in an elastic plastic sphere c) Residual hoop stress distribution d) Residual stress distribution with reversed yielding

$$\underline{\sigma}(t) = \lambda(t)\underline{\sigma}_{max} + [1 - \lambda(t)]\underline{\sigma}_{min} \tag{2.17}$$

$\underline{\sigma}_{max}$ and $\underline{\sigma}_{min}$ represent the maximum and minimum stress field during a single cycle of loading. Guechichi assumes that the max stress occurs at the instant of impact and the min stress is zero when the shot begins to rebound. Therefore, the total stress field and elastic stress field have the form

$$\underline{\sigma}(t) = \lambda(t)\underline{\sigma}_{max} \tag{2.18}$$

$$\underline{\sigma}^{el}(t) = \lambda(t)\underline{\sigma}^{el}_{max} \tag{2.19}$$

Guechichi [11] does not provide the time dependent strain or residual stress field, $\underline{\sigma}^r(t)$, in terms of $\lambda(t)$. We now move our attention to the strain fields. The total strain field is written in terms of an inelastic portion and elastic portion

$$\underline{\epsilon}(z,t) = \underline{\epsilon}^{el}(z,t) + \underline{\epsilon}^{ine}(z,t) \tag{2.20}$$

The inelastic portion is a superposition of the elastic strain resulting from the residual stress and the irreversible plastic strain. The elastic strain corresponding to the residual stress is *governed by the laws of elasticity* and in the following chapter we will utilize this condition.

$$\underline{\epsilon}(z,t) = \underline{\epsilon}^{el}(z,t) + \underline{M\sigma}^r(z,t) + \underline{\epsilon}^p(z,t) \tag{2.21}$$

$\underline{M}$ is the compliance matrix. The maximum elastic stresses are obtained from hertzian contact theory and have the form

$$\underline{\sigma}^{el}(t) = \lambda(t)\underline{\sigma}^{Hertz} \tag{2.22}$$

Guechichi assumes loading and unloading is instantaneous. Therefore, $\lambda(t)$ is equal to 1 during loading and 0 after loading giving

$$\begin{aligned} \underline{\sigma}^{el}(t) &= \underline{\sigma}^{Hertz} \quad \text{for } \lambda(t) = 1 \\ \underline{\sigma}^{el}(t) &= 0 \qquad\quad \text{for } \lambda(t) = 0 \end{aligned} \tag{2.23}$$

Where the Hertzian principal stresses have the form

$$\begin{aligned} \sigma_{rr}^{Hertz} &= p(1+\nu)\left[\frac{z}{a_e}tan^{-1}\left(\frac{z}{a_e}\right) - 1\right] + p\frac{a_e^2}{2(a_e^2+z^2)} \\ \sigma_{\theta\theta}^{Hertz} &= p(1+\nu)\left[\frac{z}{a_e}tan^{-1}\left(\frac{z}{a_e}\right) - 1\right] + p\frac{a_e^2}{2(a_e^2+z^2)} \\ \sigma_{zz}^{Hertz} &= -p\left[\left(\frac{z}{a_e}\right)^{-1} + 1\right] \end{aligned} \tag{2.24}$$

The surface is assumed to be semi infinite with positive z direction taken to be downward. The residual stress only varies through the thickness (in the z direction) not on any plane perpendicular. From loading symmetry we also obtain the stress condition $\sigma_{rr}^r = \sigma_{\theta\theta}^r = \sigma^r$. These are conditions for 100% coverage and can greatly simplify the equations of equilibrium. We must adapt conditions of a single impact for 100% coverage. To do this lets derive the equilibrium conditions. Equilibrium of the residual stress field in component form is

$$\begin{aligned} \frac{\partial\sigma^r(z)}{\partial r} + \frac{\partial\sigma_{r\theta}^r(z)}{\partial\theta} + \frac{\partial\sigma_{rz}^r(z)}{\partial z} &= 0 \\ \frac{\partial\sigma^r(z)}{\partial\theta} + \frac{\partial\sigma_{r\theta}^r(z)}{\partial r} + \frac{\partial\sigma_{\theta z}^r(z)}{\partial z} &= 0 \\ \frac{\partial\sigma_{zz}^r(z)}{\partial z} + \frac{\partial\sigma_{rz}^r(z)}{\partial r} + \frac{\partial\sigma_{\theta z}^r(z)}{\partial\theta} &= 0 \end{aligned} \tag{2.25}$$

And since the residual stress tensor is independent of r and θ all partial derivatives with respect to r and θ go to zero. To better conceptualize these conditions imagine after 100% coverage choosing various points on the surface or below, as long as the chosen points have identical depths, you should not find a different value for the residual stress because the surface is uniformly deformed. This leaves us with the equilibrium relations

$$\begin{aligned}\frac{\partial \sigma^r_{rz}(z)}{\partial z} &= 0 \\ \frac{\partial \sigma^r_{\theta z}(z)}{\partial z} &= 0 \\ \frac{\partial \sigma^r_{zz}(z)}{\partial z} &= 0\end{aligned} \tag{2.26}$$

Plane stress conditions exist at the surface $\sigma^r_{rz}(0) = \sigma^r_{zz}(0) = \sigma^r_{\theta z}(0) = 0$ allowing the equilibrium equations to be solved such that

$$\begin{aligned}\int_0^{z'} d\sigma^r_{rz}(z) = \sigma^r_{rz}(z') - \sigma^r_{rz}(0) = 0 \Rightarrow \sigma^r_{rz}(z') = \sigma^r_{rz}(0) = 0 \\ \int_0^{z'} d\sigma^r_{r\theta}(z) = \sigma^r_{r\theta}(z') - \sigma^r_{r\theta}(0) = 0 \Rightarrow \sigma^r_{r\theta}(z') = \sigma^r_{r\theta}(0) = 0 \\ \int_0^{z'} d\sigma^r_{zz}(z) = \sigma^r_{zz}(z') - \sigma^r_{zz}(0) = 0 \Rightarrow \sigma^r_{zz}(z') = \sigma^r_{zz}(0) = 0\end{aligned} \tag{2.27}$$

From which the more general conditions are obtained

$$\sigma^r_{rz}(z) = \sigma^r_{zz}(z) = \sigma^r_{\theta z}(z) = 0 \tag{2.28}$$

With these relations the residual stress tensor now has the simplified form

$$\underline{\sigma}^r(z) = \begin{pmatrix} \sigma^r(z) & 0 & 0 \\ 0 & \sigma^r(z) & 0 \\ 0 & 0 & 0 \end{pmatrix}$$

From incompressibility conditions and symmetry we have the plastic strain tensor

$$\underline{\epsilon}^p(z) = \begin{pmatrix} \epsilon^p(z) & 0 & 0 \\ 0 & \epsilon^p(z) & 0 \\ 0 & 0 & -2\epsilon^p(z) \end{pmatrix}$$

After 100% coverage surface deformation is uniform and only occurs in the z direction acting to compress the surface. Therefore, the inelastic strains are zero

$$\epsilon_{rr}^{ine}(z) = \epsilon_{\theta\theta}^{ine}(z) = 0 \tag{2.29}$$

which yields an important result

$$\epsilon^{p}(z) + \left(\frac{1-\nu}{E}\right)\sigma^{r}(z) = 0 \tag{2.30}$$

And so the residual stress is related to the plastic strain via Hooke's law and behaves linear elastically. Quechichi also utilizes the Von Mises yield criterion to relate the residual stress to the elastic stress field which has the form

$$f(\underline{S}, \underline{\alpha}) = \frac{1}{2}(\underline{S} - \underline{\alpha})^{T}(\underline{S} - \underline{\alpha}) - (R_0 + \Delta R)^2 \leq 0 \tag{2.31}$$

This yield surface incorporates both kinematic and isotropic hardening. The back stress α, is a tensorial variable which relocates the yield surface in stress space to model kinematic hardening. ΔR represents an increase in the elastic domain associated with isotropic hardening and $R_0 = \sqrt{\frac{2}{3}}\sigma_s$ where σ_s is assumed to be the cyclic stable elastic limit.

The internal variable $\underline{\alpha}$ is related to the plastic strain by

$$\underline{\alpha} = \underline{C\epsilon}^{p} \tag{2.32}$$

Guechichi introduces a second tensorial internal variable

$$\underline{\tilde{\alpha}} = \underline{\alpha} - dev(\underline{\sigma}^{r}) \tag{2.33}$$

Expressing the residual stress in terms of the new tensor variable

$$\underline{\sigma}^{r}(z) = \underline{\tilde{\alpha}}(z)\left(\frac{3E}{3C(1-\nu) - E}\right) \tag{2.34}$$

The new internal variable must also obey incompressibility, giving $\underline{\tilde{\alpha}}(z)$ in matrix form as

$$\underline{\tilde{\alpha}}(z) = \begin{pmatrix} \tilde{\alpha}(z) & 0 & 0 \\ 0 & \tilde{\alpha}(z) & 0 \\ 0 & 0 & -2\tilde{\alpha}(z) \end{pmatrix}$$

Now redefining our yield function in terms of this new internal variable

$$f(\underline{S}, \underline{\tilde{\alpha}}) = \frac{1}{2}(\underline{S} - \underline{\tilde{\alpha}})^T(\underline{S} - \underline{\tilde{\alpha}}) - (R_0 + \Delta R)^2 \leq 0 \tag{2.35}$$

and so the modified backstress, $\underline{\tilde{\alpha}}$, serves to relocate the yield surface to a location in stress space depending on our residual stress. From Eqn. 2.35 the residual stress can be solved but we must first specify a value for $\underline{\tilde{\alpha}}$ which of course depends on the material behavior.

In general a material will respond to shot peening two different ways. The material will shakedown either elastically or plastically. The difference between the two depends on the initial and final states (location and size) of the yield surface. Figures 2.6 and 2.7 show the two conditions. Guechichi describes elastic shakedown as two yield surfaces with a nonzero intersection and plastic shakedown consisting of two yield surfaces with no common section.

The plastic strain and strain rate behave differently with respect to time for elastic and plastic shakedown. The defining feature of elastic shakedown is for the plastic strain to reach a steady state as time goes to infinity. This results in a plastic strain rate of zero after a suitable length of time which implies successive shot impacts will not induce plastic flow. For elastic shakedown there is no increase in the radius of the yield surface and the residual stress can be calculated from the plastic strain by using Eqn. 2.30.

During plastic shakedown there are closed cycles of plastic strain therefore $\dot{\epsilon}^p \neq 0$. And accumulation of plastic strain must be accounted for using

$$\epsilon^p(z) + \left(\frac{1-\nu}{E}\right)\sigma^r(z) + \Delta\epsilon^p(z) = 0 \tag{2.36}$$

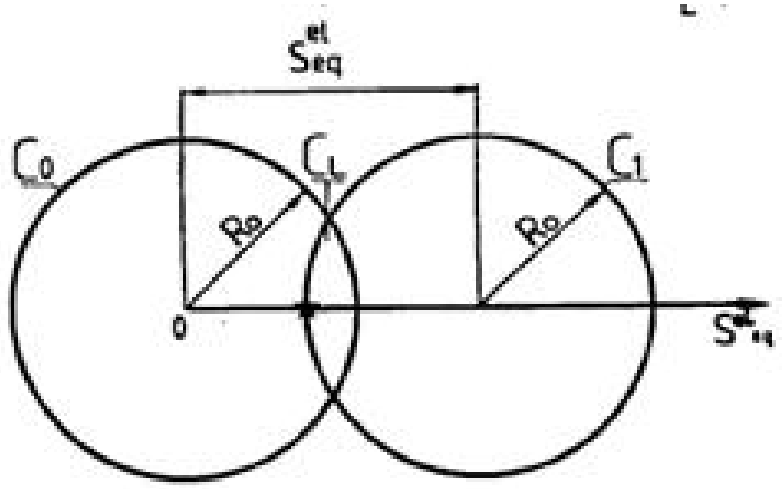

Figure 2.6: Elastic shakedown occurs with two intersecting elastic domains.

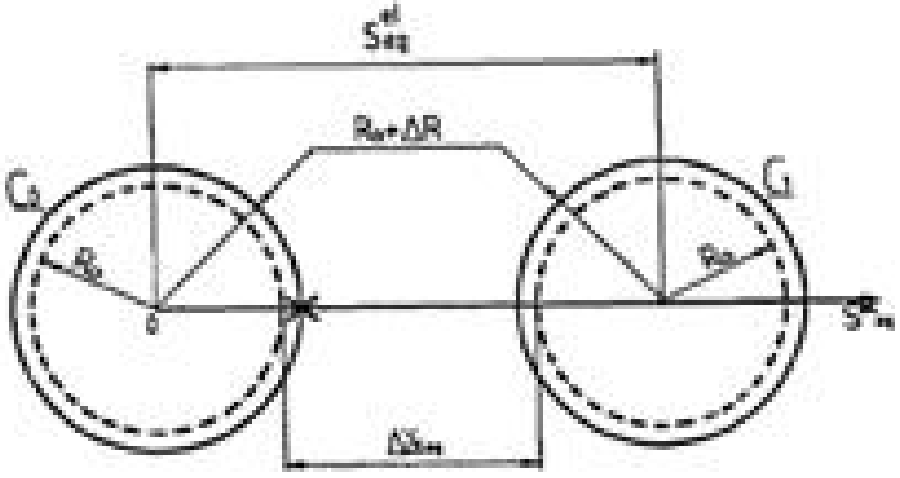

Figure 2.7: Plastic shakedown occurs when the elastic domains do not share a common intersection.

The modified internal variable must be characterized differently for each case. For elastic shakedown an equivalent modified internal variable of the form

$$\tilde{\alpha}_{eq}(z) = S^{el}_{eq}(z) - R_0 = \sqrt{6}\tilde{\alpha}(z) \tag{2.37}$$

is used by Guechichi. Under plastic shakedown conditions the analysis is a little more involved and isotropic hardening must be accounted for. This can be accomplished by expressing the transformed parameter α as

$$\tilde{\alpha}_{eq}(z) = R_0 + \Delta R(z) \tag{2.38}$$

$\Delta R(z)$ is the variation in the yield surface size and is related to $\Delta\epsilon^p$ by a power law

$$\Delta R(z) = k[\Delta\epsilon^p_{eq}(z)]^n \tag{2.39}$$

and the change in equivalent plastic strain, $\Delta\epsilon^p_{eq}(z)$, is related to the change in plastic strain by

$$\Delta\epsilon^p_{eq}(z) = \sqrt{6}\Delta\epsilon^p(z) \tag{2.40}$$

k and n are the usual material behavior coefficients. From Eqn. 2.30 and 2.34 the change in equivalent plastic strain can be calculated in terms of $\Delta\tilde{\alpha}_{eq}(z)$. $\Delta\tilde{\alpha}_{eq}(z)$ can then be related back to known elastic quantities by using $\Delta\tilde{\alpha}_{eq}(z) = S^{el}_{eq}(z) - 2R_0$

$$\Delta\epsilon^p_{eq}(z) = \Delta\tilde{\alpha}_{eq}(z)\left(\frac{3(1-\nu)}{3C(1-\nu)+E}\right) \tag{2.41}$$

The residual stress analysis so far has been for a semi infinite surface not for a finite surface. But to obtain the residual stress in a finite surface the stress field of a semi infinite surface must be known. The residual stress in a semi infinite surface ***does not satisfy equilibrium*** because the balancing tensile stress is absent Guechichi [11].

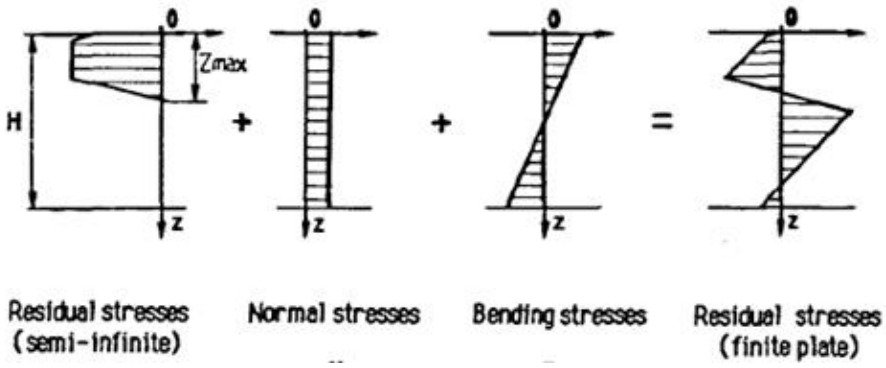

Figure 2.8: Residual stress in a finite structure is composed of three components. The residual stress in a semi infinite surface, normal stresses and bending stresses. Note the residual stress in a semi infinite surface is ***not in equilibrium*** and completely lacks any balancing tensile stress.

Guechichi states that the semi infinite residual stress will decay until it disappears entirely. Plots of the residual stress in a semi infinite surface are shown in Fig. 2.8.

To find the residual stresses in a thin plate Guechichi uses superposition. The axial and bending stress must be superimposed with the semi infinite residual stress, $\sigma^r(z)$. Thus our finite plate solution is

$$\sigma^r_{finite}(z) = \sigma_{bending}(z) + \sigma_{axial}(z) + \sigma^r(z) \tag{2.42}$$

Eqn. 2.42 is the same as Eqn. 2.5, Flavenot's equation for the residual stress in a thin plate, except that the stress source has been replaced by the residual stress in a semi infinite surface. Furthermore, if plastic shakedown does not occur then both the semi infinite residual stress and stress source are governed by Hooke's law.

2.3.4 Khabou et al.

Other researchers have made contributions to Guechichi's model. M.T. Khabou [27] adds that with isotropic hardening, Guechichi's analysis models some materials, for example plain carbon steels and titanium alloys, more accurately than with kine-

matic hardening alone. Plain carbon steels and titanium alloys have a well defined yield stress but for materials with an ill defined yield stress, such as aluminum alloys, stainless steel and nickel alloys, the latter approach falls short in predicting the residual stress behavior. Khabou states that the FCC structure of these materials make prediction of the residual compressive stress difficult because isotropic hardening cannot be modeled accurately with a simple increment of the yield surface. Therefore, Khabou devises a simple rheological model constructed of two coupled yield blocks. Khabou follows the same approach as Guechichi and uses the simplified technique of J. Zarka [29], G. Inglebert [30] and G. Inglebert [31] to solve for the inelastic strain fields and residual stress fields. This rheological model provides more realistic results for 7075 aluminum alloy.

A more recent publication R. Fathallah [32] based on the work of Guechichi and Khabou takes into account major controlling factors such as impingement angle, friction, shot and material hardness ratio. Fathallah reproduces the residual stresses in a thick plate made of base superalloy Udimet 720 measured by X-ray diffraction. The results are in good agreement.

2.3.5 Li et al.

Here we primarily discuss the work of J.K. Li [12] and show what other authors have contributed to his theoretical framework. Like previous research, the theory of Hertzian contact is used to evaluate the principal stress field in the surface layer of the target material see Johnson [3] or Herts [2]. The residual stress field is homogenous with associated plastic strain in the work piece which is taken as a semi-finite body. Loading of the surface is assumed to be uniform therefore the residual stress fields stay constant along the surface and only vary through the depth. The goal of most elastic plastic models is to simplify the analysis by relating plastic quantities to elastic quantities. So, basic Hertzian elasticity quantities such as the deviatoric stress and strain are solved and connected to elastic plastic relations of the loading and unloading

process after yielding occurs. The basic parameters developed from Hertzian contact theory include the indentation radius and maximum normal elastic pressure, which can be found in any impact mechanics book for example see Johnson [3], and have the form

$$a_e = R^* \left(\frac{5}{2} \pi k \rho \frac{V^2}{E_0} \right)^{\frac{1}{5}} \tag{2.43}$$

$$p = \frac{1}{\pi} \left(\frac{5}{2} \pi \rho k V^2 E_0^4 \right)^{\frac{1}{5}} \tag{2.44}$$

respectively with

$$\frac{1}{E_0} = \frac{1-\nu^2}{E} + \frac{1-\nu_s^2}{E_s} \tag{2.45}$$

The unknowns R^* and V are the shot radius and velocity respectively. E_0 is the combined modulus of elasticity of the target and shot, ν and ν_s are the Poisson's ratio of the target and shot, respectively. The constant k is an efficiency coefficient used to take into account elastic and thermal dissipation during impact Johnson [3]. The Hertzian stresses are given in Eqn. 2.24 and are derived for a position directly below the indenter which is a state of zero shear stress so these are principal stresses

$$\begin{aligned}
\sigma_{11}^e &= p(1+\nu) \left[\frac{z}{a_e} tan^{-1} \left(\frac{z}{a_e} \right) - 1 \right] + p \frac{a_e^2}{2(a_e^2 + z^2)} \\
\sigma_{22}^e &= p(1+\nu) \left[\frac{z}{a_e} tan^{-1} \left(\frac{z}{a_e} \right) - 1 \right] + p \frac{a_e^2}{2(a_e^2 + z^2)} \\
\sigma_{33}^e &= -p \left[\left(\frac{z}{a_e} \right)^{-1} + 1 \right]
\end{aligned} \tag{2.46}$$

A derivation of these stresses can be found in Johnson [3]. The corresponding mean stresses are

$$\sigma_m^e = \frac{1}{3} (\sigma_{11}^e + \sigma_{22}^e + \sigma_{33}^e) \tag{2.47}$$

With Hooke's law the principal strains are easily found

$$\begin{aligned}\epsilon^e_{11} &= \frac{1}{E}[\sigma^e_{11} - \nu(\sigma^e_{22} + \sigma^e_{33})] \\ \epsilon^e_{22} &= \frac{1}{E}[\sigma^e_{22} - \nu(\sigma^e_{11} + \sigma^e_{33})] \\ \epsilon^e_{33} &= \frac{1}{E}[\sigma^e_{33} - 2\nu\sigma^e_{11}]\end{aligned} \tag{2.48}$$

the corresponding mean strain is

$$\epsilon^e_m = \frac{1}{3}(\epsilon^e_{11} + \epsilon^e_{22} + \epsilon^e_{33}) \tag{2.49}$$

The elastic deviatoric stresses are

$$\begin{aligned}s^e_{11} &= \sigma^e_{11} - \sigma^e_m = \frac{1}{3}\sigma^e_i \\ s^e_{22} &= \sigma^e_{22} - \sigma^e_m = \frac{1}{3}\sigma^e_i \\ s^e_{33} &= \sigma^e_{33} - \sigma^e_m = -2s^e_{11} = -\frac{2}{3}\sigma^e_i\end{aligned} \tag{2.50}$$

Therefore, from the principle stresses and strains the Von Mises equivalent stress and strain are

$$\sigma^e_i = [(\sigma^e_{11} - \sigma^e_{22})^2 + (\sigma^e_{33} - \sigma^e_{22})^2 + (\sigma^e_{11} - \sigma^e_{33})^2]^{\frac{1}{2}} \tag{2.51}$$

$$\epsilon^e_i = \frac{\sigma^e_i}{E} \tag{2.52}$$

E is the materials Young's modulus. The strain deviators are

$$\begin{aligned}e^e_{11} &= \epsilon^e_{11} - \epsilon^e_m = \frac{1}{3}(1+\nu)\epsilon^e_i \\ e^e_{22} &= \epsilon^e_{22} - \epsilon^e_m = \frac{1}{3}(1+\nu)\epsilon^e_i \\ e^e_{33} &= \epsilon^e_{33} - \epsilon^e_m = -2s^e_{11} = -\frac{2}{3}(1+\nu)\epsilon^e_i\end{aligned} \tag{2.53}$$

Note, the analysis this far has followed a traditional elasticity approach to solve the stress and strain deviators. Now the task is to express the elastic plastic equations

in terms of these fundamental elasticity quantities. Permanent deformation occurs when the equivalent stress in the target material is greater than the yield stress. A series of simplified linear relations is used in the elastic-plastic analysis of the loading process to avoid the difficulty that arises from applying a more rigorous plasticity theory. J.K. Li [12] adopts a modifying coefficient α defined as the ratio of the plastic indentation diameter and elastic indentation diameter

$$\alpha = \frac{D_p}{2a_e} \tag{2.54}$$

Where D_p is the diameter of the plastically deformed indentation. This modifying coefficient allows us to relate our plasticity quantities, specifically the effective plastic strain, to the effective elastic strain. With this we have

$$\epsilon_i^p = \begin{cases} \epsilon_i^e & \text{for } \epsilon_i^e \leq \epsilon_s \\ \epsilon_s + \alpha(\epsilon_i^e - \epsilon_s) & \text{for } \epsilon_i^e > \epsilon_s \end{cases} \tag{2.55}$$

A convenient empirical relation to solve for the plastic diameter is J.K. Li [12]

$$D_p = \beta F^n \tag{2.56}$$

Where $\beta = (16+15R^*)+1.66(1+2R^*)\times\left[2.3-\left(\frac{S_b}{1000}\right)^3\right]$ with $n = 0.482(1-0.2R^*)$. This empirical relation assumes a static load, F, is applied to the surface by a shot of radius R^*. This is of course one drawback of the empirical relation. S_b is the true stress that corresponds to the maximum engineering stress. By assuming a multi-linear relationship between the elastic-plastic stress and strains, the elastic-plastic stress can be written as

$$\sigma_i^p = \begin{cases} \sigma_i^e & \text{for } \epsilon_i^e < \epsilon_s \\ \sigma_s + k_1(\epsilon_i^p - \epsilon_s) & \text{for } \epsilon_s \leq \epsilon_i^p < \epsilon_b \\ S_b + k_2(\epsilon_i^p - \epsilon_b) & \text{for } \epsilon_i^p \geq \epsilon_b \end{cases} \tag{2.57}$$

The unknowns k_1 and k_2 are hardening coefficients for the different linear stages of plastic deformation. σ_s and ϵ_s are the yield strength and strain respectively. The quantities S_b and ϵ_b are true stress and strain corresponding to the ultimate tensile strength or the maximum stress on the engineering stress strain curve. Fig. 2.9 represents the corresponding stress strain curve with the parameter definitions for this loading process. A great simplification can be made by assuming that the plastic strain deviators take on a similar form as the elastic strain deviators. Li claims that because of axisymmetric loading and geometric considerations the elastic-plastic strain deviators, e^p_{ij}, can be calculated from

$$\begin{aligned} e^p_{11} &= \frac{1}{3}(1+\nu)\epsilon^p_i \\ e^p_{22} &= \frac{1}{3}(1+\nu)\epsilon^p_i \\ e^p_{33} &= -2s^p_{11} = -\frac{2}{3}(1+\nu)\epsilon^p_i \end{aligned} \tag{2.58}$$

The next goal is to derive the elastic plastic stress deviator. Iliushins elastic plastic theory [33] is applied

$$s^p_{ij}\epsilon^p_i = \frac{1}{1+\nu}e^p_{ij}\sigma^p_i \tag{2.59}$$

Or written out in component form the elastic plastic stress deviators are

$$\begin{aligned} s^p_{11} &= \frac{1}{1+\nu}\frac{e^p_{11}}{\epsilon^p_i}\sigma^p_i = \frac{1}{3}\sigma^p_i \\ s^p_{22} &= \frac{1}{1+\nu}\frac{e^p_{22}}{\epsilon^p_i}\sigma^p_i = \frac{1}{3}\sigma^p_i \\ s^p_{33} &= -2s^p_{11} = \frac{1}{1+\nu}\frac{e^p_{33}}{\epsilon^p_i}\sigma^p_i = -\frac{2}{3}\sigma^p_i \end{aligned} \tag{2.60}$$

This is an equibiaxial state of stress. Let us summarize the process development this far. The principle stresses for Hertzian contact are given as equations 2.46 which can be derived by considering a ring of concentrated force acting at some radius. As was stated earlier these are principle stresses because there is no shear directly below

the indentation in the z direction. The stresses located elsewhere throughout the material have been found and we refer the reader to Huber (1904) and Morton & Close (1922). An elastic analysis is then performed to obtain the elastic deviatoric stress and strain tensors in terms of the hertzian principle stresses. Simple expressions for the elastic-plastic deviatoric stress tensor are obtained by using Iliushin's plasticity theory along with the multi linear equivalent elastic-plastic stress strain curve. Because of axisymmetry and geometry a simple relation between the deviatoric elastic plastic strain tensor and the equivalent plastic strain is given by Eqn. 2.58. With these fundamental elastic and elastic-plastic quantities the residual stress fields after unloading can be solved.

Throughout the shot peening literature the residual stresses are typically defined two ways: (1) as the difference between the plastic and elastic stress deviators or (2) in terms of the plastic strain tensor as given by the relations Eqn.'s 2.30 and 2.36. For this analysis we will define the residual stress from (1) as

$$\sigma_{ij}^r = s_{ij}^p - s_{ij}^e \tag{2.61}$$

Defining in the elastic and plastic regions

$$\sigma_{ij}^r = \begin{cases} 0 & \text{for } \sigma_i^e < \sigma_s \\ s_{ij}^p - s_{ij}^e & \text{for } \sigma_s \leq \sigma_i^e \leq 2\sigma_e^p \end{cases} \tag{2.62}$$

Or in component form

$$\begin{aligned} \sigma_{11}^r &= \frac{1}{3}(\sigma_i^p - \sigma_i^e) \\ \sigma_{22}^r &= \frac{1}{3}(\sigma_i^p - \sigma_i^e) \\ \sigma_{33}^r &= -2\sigma_{11}^r \end{aligned} \tag{2.63}$$

Based on isotropic hardening the material will experience reverse yielding and hardening if the equivalent elastic stress exceeds twice the value of the equivalent

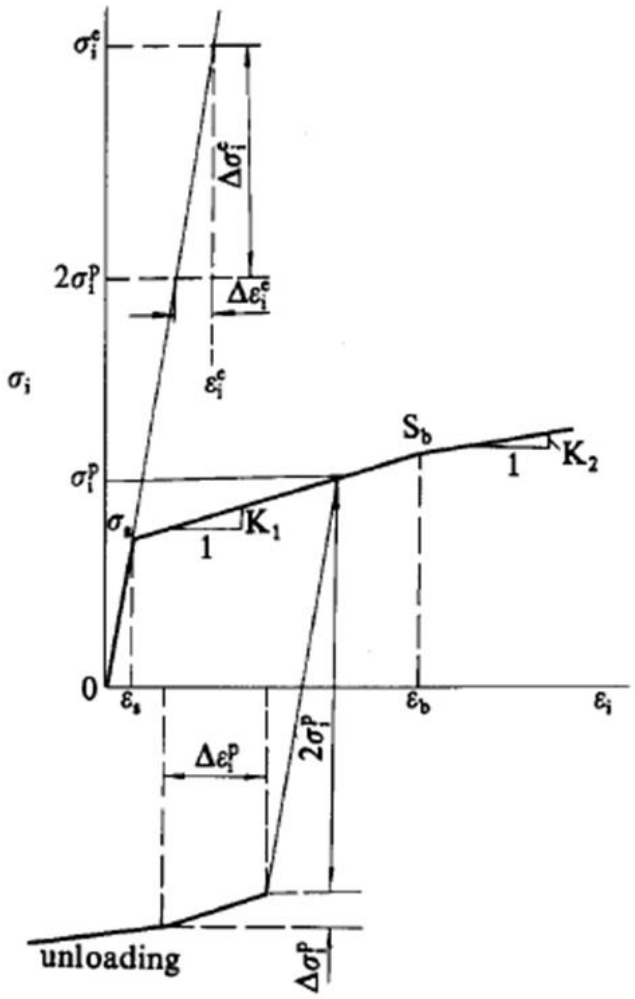

Figure 2.9: Plot of the loading and unloading process [12]

plastic stress. This behavior is observed in the equivalent stress strain curve, Fig. 2.9, reverse yielding occurs at an unloaded stress value of $2\sigma_i^p$ and so the elastic domain is growing which indicates isotropic hardening. Reverse yielding will just occur after an amount of stress equal to $2\sigma_i^p$ unloads. And any remaining elastic stress that has not unloaded will induce plastic flow and hence reverse yielding in compression. The amount of stress that has not unloaded is

$$\Delta\sigma_i^e = \sigma_i^e - 2\sigma_i^p \tag{2.64}$$

One can see from Fig. 2.9 after reverse yielding has occurred a modification to Eqn. 2.63 is required. The residual stresses take on the form

$$\begin{aligned} \sigma_{11}^r &= \frac{1}{3}(\sigma_i^p - 2\sigma_i^p - \Delta\sigma_i^p) \\ \sigma_{22}^r &= \frac{1}{3}(\sigma_i^p - 2\sigma_i^p - \Delta\sigma_i^p) \\ \sigma_{33}^r &= -2\sigma_{11}^r \end{aligned} \tag{2.65}$$

We are again faced with the task of solving our elastic plastic quantities in terms of known elastic quantities. And solve for the unknown, $\Delta\sigma_i^p$, in terms of elastic relations. From the figure we know

$$\Delta\sigma_i^p = k_1\Delta\epsilon_i^p \tag{2.66}$$

And define the change in effective plastic strain by again using α from 2.54

$$\Delta\epsilon_i^p = \alpha\Delta\epsilon_i^e \tag{2.67}$$

Where k_1 is defined in Eqn. 2.57. Again using Hooke's law

$$\Delta\epsilon_i^e = \frac{\Delta\sigma_i^e}{E} \tag{2.68}$$

Upon substituting equation 2.64 into 2.68 we can solve for the residual stress fields after reverse yielding occurs in terms of known elastic expressions. Furthermore, this

model can be easily modified to include kinematic or mixed hardening if desired. Calculating the residual stress from the equivalent stress strain curve results in much convenience.

The latter formulation is for a single shot impact. Modifications of the residual stress boundary conditions are necessary for a surface that is completely deformed. After 100% coverage the residual stress fields are uniform and continuous and the work piece is assumed to stay flat J.K. Li [12]. The boundary conditions for this scenario are

$$\sigma_{11}^r = \sigma_{22}^r = g_1(z) \tag{2.69}$$

$$\sigma_{33}^r = 0 \tag{2.70}$$

$$\epsilon_{33}^r = g_2(z) \tag{2.71}$$

$$\epsilon_{11}^r = \epsilon_{22}^r = 0 \tag{2.72}$$

Notice that with these boundary conditions equilibrium is no longer satisfied. Therefore the residual stresses must be relaxed. The relaxed residual stress can be solved from Hooke's law

$$\sigma_{11}^{rel} = \sigma_{22}^{rel} = \frac{\nu}{1-\nu}\sigma_{33}^r \tag{2.73}$$

Subtracting Eqn. 2.73 from our unrelaxed residual stresses yields

$$\begin{aligned} \sigma_{11}^R &= \sigma_{11}^r - \frac{\nu}{1-\nu}\sigma_{33}^r = \frac{1+\nu}{1-\nu}\sigma_{11}^r \\ \sigma_{22}^R &= \sigma_{22}^r - \frac{\nu}{1-\nu}\sigma_{33}^r = \frac{1+\nu}{1-\nu}\sigma_{11}^r \end{aligned} \tag{2.74}$$

Again, Eqn. 2.74 give the residual stress in a semi-infinite surface and are ***not self equilibrated***. The residual stresses are only equilibrated in a thin structure because it is allowed to bend and stretch.

S. Shen [34] claims that one of the major drawbacks of Li's analysis is the use of an empirical relation that relies on the static force. And so to remedy this physical inconsistency Shen calculates the plastic indentation by using an average pressure distribution Al-Hassani [35], $\bar{p}$, that acts to counter the force of the impinging shot and accelerate it away from the surface. The equation of motion of the shot is

$$M\frac{dv}{dt} = -\pi a_p^2 \bar{p} \tag{2.75}$$

M is the projectile mass and a_p the plastic indentation. The pressure distribution has the form Al-Hassani [35]

$$\frac{\bar{p}}{\sigma_s} = 0.6 + \frac{2}{3} ln \frac{E a_p}{\sigma_s R^*} \tag{2.76}$$

the indentation depth is also related to the impinging pressure from

$$\frac{\bar{z}}{R^*} = \left(\frac{2}{3}\right)^{\frac{1}{2}} \left(\frac{V^2 \rho}{\bar{p}}\right)^{\frac{1}{2}} \tag{2.77}$$

Simple geometric considerations give the plastic indentation size in terms of the depth

$$a_p^2 = 2\bar{z}R^* - \bar{z}^2 \tag{2.78}$$

From Eqn.'s 2.77 and 2.78 the indentation radius can be solved without any empiricism. Furthermore, the indentation is a function of the pressure resisting the motion of the shot. Primary shot peening parameters such as shot velocity and material characteristics are taken into consideration.

An alternate approach by B. Bhuvaraghan [36] avoids the parameter α all together by applying Nuebers relation. Nuebers equation assumes the strain energy corresponding to the elastic-plastic stress is equal to the strain energy of a psuedo elastic stress see Fig. 2.10. And is given by

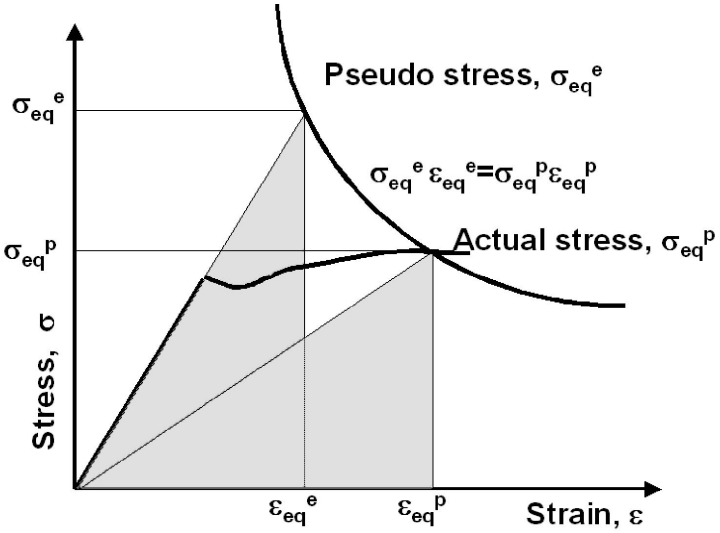

Figure 2.10: Graphical depiction of Nuebers theory relating the strain energy from the psuedo elastic stresses to the strain energy of the elastic plastic stresses

$$\sigma_i^p \epsilon_i^p = \sigma_i^e \epsilon_i^e \tag{2.79}$$

The elastic plastic stress is also approximated from the Johnson-Cook model. This model relates the elastic plastic stress and strain. With Eqn. 2.79 strain rate effects and strain hardening can be included in the effective stress strain curve

$$\sigma = [A^* + B^*(\epsilon)^n] \left[1 + C^* ln\left(\frac{\dot{\epsilon}}{\dot{\epsilon}_0}\right)\right] \left[1 - \left(\frac{T - T_0}{T_m - T}\right)^m\right] \tag{2.80}$$

Miao has also followed Li's formulation and applies it to calculate the Almen intensity of an Almen strip. H.Y. Miao [37] treats the residual stress from Eqn. 2.74 as an induced stress which is a stress that is not equilibrated. Superposition of the induced stress, axial stress and bending stress provides the complete equilibrated residual stress field in an Almen strip.

2.3.6 Tirosh

Other approaches to calculate the stress field of a spherical indentation have been used. Tirosh [13] conducts a theoretical residual stress analysis based on a simplified geometric model of the indentation. Tirosh derives the residual stresses with fundamental elasticity principles. Specifically, equilibrium and compatibility are used to express the in plane residual stress field in terms of a uniform hydrostatic pressure p. Clearly, Tirosh chose to use a classic elastic solution to solve the residual stress. He also applies the so called inclusion model of Muskhelishvili to obtain a closed form solution of this in-plane pressure. *A necessary assumption of the inclusion model is that the plastically deformed zone is an incompressible inclusion with a penny shaped configuration.* If the impact crater is much smaller than the radius of the indenter then it can be considered as flat and shallow. Therefore, the residual plastic zone has a penny-shaped form, with radius a and height h. These assumptions allow for a simplified approximation of the mechanical behavior of the material. Certain boundary conditions must also be satisfied, these are discussed below. Along with the inclusion model, Tirosh develops a fatigue model based on Melan's lower bound shakedown theorem. Melan's shakedown theorem allows Tirosh to estimate the allowable safe stress amplitude of a shot peened structure.

Inclusion Model of a Residual Stress

The basis of Tirosh's simplified residual stress model is the bi-harmonic airy stress functions used with simplified boundary conditions. Recall, the equations of stress compatibility in terms of the Airy stress function has the form

$$\sigma_{rr} = \frac{\partial \Phi}{r \partial r} + \frac{\partial^2 \Phi}{r^2 \partial \theta^2}; \quad \sigma_{\theta\theta} = \frac{\partial^2 \Phi}{\partial r^2}; \quad \sigma_{\theta r} = -\frac{\partial}{\partial r^2}\left(\frac{1}{r}\frac{\partial \Phi}{\partial \theta}\right) \tag{2.81}$$

The solution of Eqn. 2.81 is a function of only the radial component r because of azimuthal symmetry (angular symmetry of θ) of a single sphere impacting the surface.

Therefore, the solution has the form

$$\Phi = Aln(r) + Br^2 + Cr^2 + D \tag{2.82}$$

The required boundary conditions for Eqn. 2.82 are Tirosh [13]

1. at r=0 the stresses are finite;

2. at r=a the radial stress, σ_{rr}^{res}, is the residual stress of magnitude p induced by the surrounding elastic region

3. for radial distances much greater than the indentation radius the structure is stress free, i.e. the material is absent of any residual stress

With these boundary conditions the solutions to the residual stress components in Eqn. 2.81 are

$$\begin{aligned} &\sigma_{rr}^{(res)} = \sigma_{\theta\theta}^{(res)} = 2B, \quad B = \frac{p}{2} \;\; along \; 0 \leq r \leq a \\ &\sigma_{rr}^{(res)} = \frac{p}{\rho^2}, \quad \sigma_{\theta\theta}^{(res)} = -\frac{p}{\rho^2} \\ &where \; \rho = \frac{r}{a} \; along \; a < r \leq \infty \end{aligned} \tag{2.83}$$

Two apparent observations can be made based on the solutions in Eqn. 2.83. First, the residual stress field within the plastically deformed zone, $r \leq a$, is subject to a uniform hydrostatic state of $p/2$. Secondly, the radial compressive residual stress outside this region decays to zero rapidly. However, the hoop stress, $\sigma_{\theta\theta}^{res}$, outside the interface at $r = a$ becomes tensile.

The magnitude of the residual stress, p, requires a different approach to solve. Tirosh envisages the inclusion of radius a being forced into a penny shaped cavity with smaller radius $a - \Delta a$ in the surface layer of the structure. The geometrical mismatch vanishes because continuity of displacements is required. As a result, the surrounding elastic domain compensates by exerting a pressure on the inclusion. The pressure necessary to preserve the geometrical compatibility is the residual stress.

The plane solution to this type problem has been provided by Muskhelishvili [38] and has the form

$$p = \frac{4\mu_0\mu\delta}{s\mu_0 a + \mu(\chi_0 - 1)(a - \delta)}, \quad \delta = \Delta a \tag{2.84}$$

for plane strain or plane stress respectively.

Because the indentation size is small compared to the ball diameter, we have $\Delta a/a \ll 1$. By substituting the material properties, $\nu = 1/3$ and $E \approx 8/3\mu$, into Eqn. 2.84

$$\begin{aligned} \frac{p}{\sigma_0} &= -\frac{3}{8}\frac{E}{\sigma_0}\epsilon^p \quad for\ plane\ strain \\ \frac{p}{\sigma_0} &= -\frac{9}{32}\frac{E}{\sigma_0}\epsilon^p \quad for\ plane\ stress \end{aligned} \tag{2.85}$$

A close approximation of the plastic strain, ϵ^p is the yield strain, ($\epsilon_p \approx \epsilon_y \approx \sigma_y/E$) because the inclusion is confined to its plane by the elastic domain. Substituting the yield strain into Eqn. 2.85 gives the range of values for the residual stress

$$\frac{9}{32} \leq \left|\frac{p}{\sigma_0}\right| \leq \frac{3}{8} \tag{2.86}$$

Tirosh's analysis neglects the interaction of multiple impacts, but from the range of values above, he obtains a reasonable approximation for the residual stress

$$p \approx -\frac{1}{3}\sigma_0 \tag{2.87}$$

This value is on the lower limit of experimental measurements, which predicts the residual stress to be $p \approx -1/2\sigma_y\ to\ -\sigma_y$ [13, 16].

Lower Bound Shakedown Analysis

The key concept of Melan's lower bound shakedown principle is that a structure subjected to a fluctuating load will respond elastically if the unbounded elastic stress (which is identical to the applied stress $\sigma^e_{ij}(t)$) superimposed on a time independent admissible residual stress (σ^{res}_{ij}) does not exceed yielding. The unbounded elastic

stress is the stress that would form in the material assuming it responds to external loads by deforming elastically, even if loads are large enough to cause yielding. Note, the unbounded elastic stress is not the actual elastic-plastic stress within the material. Mathematically, shakedown occurs when the following criterion is met

$$F = [\sigma_{ij}^{(res)} + \sigma_{ij}^{(e)}(t)] \leq \sigma_0 \tag{2.88}$$

F is some specified yield criterion. For convenience write the sum of the elastic residual stress and applied stress as

$$\sigma_{ij}^{(sum)} = \sigma_{ij}^{(res)} + \sigma_{ij}^{(e)}(t) \tag{2.89}$$

By substituting the equation above into the Von Mises yield criterion, the shakedown condition becomes

$$F = \frac{1}{2}[(\sigma_{rr}^{(sum)} - \sigma_{\theta\theta}^{(sum)})^2 + (\sigma_{\theta\theta}^{(sum)} - \sigma_{zz}^{(sum)})^2 + (\sigma_{zz}^{(sum)} - \sigma_{rr}^{(sum)})^2] + 3\tau_{r\theta}^{(sum)2} = \sigma_0^2 \tag{2.90}$$

Muskhelishvili [38] solves the elastic stress distribution caused by an in-plane remote fluctuating stress inside and outside of an inclusion. Tirosh uses these stress relations as the applied stress components, $\sigma_{ij}^{(e)}$. The derivation for the fluctuating stresses are lengthy and involved, so the results are referred to here. With $\sigma_{ij}^{(res)}$ and $\sigma_{ij}^{(e)}$ defined, Tirosh obtains a closed form solution of the stress amplitude ($\frac{\sigma_\infty(t)}{\sigma_0}$) as a function of the normalized residual stress components ($\frac{p}{\sigma_0}$) from Eqn. 2.90

$$K_{11}\left(\frac{\sigma_\infty(t)}{\sigma_0}\right)^2 + K_{12}\left(\frac{\sigma_\infty(t)}{\sigma_0}\right)\left(\frac{p}{\sigma_0}\right) + K_{22}\left(\frac{p}{\sigma_0}\right)^2 = 1 \tag{2.91}$$

The coefficients in Eqn. 2.91 have the values $K11 = 1$, $K12 = 1$, and $K22 = 1$ for plane strain. In plane stress we have $K11 = 273/256$, $K12 = 9/8$, and $K22 = 1$. The difference between the two stress states is almost indistinguishable.

The total area under the residual stress vs depth curve must sum to zero because equilibrium has to be satisfied. Each part of the residual stress, the compressive and

the tensile, must balance. In a thick structure the tensile region of the residual stress is stretched out over a larger depth, therefore, the magnitude is reduced. However, there are relatively large tensile residual stresses in a thinner shot peened structure. In general, the fatigue benefits diminish for a thinner structure (plane stress). Tirosh's results are not entirely accurate because they do not capture the aforementioned behavior.

The applied stress σ_∞ caused by cyclic loading is fatigue safe if it falls inside (including the boundary) the ellipse. If the stress amplitude falls somewhere outside the ellipse the structure will fail from an accumulation of plastic deformation (ratcheting). Tirosh verifies his analysis by comparing the predicted safe life stress amplitude (the stress amplitude at which the structure will survive at least 10^7 cycles) with experimental fatigue data. An improvement of 10% to 32% in the allowable fatigue limit amplitude is predicted for an applied mean stress, σ_m, equal to zero and σ_0 (yield strength of the material) respectively. Test results for $R = -1$, corresponding to $\sigma_m = 0$, give an improvement in the stress amplitude equal to 40%, in close agreement with the theoretical value of 32%.

2.4 Numerical Simulations of Shot Peening Residual Stresses

There have been a large abundance of numerical simulations produced for shot peening. Numerical modeling is crucial to our understanding of the complicated interaction between the shot media and target material. Even though numerical modeling fails to provide a fundamental relation to the physics of the phenomenon it does shed light on the physical behavior that occurs during shot peening. And having this understanding is crucial for developing an analytical model.

There are six main types of finite element models that have been used to simulate the shot peening residual stress problem. And each model can be categorized by both the degrees of freedom and the number of symmetry surfaces utilized. The first was introduced by K. Mori [39] and is a 2D axisymmetric model. This model simulates

the plastic deformation of the target. The 2D model has the fewest degrees of freedom and is computationally inexpensive. The second development, mentioned previously, consists of a 3D axisymmetric construction implemented by S.A. Meguid [16]. This 3D model was composed of four symmetry surfaces. In the third approach K. Schiffner [40] also used a 3D model but instead modeled the surface as an equilateral triangle. The goal of the investigation was to study the effect of adjacent impacts on the stress fields in the target workpiece. They concluded that adjacent shots have a non negligible influence on the residual stress fields. The fourth numerical model was used by J. Edberg [41]. By using a 3D model with 2 symmetry surfaces Edberg et al. was able to simulate multiple shot impingements. This model was also implemented by S.A. Meguid [15] and S.A. Meguid [42]. The fifth type of model was made by S.T.S. Al-Hassani [43]. His simulation consisted of only a single symmetry surface because he used a target workpiece in the shape of a half circle. The sixth type of model established by J. Schwarzer [44] does not consist of any symmetry surfaces. It is capable of modeling each individual impact zone and is more indicative of what occurs in reality during the peening process.

Some of the earliest contributions of finite element modeling in shot peening was performed by Meguid et al.. Over the past two decades Meguid has made some of the most substantial contributions to the finite element modeling of residual stresses. His work dates back to 1984 when S.A. Meguid [45] studied the influence of punch separation and plastic zone interactions on the residual stress field. In S.A. Meguid [46] the effect of two simultaneous impacting flat rigid punches on a bounded solid is investigated. His work successfully predicts the influence of different strain hardening behavior on residual stresses. Specifically, he discovers a decrease in strain hardening results in a decrease in magnitude of the maximum compressive residual stress. Further contributions have again been made by Meguid. In 1999 S.A. Meguid [15] published a finite element investigation of the dynamic nature of the loading process from shot peening. He reports the influence of shot properties on the time dependent

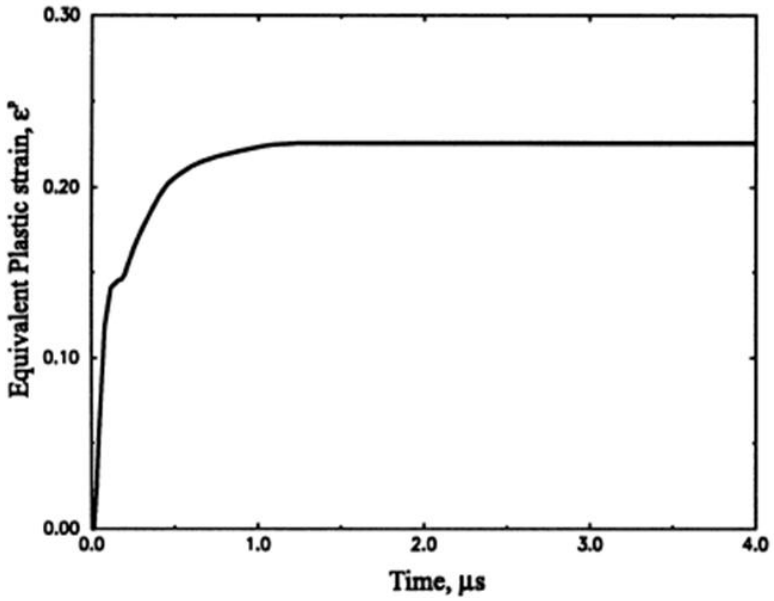

Figure 2.11: Plastic strain, $\epsilon^p(t)$, versus time obtained from [15].

contact force, velocity history, plastic zone and residual stresses. Fig. 2.11 shows the equivalent plastic strain versus time. The behavior is expected a sharp increase in plastic strain during loading followed by a constant strain.

For this investigation S.A. Meguid [15] uses eight noded brick elements isolated around the indentation zone and tetrahedral finite elements elsewhere. The interface of the shot and target was constructed with contact elements. The model revealed some interesting results: i) the velocity, which was varied between 50 and 100 m/s, had an almost negligible influence on the magnitude of the maximum residual stresses occurring below the surface and ii) the velocity did however have a large influence on the depth of the residual stress. For larger velocities a deeper residual stress was observed. A possible reason for this may include hardening of the plastic core. An increase in shot size and shape results in a deeper stress. Another noteworthy result is target hardness had a limited influence on the magnitude of the maximum subsurface compressive residual stress. But an increase in hardness did induce a deeper stress.

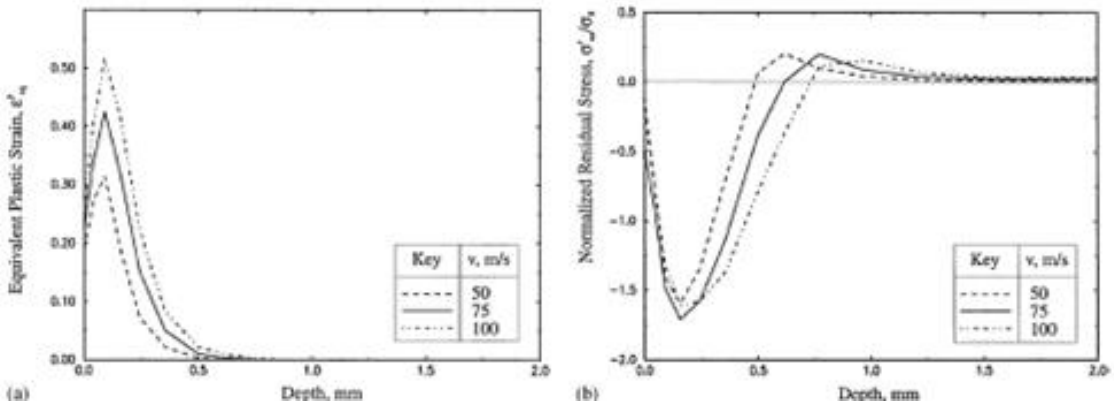

Figure 2.12: Influence of variable velocity on the equivalent plastic strain and residual stress

The dynamic aspect of the work revealed that loading and unloading of the equivalent stress and strain quantities occur on a microsecond time scale.

S.A. Meguid [42] published their findings from a similar finite element model as previously described in S.A. Meguid [15] but considers two impacting shots not just a single impact. S.A. Meguid [42] again studies the effect of shot velocity, size and shape on the equivalent elastic and plastic quantities as well as residual stresses. Similar behavior for these variables on the residual stress field was found. Fig. 2.12 shows both the equivalent plastic strain and residual stress versus depth. The behavior of the two is similar. Each have large stress and strain gradients before and after a maximum value below the surface. However, for an increase in velocity the residual stress does not increase substantially. This is likely because of hardening. They also discuss how the separation distance between impacts affect the compressive stress field. The separation distance between impacts drastically influences the compressive stress distribution. Implying that a large variation in residual stresses will also occur for partial coverage.

S.A. Meguid [16] used a 3D axisymmetric finite element model to study the influ-

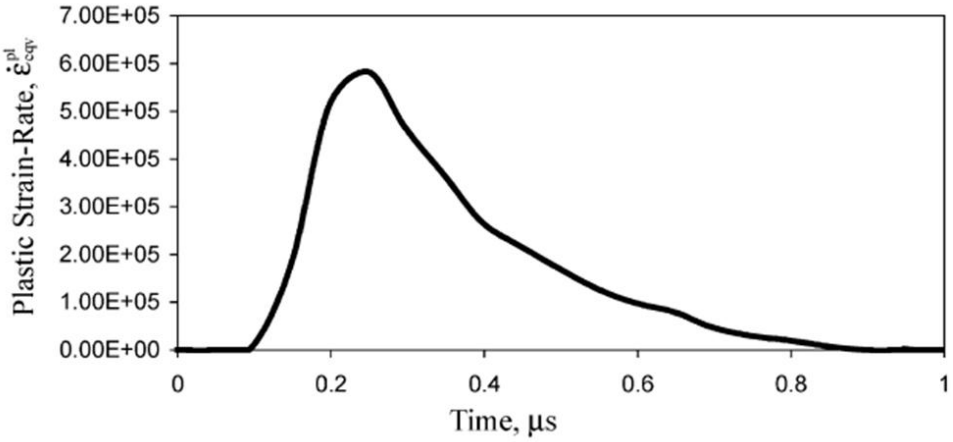

Figure 2.13: Plot of plastic strain rate versus time obtained from LS Dyna [16]

ence of strain rate sensitivity on the residual stresses. Strain rate sensitive materials exhibit an increase in yield strength with an increase in strain rate. Shot peening involves strain rates on the order of $10^5 1/s$ S.A. Meguid [16] which is quite large and so strain rate effects should be incorporated in any modeling if at all possible. They discovered that these high strain rates increased the maximum compressive residual stress by as much as 32% and decrease the depth by 45%. S.A. Meguid [16] also extended the finite element model to incorporate multiple impingements so as to replicate coverage effects. A smaller separation distance creates a more uniform residual stress and plastic strain in the impacted surface. Plots of the equivalent plastic strain rate versus time shown in Fig. 2.13, clearly, the plastic strain rate increases sharply during loading and then decreases over a longer period of time displaying a characteristic tale until finally the strain rate decreases to zero.

More recent work by S.A. Meguid [47] models the compressive stresses with an enhanced symmetry cell rather than the original symmetry cell used throughout S.A. Meguid [16]. This enhanced symmetry cell is capable of modeling closer shot spacing. They conclude however that either the original or enhanced symmetry cell is

acceptable for modeling the residual stresses because both compare well with experimentally measured residual stresses. But this indicates that the differences between the two are not substantial.

Another early contributor to the numerical modeling of shot peening is Y.F. Al-Obaid. Al-Obaid [48] develops a finite element program to incorporate dynamic loading for repeated impact along with strain and work hardening. The model also allows for shakedown of each location resulting from repeated shot impacts. The numerical model provides consistent results with previous numerical and analytical models. S.T.S. Al-Hassani [43] has performed a numerical simulation of multiple shot impacts. The model was created in ABAQUS and considers strain rate dependency and non linear work hardening for multiple normal impacts and a single oblique impact. M.S. EITobgy [49] also uses ABAQUS for a three dimensional elastoplastic finite element model to obtain the residual stresses from shot peening. This numerical formulation uses the Johnson-Cook model to evaluate the flow stress of the target material. The Johnson-Cook model is an analytical expression that relates the flow stress to realistic material behavior such as strain rate, hardening and temperature dependence. M.S. EITobgy [49] also models the shot as deformable instead of rigid as is common in some finite element simulations. Using a deformable shot in the model shows a decrease in both the depth and magnitude of the compressive stress below the surface. Compressive residual stresses obtained from the model are in good agreement with experiment.

H.Y. Miao [50] considers a random distribution of impacts along the surface. This random generation of impacts more realistically represents the actual peening process. This is possible by combining the ANSYS preprocessor with a Matlab program. The explicit solver LS-DYNA was used to model the shot impacting. With this random 3D model it is possible to simulate shot peening intensity, surface coverage and surface roughness for normal and oblique impacts. The average residual stress fields were also produced for 48 impacts. Comparisons with other numerical models are made,

however the study is absent of experimental verification.

2.5 Experimental Findings

This section provides a brief description of the influence the compressive residual stress has on the fatigue behavior of commonly shot peened metals. The review of research here is not directly connected with the analytical modeling in the following chapters but is provided for completeness and to motivate the need for analytical analysis of the residual stresses. The amount of experimental research conducted for shot peening is vast to say the least. Some of the earliest experiments date back to the early 20th century. This work was motivated by frequent fatigue failure of metal parts. Engineers, designers and metallurgists were desperate to understand why these failures occur and how they could extend the lifetime of these parts or prevent failure all together. In 1927, E.G. Herbert [51] published his findings on the work-hardening of steel by abrasion. Herbert investigated the hardening behavior of locomotive tyres and rails as well as steel gears and cams from motor cars that underwent severe abrasion. Another early innovator of the field is J.O. Almen. Almen was the inventor of the Almen strip and gage, measurement tools that provide process consistency, and was a metallurgist that frequently studied fatigue induced fracture of metals. His peening research dates back to 1943. Almen [52] points out that the fatigue strength of most specimens will increase in the presence of a pre-stressed compressive surface layer induced from hammering, swaging, tumbling, by pressure operations with balls or rollers and of course from shot blasting. He also introduces a simple and practical way of measuring the magnitude and depth of the residual stress of the machine part by shot peening a thin metal strip (Almen strip) with the same intensity that is given to the machine part. After peening, the convex curvature of the Almen strip is measured using an Almen gage. Almen claimed this arc height provided a measurement of the residual stress. Even though we now know this is an inadequate method for estimating residual stresses the technique is a cornerstone

for process control in shot peening. The Almen strip and gage are by far the most common measuring tools and practice in shot peening.

Fatigue studies of shot peened metals date to 1943 when Almen [53] performed fatigue tests to determine the increased fatigue durability or life improvement of machine parts. He concluded that fatigue durability increased for hard carburized gears and soft parts whether the stress is completely reversed or if the stress range is small. This is not completely correct because certain steels may experience stress relaxation under the right cyclic loading conditions see S. Taira [54] but these were the first experimental steps toward understanding the nature and behavior of shot peening in fatigue strength and lifetime enhancement. Fatigue remains the largest area of experimental research. And when it comes to fatigue, the more research the better. Thousands of shot peening fatigue studies have been conducted and many focus on such topics as influence of residual stress on fatigue, fatigue strength and life enhancements, corrosion fatigue and high temperature fatigue. These topics will be discussed in detail with a strong emphasis on residual stress effects. In general, the fatigue life for steel, aluminum or titanium can increase under appropriate conditions even though the material response to shot peening is different. However, each study is only relevant for a particular metal and so the following section is organized by fatigue behavior of the most commonly shot peened metals including steel, aluminum and titanium.

2.5.1 Fatigue Behavior of Shot Peened Metals

Steel Alloys

The fatigue behavior of steel is by far the most commonly investigated area. In 1999 Tosha [55] conducted a thorough study of 1507 publications related to fatigue, wear, stress corrosion cracking and peen forming. He found that fatigue is the most common research topic among low alloy steel, carburized steel, spring steel, stainless steel, high

strength steel, aluminum alloys and titanium alloys. Of all these materials low alloy steel, spring steel and carburized steel are the most frequently investigated.

Influence of Residual Stress on Crack Initiation and Propagation

Even though fatigue research is abundant for steels the amount of work investigating the effect of residual stresses on crack initiation is comparatively limited. This is because of the considerable difficulty associated with observing the formation and growth of such small cracks. But even with the associated difficulty a few investigations have revealed the crack initiation behavior of some shot peened steels. For example, in the case of A316 stainless steel, crack initiation is delayed and crack propagation is slowed by the act of shot peening E. R. de los Rios [56]. E. R. de los Rios performed fatigue tests in pure bending with a stress ratio of -0.8 on shot peened hourglass shaped specimens both polished and unpolished. He reported that the number of cycles needed to form a detectable crack was increased from 8000 to 500000 post peening. They also found that unpolished peened specimens have longer initiation and total fatigue lives than polished peened specimens. Work hardening of the surface and heavy distortion of the grains from the deformation is found to be a contributing factor in the delayed crack initiation and growth. Indicating that the residual stress from shot peening is not solely responsible for the improvement in fatigue behavior. Their results also revealed that shot peening improved the fatigue life in all cases. Another investigation conducted by K. Lang [57] of shot peened AISI 304 steel showed that crack formation occurs later than untreated material see Fig. 2.14. Crack propagation is also slower because of the residual stress. This crack behavior is also a result of increased dislocations, grains and twin boundaries in the work hardened layer that act as obstacles preventing localized slip. Furthermore, I. Altenberger [58] also reported similar behavior for normalized steel SAE 1045. Similar results are also found for plain carbon steel SAE 1080 J. Lamer [59] and high strength spring steel AISI 6150 in H. Berns [60] and H. Berns [61]

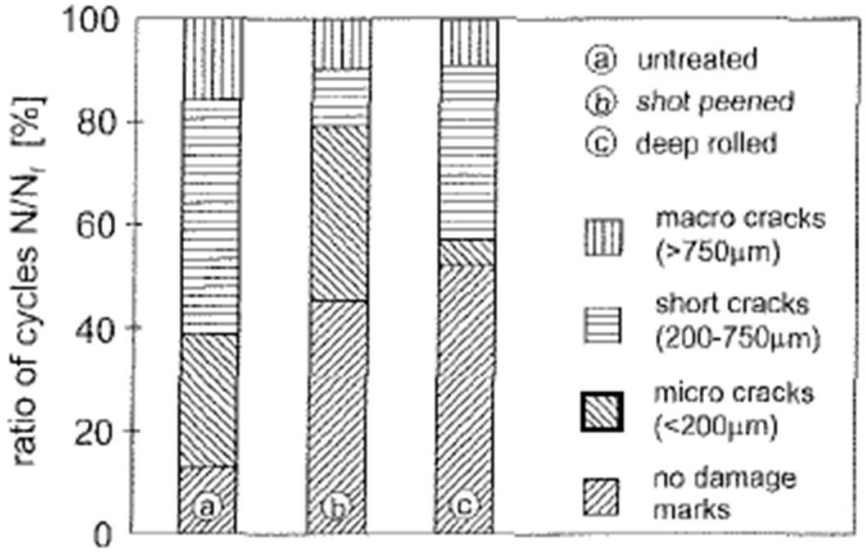

Figure 2.14: Effect of shot peened and deep rolled treatments on fatigue life of austenitic steel AISI 304 [57]

The physical location of crack initiation is also important and can reveal much about the nature of failure. Researchers have found that crack initiation in shot peened surfaces can occur from the top surface or subsurface layers. Some early work done by P. Starker [62] reported that only under certain loading conditions does crack initiation occur at the surface for shot peened carbon steel. Under reversed bending, Starker showed crack initiation started below the surface, approximately 0.3 mm, with a stress amplitude at or less than 1100 N/mm^2. For stress amplitudes between 1200 and 1300 N/mm^2 initiation occurred at the surface. S. Wang [63] also concluded that shot peening of steel pushes the crack source below the surface hardened layer to the tensile region of the residual stress. This results in optimum strengthening of the material.

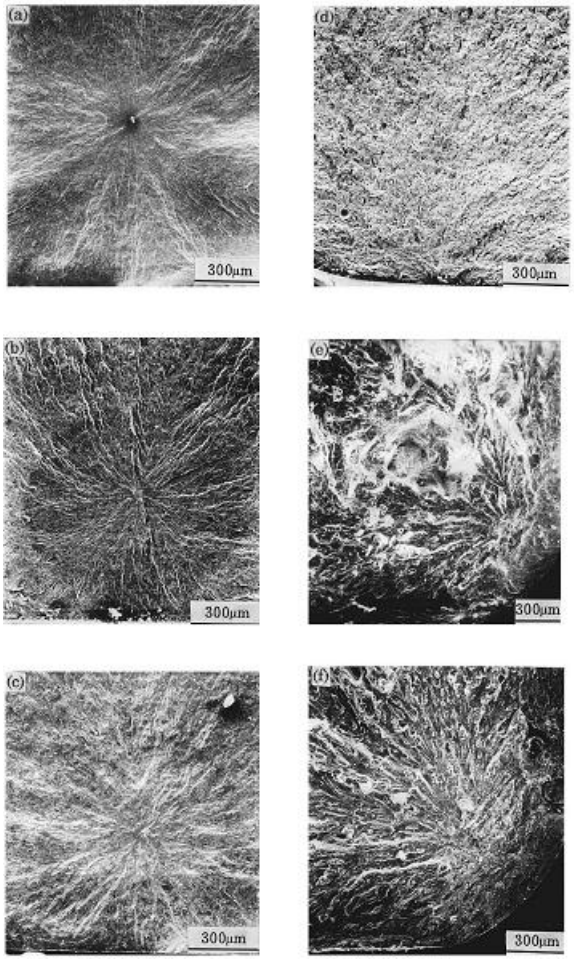

Figure 2.15: SEM photographs of crack initiation below the surface [63]

Fatigue Strength and Life Enhancement of Steel Due to Shot Peening

The key to the increased fatigue life from shot peening resides in its ability to retard crack initiation because crack initiation dominates the cycle life for high cycle fatigue. So all previously discussed benefits of shot peening, for example work hardening of the surface, increase in dislocation density, and especially the residual stress, are responsible for improved fatigue life and strength because crack initiation is delayed. An improved fatigue life is the primary reason for shot peening. And many studies have reported the improved fatigue limit of a large variety of steel. K. Iida [64] found that peening improved the fatigue limit of carburized steel by 25%. R. A. Everett. Jr. [65] investigated the increase in fatigue life of high strength 4340 steel by shot peening. However, only a 10% increase in endurance limit was achieved. Tekeli [66] documented an increase in fatigue life of SAE 9245 steel, used for helical spring production, of approximately 30%. A broader study was conducted by Bignonnet [67] on the influence of the endurance limit from four types of stress loading (rotating-bending, tension-compression, alternating torsion and alternating torsion-bending) on shot peened grade 35 NCD 16 steel. Bignonnet [67] observed that the endurance limit increases by 10 to 20% depending on the type of loading. The list of studies on the increase in fatigue life and strength is endless, our intention is to only discuss a handful so the reader has an idea of how much these crucial fatigue properties increase because of the positive attributes of shot peening.

Relaxation and Stability of Residual Stresses

Another critical topic related to the fatigue behavior of steel is the stability of residual stresses during fatigue. It has been well researched McClung [5] that under specific loading situations a redistribution of the residual stress will occur. For example, if an applied load causes yielding in a material with a residual stress then said residual stress will change upon removal of the applied load. Alternatively, relaxation of the

residual stress can also occur during cyclic loading even if the induced stress is below the yield strength of the material. A modification of a residual stress field can also occur if a crack extends into the initial stress field.

Bignonnet [67] found that relieving of the residual stress increases with an increase in applied stress amplitude along with a greater number of cycles. He also documented that even though the magnitude of the residual stress decreases, the maximum depth of the compressive layer, in this case approximately 0.3mm, remains relatively unaffected. J. T. Cammett [68] performed uniaxial static tension and static bend tests of shot peened 17Cr-7Ni austenitic stainless steel specimens to observe the behavior of the residual stresses under static loading. The shot peened specimens (peened at 0.018 A and 0.020 N mm) under went a strain corresponding to the 0.02 percent offset yield stress in both tests (at the surface for the bend test). A reduction in magnitude of sub surface residual stresses occurred for both tests. However, the residual stress relaxation for the bend test specimens are more severe than the relaxation experienced for uniaxial loading tests. The study also showed that the relaxation effects from tensile strains were greater than compressive strains. J. T. Cammett [68] also conducted cyclic bend tests with an $R = 0$ and a surface strain again corresponding to a 0.02 percent offset yield stress. He found that the residual stress distribution between the static and cyclic loading tests were the same. McClung [5] provides an extensive list of influential fatigue studies on the cyclic relaxation of shot peening induced residual stresses in steels between 1960 and 2004. This list is reproduced in Fig. 2.16. McClung [5] states the general consensus of the compiled work is that a larger stress amplitude has a greater influence on relaxation.

Aluminum Alloys

Shot peening of aluminum is a delicate process. Aluminum is much more prone to surface damage compared to steel. Cracks, folding and stress concentrations from pitting can form because of shot peening. All of which have an adverse effect on the

Authors	Date	Steel Grade	Special Notes
Taira and Murakami	1960	S40C medium C	Reversed bending
Esquivel and Evans	1968	4130	
Kodama	1972	JIS SS41	Reversed bending
Neff	1981	cast 0.28C	Four-point bending, $R = 0$
McClinton and Cohen	1982	1040	
Bergström and Ericsson	1984	4140	Smooth and notched, $R = 0$ & -1
Bergström and Ericsson	1986	4140	Smooth and notched, $R = 0$ & -1
Berns and Weber	1986	50CrV4	Bending
Bergström and Ericsson	1987	4140	Smooth and notched, $R = 0$ & -1
Bignonnet *et al.*	1987	E460 and E550	Welded T-joints
Bignonnet	1987	35 NCD 16	Four different loading types
Misumi and Ohkubo	1987	S45C	Reversed bending with small hole
Qiu and Wang	1987	GC-4 superhigh strength	
Cao and Castex	1988	4135	Plane bending
Meguid and Hammond	1989	080M40 (medium C)	
Hammond and Meguid	1990	080M40 (medium C)	
Cammett *et al.*	1993	301 SS	
Zeller	1993	Ck 45, X5 CrNiMo 18 10	Rotating bending
Eigenmann *et al.*	1994	4140	
Farrahi *et al.*	1995	60SC7 spring steel	Torsion, $R = -1$
Iida and Taniguchi	1996	S45C	Reversed bending
Schulze *et al.*	1996	4140	Stress control vs. strain control
Holzapfel *et al.*	1996	4140	Bending, elevated temperature
Holzapfel *et al.*	1998	4140	Bending, elevated temperature
Iida and Hirose	1999	0.45% C carburized	Reversed bending
Wick *et al.*	1999	4140	Warm peening, cyclic bending
Wick *et al.*	1999	4140	Warm peening, cyclic bending
Wick *et al.*	2000	4140	Warm peening, cyclic bending
Batista *et al.*	2000	Carbo-nitrided 4130	Contact fatigue (gears)
Smith *et al.*	2001	En15R	Tension-compression cycling
Menig *et al.*	2002	4140	Warm peening, torsion
Menig *et al.*	2002	4140	Warm peening, diff heat treats
Torres *et al.*	2002	4340	Rotating bend, diff hardnesses
Torres and Voorwald	2002	4340	Rotating bend, diff SP intensities
Teodosio *et al.*	2003	API 5L X70, 31803 SS	Complex changes in weldments
Capello *et al.*	2004	C45, 39NiCrMo3	$R = -1$
Nikitin *et al.*	2004	304SS	LSP, DR at elevated T, $R = -1$

Figure 2.16: Compiled list of published research on cyclic relaxation of residual stresses for steel [5]

fatigue life and strength. Therefore, care must be taken so that over peening does not occur.

Influence of Residual Stress on Crack Initiation and Propagation

We have shown there is ample research reporting delayed crack initiation and propagation of many steels. However, aluminum research of the same phenomenon is limited and contradictory to say the least. Researchers have generally accepted that shot peening does not significantly influence the initiation life of cracks. For low stress amplitudes crack nucleation constitutes up to 90% of the fatigue life. G. S. Was [69] has cited that since we observe nearly identical fatigue lives during high cycle fatigue of peened and unpeened specimens that crack nucleation is not affected by shot peening. However, crack initiation still occurs below the surface. McClung [5] also states that the fatigue nucleation life depends not on the mean stress but on the alternating stress implying that residual stresses have little effect on crack nucleation. But crack propagation may be influenced significantly.

X. Y. Zhu [70] assessed the shot peening effect on pre-cracked shot peened 7075-T6 aluminum compact specimens. He shot peened select locations along the pre-crack to study its effect on crack growth rates and crack re-initiation. He found that peening the frontal region of the crack tip had a moderate influence on the retardation of crack growth. But peening along the entire length of the pre-crack resulted in significant improvement. A thorough study on the fatigue crack growth in 7075-T735 single edge notch bend and three point bend specimens was conducted by T. Honda [71]. T. Honda [71] found severe shot peening of the SENB specimen did not significantly change the fatigue crack growth rate at the surface. Implying that shot peening has little effect on the crack growth behavior of preexisting cracks.

E. R. de los Rios [72] studied the shot peening affect on fatigue damaged 2024-T351 aluminum alloy. Using an in situ four point bending fatigue machine Rios showed that for cracks shorter than the peening depth shot peening completely healed the prior

fatigue damage. However, for cracks longer than the peening depth there was little improvement in life extension.

Wagner [73] studied the fatigue behavior of age hardenable aluminum alloy Al 2024 between T3 (under-aged) and T6 (peak-aged) with an emphasis on microcrack growth. It was observed that microcrack growth rates are much less in T3 as compared to T6 because of larger compressive stresses in T3. Wagner [73] summarized the influence the compressive residual stress, surface roughness and cold work have on crack nucleation and propagation. He states the surface roughness accelerates crack nucleation but does not influence propagation. Whereas cold work retards crack nucleation but accelerates propagation. And as already stated the residual stress from shot peening will have a limited effect on crack nucleation but retards crack propagation.

Fatigue Strength and Life Enhancement of Aluminum Due to Shot Peening

Shot peening can significantly increase the fatigue life of aluminum. However, research shows that there are limitations to this increase in fatigue life. G. S. Was [69] showed for uniaxial fatigue tests with zero mean stress of 7075-T6 specimens there was little difference in the fatigue life of the peened and unpeened specimens for stresses below 200 MPa. However, a marked increase in fatigue life occurred for stress amplitudes above 275 MPa. Therefore benefits in fatigue life occur at stress levels higher than stress levels near the long life fatigue strength for uniaxial fatigue tests at R=-1. For the same material again at R=-1 but in reverse bending fatigue tests an increase in fatigue life did occur near the long life fatigue strength. This is more in line with our expectations of the fatigue behavior of shot peened aluminum.

D. W. Hammond [74] also performed rotating fatigue bend tests and a repeening study on 7075 T7351 aluminum zinc alloy. Although the test was focused on the cycle range $10^5 - 10^6$ there was up to a 20% increase in fatigue life. It should also be noted that repeening of this aluminum alloy after a fraction of its fatigue life had been used

up did not substantially recover its life.

L. Wagner [75] evaluated the individual contributions of the compressive residual stress, high dislocation densities and surface roughness from shot peening to the improved fatigue life of Al 2024 for T3 (naturally aged and prestrained) and T6 (artificially aged) conditions. He used an electropolished specimen as his reference and compared the fatigue behavior of shot peened, shot peened and polished, shot peened and stress relieved, and shot peened stress relieved with polishing. L. Wagner [75] found for the shot peened only condition the fatigue life of T3 exceeded that of T6. The electropolished samples exhibited the same trend but were less pronounced and both had lower fatigue lives. In general, T3 out performed T6 because of lower microcrack propagation rates and higher compressive stresses. Fig. 2.17 shows measurements of the residual stress versus depth of shot peened Al 2024-T3. The highest fatigue strength is obtained by polishing following shot peening eliminating the negative aspects (microcrack initiation sites) of a higher surface roughness.

Relaxation and Stability of Residual Stresses

Research on relaxation of residual stresses in aluminum alloys is scarce and results are mixed. Several studies have shown a moderate relaxation behavior. On the other hand others have shown relaxation was minimal. One of the first studies of this phenomenon was published by Seppi [76]. He observed a 20% reduction of residual stresses in 7075-T6 that underwent tensile fatigue testing. C. Bathias [77] conducted an X-ray diffraction and acoustic emission study of fatigue damage in aluminum alloys. He noted a 10 to 40% relaxation of shot peening residual stresses in 2024 and 7075. W. Zinn [78] also observed a 30 to 40% relaxation of residual stresses in 7020, 6082, 5754, 5083 and 2017 for reverse bending. Bending fatigue tests of 6082-T5 was performed by V. Fontanari [79]. He reported 5 to 20% relaxation.

Several researchers have observed no relaxation of shot peened residual stresses in aluminum. For example, D. W. Hammond [74] did not observe relaxation behavior

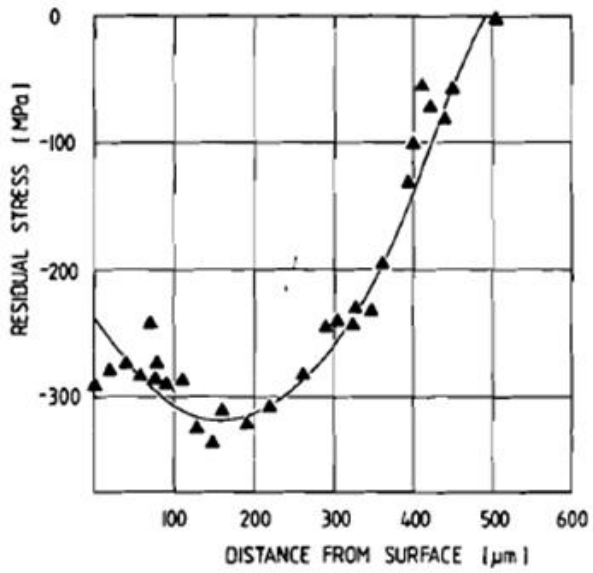

Figure 2.17: Experimental residual stress versus depth measurements of shot peened Al 2024-T3 [75]

of 7075-T6 during rotating bending fatigue tests nor did J.M. Potter [80] for R=-1 and R=0.5 of the same aluminum alloy.

Titanium Alloys

The influence shot peening on titanium alloys is more substantial compared to aluminum alloys. Fatigue hardening as well as softening plays an important role in the stability of the residual stresses and hence fatigue behavior of shot peened titanium. There also exists a drastic difference in the fatigue behavior of shot peened titanium undergoing uniaxial fatigue tests compared with bending tests as reported by L. Wagner [81]. Researchers observed in vacuum shot peened Ti-6Al-4V under performed electropolished specimens in push pull tests. But out performed the electropolished specimens in rotating beam tests. Results reported by L. Wagner [82] show residual stresses can either increase or decrease the fatigue life of titanium alloys.

Influence of Residual Stress on Crack Initiation and Propagation

Like steel or aluminum, crack initiation in shot peened titanium can occur on the surface or internally. Internal crack initiation is also caused by the tensile residual stress from peening. And the surface roughness still induces nucleation sites at the surface. The initiation site of the crack is strongly dependent on the residual stress and its stability as well as the stress amplitude, stress gradient, surface roughness, dislocation density and environmental factors L. Wagner [82]. H. Boeckels [83] studied the fatigue behavior of shot peened Ti-2.5Cu that was cold worked prior to aging. He noted that in HCF the crack initiation always occurred from below the surface.

A. Drechsler [84] compared the fatigue behavior of shot peened α, $\alpha + \beta$ and β titanium alloys. Crack initiation occurred below the surface for both α and $\alpha+\beta$ alloys however the β exhibited crack initiation originating at the surface. A. Drechsler [84] argues that the α and $\alpha + \beta$ alloy classes have cyclicly stable residual tensile stresses. However, for cyclicly softening materials the residual stress relaxes therefore initiation occurs on the surface. He also pointed out that the compressive residual stress can slow or even arrest microcrack growth from the surface. Crack propagation is hindered in the usual way from the compressive residual stress. L. Wagner [81] noted a small increase in the fatigue limit for shot peened Ti-6Al-4V tested in rotating beam loading. This can be attributed to the residual stress inhibiting microcrack propagation.

Fatigue Strength and Life Enhancement of Titanium Due to Shot Peening

There is a substantial amount of work reporting the fatigue life and strength improvement of many titanium alloys resulting from shot peening. T. Ludian [85] cited a large increase in fatigue life of Ti-6Al-4V in reverse bending fatigue tests. The increase in fatigue life occurred in the finite life region, for higher stress amplitudes, as well as the high cycle fatigue region. But at low stress amplitudes Ludian stresses the need to consider the influence of the mean stress sensitivity on fatigue strength.

The fatigue life at low stress amplitudes will be relatively unaffected by shot peening for those titanium alloys that have an abnormal sensitivity to mean stresses. This is the case for Duplex/AC (air cooled) microstructure of Ti-6Al-4V T. Ludian [85].

In some of the early work by E. C. Reed [86] a 25% increase in the endurance limit of Ti-6Al-4V by glass bead peening was observed. T. Dorr [87] reported fatigue life improvements for select titanium alloys between 5 to 100x. A decrease in fatigue life for certain titanium alloys has been reported as well. B. R. Sridhar [88] found for IMI318 and IMI685 titanium alloys a decrease in fatigue life at high stress amplitudes for both room temperature and temperatures up to 450 C. It was reasoned that the high stress amplitudes were responsible for relaxation of the residual stress.

Relaxation and Stability of Residual Stresses

As highlighted throughout the last couple sections residual stress relaxation is a primary focus in the study of titanium fatigue behavior. G. R. Leverant [89] published a seminal article on the relaxation behavior of Ti-6Al-4V during high temperature (600 F) fatigue cycling. An increase in relaxation was observed with an increase in strain amplitude. O. Vohringer [90] observed relaxation during the first cycle and only limited relaxation thereafter for Ti-6Al-4V. W. Cheong [91] cited a 20% reduction in surface residual stress during low cycle fatigue testing of Ti-6Al-4V disk bore feature specimens at R=0.05. In some studies relaxation occurred primarily during the initial cycles of fatigue or later in fatigue life during microcrack growth.

Residual Stress Measurements

There are several different techniques that can be used to measure the residual stresses in a given structure. One of the more common is X-Ray diffraction which is used in conjunction with electropolishing or hole drilling. Each of these processes remove layers of the material so that subsurface residual stresses can be measured. They are not without their faults and are capable of modifying the residual stress via relaxation

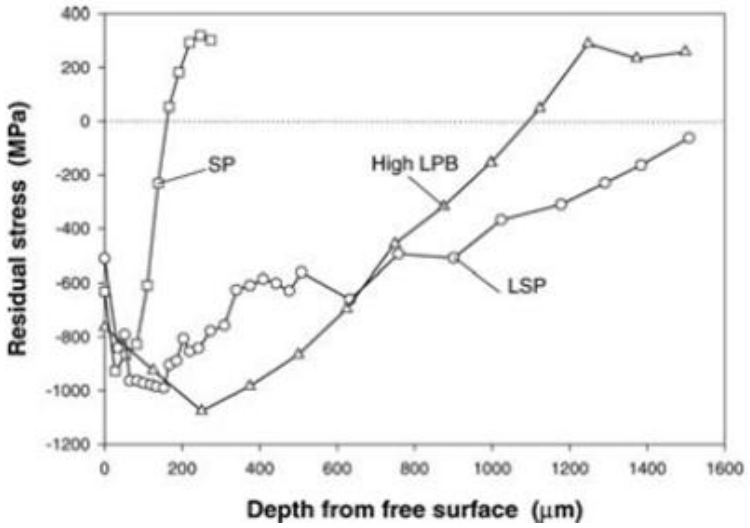

Figure 2.18: Residual stress measurements for shot peening, laser shock peening and low plasticity burnishing of IN-718 are shown [5]

that one is attempting to measure. Fortunately, for the simplest geometries such as flat plates and cylindrical bodies analytical solutions do exist to correct the false measurements.

Fig. 2.18 shows experimentally measured residual stress data McClung [5]. Three residual stress plots for shot peening, laser shock peening and low plasticity burnishing are shown. Interestingly, they all have the same behavior a maximum subsurface residual stress located below the surface. We see that shot peening induced residual stresses reach a much smaller depth than either laser shock or LPB but the subsurface residual stress magnitudes are all reasonably matched.

2.6 Summary

A comprehensive review on the shot peening process and resulting residual stress research has been discussed. Flavenot developed the stress source method. The stress source, which represents the residual stress induced in a semi-infinite structure,

is approximated with the cosine function. The cosine function is convenient at fitting experimental data and describing behavior indicative of the residual stress. The spherical cavity model of Al Hassani and Al Obaid also base their approach on the stress source method. Guechichi's research can encompass a wide variety of mechanical phenomenon such as isotropic and kinematic hardening and even shakedown. Whereas, Li applies a traditional mechanical approach to solve the residual stress. The downside is that not much new physics is introduced to the analysis and so our fundamental understanding of the problem only slightly improves. Each modeling technique offers new insights however they are not without limitations. The basis of the body of research relies on the Von Mises yield criterion. However, Edelman and Drucker suggest a yield criterion that is a function of the third invariant may predict yielding during combined loading with more success. This alternate yield criterion may also provide similar results when used to predict the residual stress from shot peening.

Finite element models show that a single shot can impact and rebound from a structure in a fraction of a microsecond. Meguid conducted a dynamic elasto-plastic finite element analysis using a rate sensitive material. His results show that the residual stress at the surface can be greater than the yield stress of the material. He also found that strain rates can be as high as $6 \times 10^5 \frac{1}{s}$. The simulations give the time history of the plastic strain and strain rate. The time dependent behavior of the plastic strain rate strongly resembles an impulse. The loading phase of the target (the time of impacting prior to shot rebound) is shorter than the unloading phase (the time of impacting when the shot is rebounding) because the shot is hitting the target with more energy than it is leaving with. On the other hand, the plastic strain increases abruptly and quickly attains a steady state value.

Chapter 3

RESEARCH SCOPE AND OBJECTIVES

3.1 Research Scope

There is a need to develop residual stress models that yield reliable results so that research scientists and design engineers have a better understanding of shot peening. The aerospace, automotive, medical and pressure vessel industries all benefit from the compressive residual stress's ability to mitigate the destructive nature of fatigue. There are several viable surface treatment processes that can be used for fatigue prevention. Shot peening is one of the most widely used processes because of its convenience, controllability and overall effectiveness at enhancing fatigue properties of metals by inducing a compressive residual stress. Therefore, predictions of the residual stresses can help engineers understand what affect they will have on fatigue and forming experiments.

Analytical models are essential to our overall understanding of the mechanical behavior of materials. The dissertation explores many seminal mechanics concepts including the influence of combined loading on the behavior of residual stresses. The reliability of an analytical model is dependent upon the assumptions used. All previous models assume the residual stress can be predicted with yield criterion found to be accurate only for simple loading. The multi-axial stress state of the structure during shot peening makes prediction of yielding difficult. The residual stress is predominately modeled with the Von Mises criterion but for complex loading this criterion fails to predict exactly when yielding will occur. Therefore, an attempt is made in this research to improve and extend upon preexisting models. A proper yield function must be selected that will adequately describe the complex state of stress

in the surface after a single impact but especially after multiple impacts. We show that when an appropriate yield model is selected, more accurate predictions of the residual stress is obtained.

To this author's knowledge, there appears to be a lack of analytical research of the time dependent behavior of the plastic strain and residual stress during the high speed impact of the shot. The lack of research presents an opportunity to make a unique, original contribution to the theoretical analysis of shot peening, and to the field of impact mechanics. A simple dynamical model is derived from the shot peening boundary conditions. The semi-analytical model was found to describe the time dependent response of a shot impact within 10% of numerical predictions, surprisingly high accuracy.

Along with the aforementioned contributions a completely new residual stress model is proposed. Analytical, experimental and numerical analysis has revealed valuable insight into the problem. Observations from all three indicate the general behavior of a sphere colliding with a flat surface at high speeds (30 - 100 m/s) results in sharp stress gradients leading and following a large subsurface maximum compressive residual stress confined to a very thin layer.

3.2 Goals and Objectives

1. A major objective of the present work is to select and incorporate a yield criterion into Li's mechanical model that will better predict yielding during shot peening. Generalized $J2$ incremental plasticity is applied to Li's formulation because his approach is favored for its overall simplicity and reliability. By combining the two techniques, more accurate residual stress predictions can be found.

2. The second objective is to develop a simple physical semi-analytical model of the time dependent stresses and strains. Description of the time dependent

behavior of plastic strains during loading and unloading of the shot is restricted entirely to numerical analysis. Therefore, a gap exists in the analytical literature and it must be filled.

3. The third objective is an empirical extension of the time dependent model. We derive an equation for the residual stress as a function of both time and depth. The model, though empirical, is based on fundamental physical concepts. Therefore, the empirical relation has predictive capabilities. Though the empirical model is derived from shot peening conditions, there may be potential for applications to different surface treatment processes. Unlike rigorous elastic plastic analysis that are restricted to a particular process, the semi-analytical model may have the capability of modeling different treatment processes. However, application to shot peening remains the primary focus.

4. The final contribution of the dissertation is based on the theory of shakedown. Specifically, we show that shakedown can still be applied to a shot peening residual stress that undergoes relaxation induced by a recovery strain. The recovery strain which is created at high temperatures because of thermal recovery, is a consequence of micro-plastic deformation. Application of shakedown provides us with the framework to calculate the infinite life fatigue limit of shot peened fatigue specimens undergoing high temperature fatigue. Predictions are within 10% of experimentally obtained values.

Chapter 4

ANALYTICAL MODELING OF SHOT PEENING RESIDUAL STRESSES BY EVALUATING THE ELASTIC-PLASTIC DEVIATORIC STRESSES USING J2-J3 PLASTICITY

4.1 Introduction

When a finite structure is shot peened, combined loading occurs because shear, axial and bending stresses are induced along with the residual stress. Even when a thick structure is shot peened shear stresses are caused by oblique impacts, and interactions occur among triaxial stress fields created by neighboring shot impacts. For complicated loading it has been found that neither the Tresca nor Von Mises yield criteria can predict exactly when yielding occurs. The complex stress state induced by the peening process makes prediction of yielding difficult. An analytical model of the residual stresses induced by shot peening has been developed for a generalized isotropic material. By using incremental plasticity, both the second and third deviatoric stress invariants, J_2 and J_3, are incorporated into the residual stress analysis thus providing more accurate predictions. The model is verified with published experimental data.

Shot peening is one of the most utilized surface treatment processes because of its convenience, controllability and overall effectiveness at enhancing fatigue properties of metals by inducing a compressive residual stress in the material. With such importance there is an urgent need to develop analytical models that yield reliable results so that research scientists and industry engineers alike have a better understanding of the process and residual stresses. There are only a few models of the residual stresses

induced during the peening process that are based on 100% coverage [23]. Flavenot and Niku Lari [9] provide the first theoretical efforts by introducing the concept of a "stress source" to calculate the residual stresses in an Almen strip. Al-Hassani [35] uses a spherical cavity model to represent the impact crater and apply Flavenots concept of a stress source to solve the residual stresses. Guechichi [11] envisages the shot peening process as a cyclic loading problem and develops a model by assuming the shot impacting is periodic and attains a stable cyclic state. J.K. Li [12], on the other hand, utilizes a mechanical approach to calculate the residual stresses from Iliushin [33]. The work of Li has received much attention from researchers because of its simplicity, easy application and ability to incorporate different types of hardening behavior with relative ease. All of these analytical residual stress models are limited to J_2 deformation plasticity.

However, when a structure is shot peened, not only is a residual stress induced, but axial and bending stresses are also produced from the redistribution of the residual stress. Therefore, the structure undergoes combined loading [17, 92]. F. Edelman [93] formulated several alternate yield criteria for materials undergoing combined loading to allow for more flexibility when predicting experimental behavior. The yield criteria developed by Edelman is a modification of the Von Mises yield criteria and incorporates the third invariant of the deviatoric stress. The purpose of this paper is to model the peening induced residual stresses by adopting Li's mechanical approach [12] and utilizing Drucker's modified Von Mises yield criterion. To the authors knowledge, no prior research has been done that investigates the influence of J_3 on the residual stresses induced by shot peening. By using a yield criteria dependent on J_2 and J_3 in the incremental plastic flow rule, along with relevant shot peening boundary conditions, we obtain a simple expression for the elastic-plastic deviatoric stress components that is easily incorporated into Li's mechanical model. Furthermore, in the appropriate limits the proposed approach simplifies to the results of Li obtained by using J_2 deformation theory.

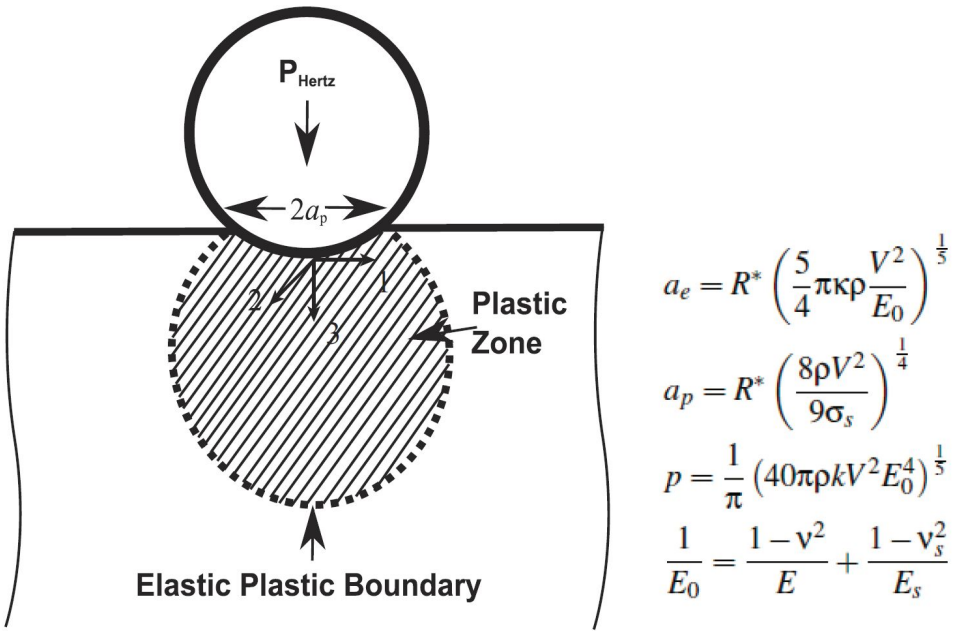

Figure 4.1: Schematic of a single shot impacting a semi-infinite surface. Elastic-plastic boundary separates the confined plastic zone and the elastic domain.

4.2 Calculating the Elasto-Plastic Deviatoric Stress Tensor

Fig. 4.1 provides an idealized illustration of a single shot impacting a surface along with expressions for the elastic and plastic indentation radius, a_e and a_p, and maximum elastic pressure, p, derived from Hertzian contact theory. For the quantities of Fig. 4.1, V is the shot velocity, R^* is the shot radius, ν is the target Poisson ratio, ν_s is the shot Poisson ratio, ρ is the shot density and κ is an efficiency coefficient based upon elastic rebound of the shot. A value of 0.8 was proposed by Johnson [3] and is used here.

The Hertzian stresses are derived for a position directly below the indenter. The reason for choosing a location exactly below the impacting shot is to simplify the problem. A state of zero shear stress exists there, thus the stresses are principal

stresses giving

$$\begin{aligned}\sigma_{11}^e = \sigma_{22}^e &= p(1+\nu)\left[\frac{z}{a_e}tan^{-1}\left(\frac{z}{a_e}\right) - 1\right] + p\frac{a_e^2}{2(a_e^2+z^2)} \\ \sigma_{33}^e &= -p\left[\left(\frac{z}{a_e}\right)^2 + 1\right]^{-1}\end{aligned} \tag{4.1}$$

The corresponding mean stress and strain are

$$\begin{aligned}\sigma_m^e &= \frac{1}{3}(\sigma_{11}^e + \sigma_{22}^e + \sigma_{33}^e) \\ \epsilon_m^e &= \frac{1}{3}(\epsilon_{11}^e + \epsilon_{22}^e + \epsilon_{33}^e)\end{aligned} \tag{4.2}$$

With generalized Hooke's law the principal strains are easily found

$$\begin{aligned}\epsilon_{11}^e &= \frac{1}{E}[\sigma_{11}^e - \nu(\sigma_{22}^e + \sigma_{33}^e)] \\ \epsilon_{22}^e &= \frac{1}{E}[\sigma_{22}^e - \nu(\sigma_{11}^e + \sigma_{33}^e)] \\ \epsilon_{33}^e &= \frac{1}{E}[\sigma_{33}^e - 2\nu\sigma_{11}^e]\end{aligned} \tag{4.3}$$

The elastic deviatoric strain components are found by subtracting the mean strains from the strain tensor (recall the strain is a sum of both the mean strain and deviatoric strain)

$$\begin{aligned}e_{11}^e &= \epsilon_{11}^e - \epsilon_m^e = \frac{1}{3}(1+\nu)\epsilon_i^e \\ e_{22}^e &= \epsilon_{22}^e - \epsilon_m^e = \frac{1}{3}(1+\nu)\epsilon_i^e \\ e_{33}^e &= \epsilon_{33}^e - \epsilon_m^e = -2e_{11}^e = -\frac{2}{3}(1+\nu)\epsilon_i^e\end{aligned} \tag{4.4}$$

The elastic deviatoric stresses are

$$\begin{aligned}s_{11}^e &= \sigma_{11}^e - \sigma_m^e = \frac{1}{3}\sigma_i^e \\ s_{22}^e &= \sigma_{22}^e - \sigma_m^e = \frac{1}{3}\sigma_i^e \\ s_{33}^e &= \sigma_{33}^e - \sigma_m^e = -2s_{11}^e = -\frac{2}{3}\sigma_i^e\end{aligned} \tag{4.5}$$

The Von Mises equivalent stress and strain can now be obtained from the principal stresses and strains,

$$\begin{aligned}\sigma_i^e &= \sqrt{3J_2} = [(\sigma_{11}^e - \sigma_{22}^e)^2 + (\sigma_{33}^e - \sigma_{22}^e)^2 + (\sigma_{11}^e - \sigma_{33}^e)^2]^{\frac{1}{2}} \\ \epsilon_i^e &= \frac{\sigma_i^e}{E}\end{aligned} \tag{4.6}$$

The necessary plasticity relations can be defined from all the fundamental elasticity relations provided. Deformation in the elastic-plastic stage occurs when the equivalent stress in the target material is greater than the yield strength. A detailed illustration is given in Fig. 4.2 of the material stress state of a small subsurface volume of material directly below a shot impacting a semi-infinite surface. The deformation in the volume element is initially elastic, as indicated by the uniaxial stress-strain representation of the impact, see Fig. 4.2a. The first and second principal stresses are tensile whereas the third is compressive. Hertzian contact predicts an indentation size equal to a_e. Shown in Fig. 4.2b, the pressure is large enough to induce plastic flow beneath the impacting shot. Upon rebound, a plastic indentation, a_p, is produced along with a triaxial residual stress that is compressive in the 11 and 22 directions and tensile in the 33. When the elastic stresses exceed a specified amount, reverse yielding occurs and the compressive stress has the new form shown in Fig. 4.2c, governed by the corresponding stress strain curve. Major assumptions of the analysis include:

(1) The residual stresses are computed assuming the hardening is isotropic

(2) The elastic-plastic deviatoric stresses are calculated using the material constitutive relation $\epsilon_i^p = a(\frac{\sigma_i^p}{b})^{2n+1}$

(3) A linear equivalent stress-equivalent strain relation is used to calculate the residual stresses during loading and unloading of the shot

(4) The analysis is done using index notation and by direct computation involving the stress and strain components; doing so simplifies the analysis.

The expression relating the equivalent plastic strain to the equivalent elastic strain is given by:

$$\epsilon_i^p = \begin{cases} \epsilon_i^e & \text{for } \epsilon_i^e \leq \epsilon_s \\ \epsilon_s + \alpha(\epsilon_i^e - \epsilon_s) & \text{for } \epsilon_i^e > \epsilon_s \end{cases} \tag{4.7}$$

Where, ϵ_i^e is the Von Mises equivalent strain and is defined in terms of Hertzian principal stresses σ_{11}^e, σ_{22}^e and σ_{33}^e [3, 12] as

$$\epsilon_i^e = \frac{\sigma_i^e}{E} = \frac{[(\sigma_{11}^e - \sigma_{22}^e)^2 + (\sigma_{33}^e - \sigma_{22}^e)^2 + (\sigma_{11}^e - \sigma_{33}^e)^2]^{\frac{1}{2}}}{E} \tag{4.8}$$

The linearity coefficient α is defined as the ratio of the plastic and elastic indentation radius, a_p/a_e, [12] and ϵ_s is the strain at yielding. The quantity α creates a connection between the elastic-plastic equations and the solvable elasticity relations, specifically the equivalent elastic and plastic strains. α is defined as the ratio of the maximum elastic and plastic indentation radii. The maximum plastic indentation radius [37] is

$$a_p = R^* \left(\frac{8\rho V^2}{9\sigma_s} \right)^{\frac{1}{4}} \tag{4.9}$$

where σ_s is the yield strength. The equivalent stress, σ_i^p, is solved by assuming a multi-linear relationship with the equivalent plastic strain

$$\sigma_i^p = \begin{cases} \sigma_i^e & \text{for } \epsilon_i^e < \epsilon_s \\ \sigma_s + k_1(\epsilon_i^p - \epsilon_s) & \text{for } \epsilon_s \leq \epsilon_i^p < \epsilon_b \\ \sigma_b & \text{for } \epsilon_i^p \geq \epsilon_b \end{cases} \tag{4.10}$$

The quantities σ_s, σ_b, and k_1 are the yield stress, ultimate tensile stress and linear strain hardening parameter respectively. A great simplification is made by assuming the deviatoric plastic strains take on a similar form as the deviatoric elastic strains. Li claims that because of axisymmetric loading and geometric considerations the plastic strain deviators, e_{ij}^p, can be calculated from

$$\begin{aligned} e_{11}^p &= \frac{1}{3}(1+\nu)\epsilon_i^p \\ e_{22}^p &= \frac{1}{3}(1+\nu)\epsilon_i^p \\ e_{33}^p &= -2e_{11}^p = -\frac{2}{3}(1+\nu)\epsilon_i^p \end{aligned} \tag{4.11}$$

The next goal is to derive the elastic-plastic deviatoric stresses. From Iliushin's deformation theory of plasticity [33] we have the expression

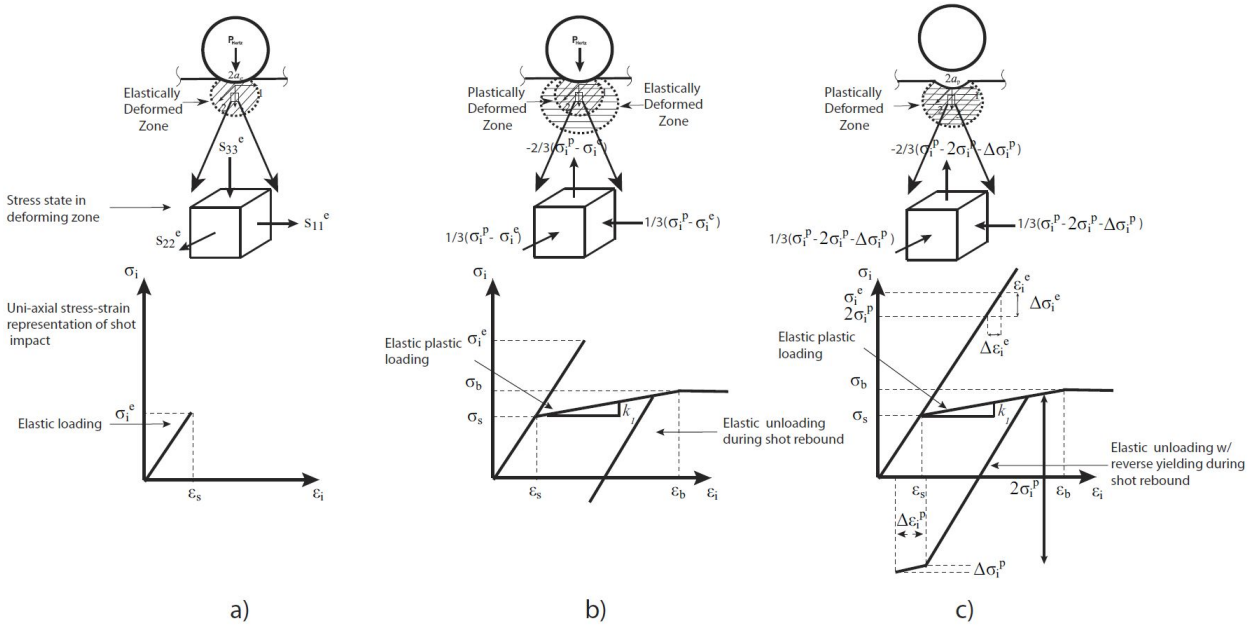

Figure 4.2: Stress strain curve of the loading/unloading process for a single shot impact. a) purely elastic deformation b) residual stress stress state with purely elastic unloading c) residual stress state with reverse yielding.

$$s_{ij}^p \epsilon_i^p = \frac{1}{1+\nu} e_{ij}^p \sigma_i^p \tag{4.12}$$

Substituting Eqn. 4.11 into Eqn. 4.12 and writing the elasto-plastic deviatoric stresses in component form gives

$$\begin{aligned} s_{11}^p &= \frac{1}{1+\nu}\frac{e_{11}^p}{\epsilon_i^p}\sigma_i^p = \frac{1}{3}\sigma_i^p \\ s_{22}^p &= \frac{1}{1+\nu}\frac{e_{22}^p}{\epsilon_i^p}\sigma_i^p = \frac{1}{3}\sigma_i^p \\ s_{33}^p &= -2s_{11}^p = \frac{1}{1+\nu}\frac{e_{33}^p}{\epsilon_i^p}\sigma_i^p = -\frac{2}{3}\sigma_i^p \end{aligned} \tag{4.13}$$

This is an equibiaxial state of stress.

4.3 Iliushin's Plasticity Theory and the Elasto-Plastic Deviatoric Stresses

The deformation theory of plasticity is hailed for its simplicity and Iliushin was one of the primary proponents. In deformation plasticity total stresses are related to total strains and so it is unable to include stress history effects. However, incremental plasticity relates incremental stresses to incremental strains and so history effects can be incorporated making it the more general of the two theories. We can calculate Eqn. 4.12 very simply by assuming the plastic strain is proportional to the deviatoric stress, as is the usual procedure in the Iliushin (also referred to as Hencky-Iliushin) theory of deformation plasticity [94]

$$\epsilon_{ij}^p = e_{ij}^p = F(J_2) s_{ij}^p \tag{4.14}$$

Note, proportionality between the plastic strain and *elasto-plastic deviatoric stress*, s_{ij}^p is assumed. The proportionality constant F is related to the second invariant, J_2, of the deviatoric stress and can be solved by multiplying both sides of Eq. 4.14 by itself and taking the square root

$$\sqrt{\epsilon_{ij}^p \epsilon_{ij}^p} = F(J_2)\sqrt{s_{ij}^p s_{ij}^p} \tag{4.15}$$

The definition of the effective plastic strain in the plastic stage provides

$$\epsilon_i^p = \sqrt{\frac{2}{3}\epsilon_{ij}^p \epsilon_{ij}^p} \tag{4.16}$$

Similarly, the effective stress in the plastic stage

$$\sigma_i^p = \sqrt{\frac{3}{2}s_{ij}^p s_{ij}^p} \tag{4.17}$$

Substituting Eqn.'s 4.16 and 4.17 into 4.15 gives

$$\sqrt{\frac{3}{2}}\epsilon_i^p = F(J_2)\sqrt{\frac{2}{3}}\sigma_i^p \tag{4.18}$$

Solving $F(J_2)$ with Eqn. 4.18 and substituting into Eqn. 4.14 yields

$$s_{ij}^p = \frac{2}{3}\frac{\sigma_i^p}{\epsilon_i^p}e_{ij}^p \tag{4.19}$$

Eqn. 4.19 is identical to Eqn. 4.12 upon using a Poisson's ratio of 0.5 which occurs during plastic deformation. We have shown with much ease Eqn. 4.12 can be derived by relating the effective stress in the plastic stage, σ_i^p, to the elasto-plastic deviatoric stress, s_{ij}^p, but we do not need to use Iliushin's theory of plasticity to obtain the elasto-plastic deviatoric stress of Eqn. 4.13 as is shown next. The simple process outlined in this section leads to the following relation between the second invariant of the elasto-plastic deviatoric stress, J_2, and the elasto-plastic deviatoric stress, s_{ij}^p

$$J_2 = \frac{1}{2}s_{ij}^p s_{ij}^p \tag{4.20}$$

Now, it follows by utilizing the equi-biaxial state of stress, $s_{11}^p = s_{22}^p$, and the first invariant $J_1 = s_{ii}^p = 0$ that the effective stress in the plastic stage is

$$\sigma_i^p = \sqrt{3J_2} = \sqrt{3\frac{1}{2}s_{ij}^p s_{ij}^p} = \sqrt{9s_{11}^{p2}} = 3s_{11}^p \tag{4.21}$$

From which all three components of the elasto-plastic deviatoric stress can be solved in terms of the effective stress in the plastic stage $s_{11}^p = s_{22}^p = -\frac{1}{2}s_{33}^p = \frac{1}{3}\sigma_i^p$.

Thus, it is not necessary to evaluate the elasto-plastic deviatoric stress by using Iliushin's deformation theory of plasticity but only define the effective stress in the plastic stage from Eqn. 4.21.

4.4 Elasto-Plastic Deviatoric Stresses From Incremental Plasticity

A more general framework for calculating the elastic-plastic stress deviator by using the plastic flow rule is now presented. The basis of the approach relies on Druckers (1960) well known linearity relation that states the incremental plastic strain is linear in incremental stress. The incremental plastic strain is characterized by the flow rule

$$d\epsilon_{ij}^{p} = d\lambda \frac{\partial f}{\partial \sigma_{ij}} \tag{4.22}$$

Where $d\lambda$ is a positive scalar proportionality factor and $\frac{\partial f}{\partial \sigma_{ij}}$ is proportional to the direction cosines of the normal to the yield surface. The positive scalar is taken as

$$d\lambda = \bar{G}\partial f = \bar{G}\frac{\partial f}{\partial \sigma_{mn}} d\sigma_{mn} \tag{4.23}$$

which gives for the incremental plastic strain

$$d\epsilon_{ij}^{p} = de_{ij}^{p} = \bar{G}\partial f \frac{\partial f}{\partial \sigma_{ij}} = \bar{G}\frac{\partial f}{\partial \sigma_{ij}}\frac{\partial f}{\partial \sigma_{mn}} d\sigma_{mn} \tag{4.24}$$

Where e is the plastic deviatoric strain and $\bar{G}$ is a scalar function which may depend upon stress, strain, and loading history but not $d\sigma_{ij}$ [94]. Let us consider a simple case in which the Von Mises yield function $f = J_2 - k^2(\epsilon_i^p)$ and the assumed uniaxial stress-strain relation, $\epsilon_i^p = a(\frac{\sigma_i^p}{b})^{2n+1}$ where a, b and n are constants, are used in Eqn. 4.24. Furthermore, the following relations are utilized

$$J_1 = s_{ii}^{p} = 0 \tag{4.25}$$

$$J_2 = \frac{1}{2} s_{ij}^{p} s_{ij}^{p} \tag{4.26}$$

$\bar{G}$ is calculated by substituting the yield function, f, into Eqn. 4.24 and from using the definition of the equivalent stress and strain

$$\bar{G} = \frac{9}{4}\frac{1}{H_p \sigma_i^{p2}} = \frac{3}{4H_p J_2} \tag{4.27}$$

$H_p = \frac{d\sigma_i^p}{d\epsilon_i^p}$ is the hardening modulus. The second invariant takes the form $J_2 = \frac{1}{2}s_{ij}^p s_{ij}^p = 3s_{11}^{p2}$ and $dJ_2 = s_{ij}^p ds_{ij}^p = 6s_{11}^p ds_{11}^p$. After substituting these quantities into Eqn. 4.24 we have

$$de_{ij}^p = \frac{3a(2n+1)}{4b} s_{ij}^p \left(\frac{3}{b^2}\right)^n \left(3s_{11}^{p2}\right)^{n-1} 6s_{11}^p ds_{11}^p \tag{4.28}$$

Taking the first principal plastic strain and integrating gives

$$e_{11}^p = \frac{6a}{4b}\left(\frac{3}{b}\right)^{2n} s_{11}^{p(2n+1)} \tag{4.29}$$

One can assume that the components of the deviatoric plastic strain tensor, e_{ij}^p, has a form similar to the deviatoric elastic strain tensor because of axi-symmetric loading and geometric considerations [12]

$$e_{11}^p = e_{22}^p = -\frac{1}{2}e_{33}^p = \frac{1}{3}(1+\nu)\epsilon_i^p \tag{4.30}$$

To express Eqn. 4.29 in terms of the equivalent elastic-plastic stress, σ_i^p, the uniaxial stress-strain relation, $\epsilon_i^p = a(\frac{\sigma_i^p}{b})^{2n+1}$, and e_{11}^p of Eqn. 4.30 must be substituted into Eq. 4.29

$$\begin{aligned} s_{11}^p &= \left[\frac{4b}{6a}\left(\frac{b}{3}\right)^{2n}\frac{1}{3}(1+\nu)a\left(\frac{\sigma_i^p}{b}\right)^{2n+1}\right]^{\frac{1}{2n+1}} = \\ &\left[\left(\frac{2}{3^{2n+1}}\right)\frac{1}{3}(1+\nu)(\sigma_i^p)^{2n+1}\right]^{\frac{1}{2n+1}} = \\ &\left[\frac{2}{3}(1+\nu)\right]^{\frac{1}{2n+1}}\frac{\sigma_i^p}{3} \end{aligned} \tag{4.31}$$

A Poisson's ratio of 0.5 yields

$$s_{11}^p = s_{22}^p = -\frac{1}{2}s_{33}^p = \frac{1}{3}\sigma_i^p \tag{4.32}$$

Notice, there is no longer any dependence on the parameters of the uniaxial power law that we initially used in our incremental plastic strain relation, Eqn. 4.28. So, by combining the usefulness of incremental plasticity and the plastic strain relation of Eqn. 4.30 we recovered the results of Li [12]. In the following section, a similar

approach is utilized with an alternate yield function that is dependent on the third invariant, J_3, which is used in place of the traditional yield function of simple J_2 plasticity. Predictions based on the model will reveal how the third invariant influences the residual stresses.

4.5 Evaluation of the Elastic-Plastic Deviatoric Stresses Based on a Generalized Isotropic Material

The physical meaning of the first and second invariants is clear. J_1 and J_2 are related to the hydrostatic stress and the octahedral shear stress, respectively. The physical interpretation of the third invariant is less clear but experimental research has found that J_3 directly influences the yield state of a material [17]. Clearly, the residual stress depends on the yield state of a material. Therefore the residual stress must be influenced by the third invariant. The process outlined in section 4.3 can be generalized to include the modified Von Mises yield function that includes the affects of the third invariant on the yield state [95]

$$f(\sigma_{ij}) = J_2(1 - c\frac{J_3^2}{J_2^3})^\beta - k^2 \tag{4.33}$$

The parameter k is the yield stress in simple shear, β is either 1 or $\frac{1}{3}$ and c has the range of values $-3.375 \leq c \leq 2.25$. The Von Mises equivalent stress for J_2 deformation used in Eqn. 4.27 is given as $\frac{\sigma_i^{p2}}{3} = J_2$. For the purpose of solving the deviatoric plastic strain from Eqn. 4.24, dependent on J_3, a similar equivalent stress must be defined in terms of J_2 and J_3. The necessary equivalent stress has the form:

$$\frac{\sigma_i^{p2}}{3} = J_2(1 - c\frac{J_3^2}{J_2^3})^\beta \tag{4.34}$$

The constant, β, is assigned the value 1 for both our equivalent stress and yield function. Note, a value of $c = 0$ gives simple J2 plasticity. Applying the chain rule to express $\frac{\partial f}{\partial \sigma_{ij}}$ in terms of the invariants gives

$$\frac{\partial f}{\partial \sigma_{ij}} = \frac{\partial f}{\partial J_2}\frac{\partial J_2}{\partial \sigma_{ij}} + \frac{\partial f}{\partial J_3}\frac{\partial J_3}{\partial \sigma_{ij}} = \frac{\partial f}{\partial J_2}s_{ij}^p + \frac{\partial f}{\partial J_3}t_{ij}^p \tag{4.35}$$

Where we have defined $s_{ij}^p = \frac{\partial J_2}{\partial \sigma_{ij}}$ and $t_{ij}^p = \frac{\partial J_3}{\partial \sigma_{ij}}$. With the equivalent elastic plastic stress and $\frac{\partial f}{\partial \sigma_{ij}}$ known, the next step is to solve $\bar{G}$. $\bar{G}$ can take the general form:

$$\bar{G} = \frac{\sqrt{\frac{3}{2}} d\epsilon_i^p}{\partial f \left(\frac{\partial f}{\partial \sigma_{ij}} \frac{\partial f}{\partial \sigma_{ij}} \right)^{1/2}} \tag{4.36}$$

Substitute $\partial f = dJ_2 = \frac{2}{3}\sigma_i^p d\sigma_i^p$ and $\left(\frac{\partial f}{\partial \sigma_{ij}} \frac{\partial f}{\partial \sigma_{ij}} \right)^{1/2} = \sqrt{\frac{2}{3}}\sigma_i^p$ into Eqn. 4.27 to compute a $\bar{G}$ based on simple J_2 plasticity. To calculate $\bar{G}$ for a generalized isotropic material, first substitute Eqn. 4.33 into Eqn. 4.35. With $\frac{\partial f}{\partial \sigma_{ij}}$, the expression $\frac{\partial f}{\partial \sigma_{ij}} \frac{\partial f}{\partial \sigma_{ij}}$ can be calculated. Substitution of $\partial f = \frac{2}{3}\sigma_i^p d\sigma_i^p$ into Eq. 4.36 gives a $\bar{G}$ that contains the hardening modulus H_p

$$\bar{G} = \frac{\sqrt{\frac{3}{2}}}{\frac{2}{3}\sigma_i^p H_p \left(\left(\frac{\partial f}{\partial J_2} \right)^2 2J_2 + \left(\frac{\partial f}{\partial J_3} \right)^2 \frac{2}{3} J_2^2 + 6 \frac{\partial f}{\partial J_2} \frac{\partial f}{\partial J_3} J_3 \right)^{1/2}} \tag{4.37}$$

Eqn. 4.37 reduces to Eqn. 4.27 when $J_3 = 0$, as is expected. The final expression for de_{ij}^p, comes after substituting $\partial f = \frac{\partial f}{\partial J_2} dJ_2 + \frac{\partial f}{\partial J_3} dJ_3$, Eqn. 4.33 and Eq. 4.37 into Eqn. 4.24

$$de_{ij}^p = \frac{\sqrt{\frac{3}{2}} \left(\frac{\partial f}{\partial J_2} s_{ij} + \frac{\partial f}{\partial J_3} t_{ij} \right) \left(\frac{\partial f}{\partial J_2} dJ_2 + \frac{\partial f}{\partial J_3} dJ_3 \right)}{\frac{2}{3}\sqrt{3}\sqrt{J_2(1 - c\frac{J_3^2}{J_2^3})} H_p \left(\left(\frac{\partial f}{\partial J_2} \right)^2 2J_2 + \left(\frac{\partial f}{\partial J_3} \right)^2 \frac{2}{3} J_2^2 + 6 \frac{\partial f}{\partial J_2} \frac{\partial f}{\partial J_3} J_3 \right)^{1/2}} \tag{4.38}$$

The invariants in this equation can be explicitly calculated from the components of the elastic plastic deviatoric stress tensor. The stress components, s_{11}^p and s_{22}^p, of s_{ij}^p, are equal because of geometric considerations. And the equation of the first invariant, $s_{ii}^p = 0$, yields $s_{33}^p = -2s_{11}^p$. These relations result in considerable simplification of J_2, J_3, dJ_2 and dJ_3, namely

$$\begin{aligned}
J_2 &= \frac{1}{2} s_{ij}^p s_{ji}^p = \frac{1}{2}(s_{11}^{p2} + s_{11}^{p2} + 4s_{11}^{p2}) = 3s_{11}^{p2} \\
J_3 &= \frac{1}{3} s_{ij}^p s_{jk}^p s_{ki}^p = \frac{1}{3}(s_{11}^{p3} + s_{11}^{p3} + (-2s_{11}^p)^3) = -2s_{11}^{p3} \\
dJ_2 &= 6 s_{11}^p ds_{11}^p \\
dJ_3 &= -6 s_{11}^{p2} ds_{11}^p
\end{aligned} \tag{4.39}$$

Solving e^p_{11} by inserting $t^p_{11} = s^{p2}_{11} - \frac{2}{3}J_2\delta_{11} = -s^{p2}_{11}$, and H_p after much algebra gives

$$e^p_{11} = \frac{a(27-4c)s^{p3}_{11}}{2b^3\sqrt{3}}\left(3-\frac{4c}{9}\right)^{\frac{1}{2}} \tag{4.40}$$

We solve e^p_{11} of Eqn. 4.40 by employing the same approach outlined in section 4.4 for the simple J_2 analysis. Substitute ϵ^p_i of the uniaxial stress-strain equation into Eq. 4.30 to get $e^p_{11} = \frac{1}{3}(1+\nu)\epsilon^p_i = \frac{a\sigma^{p3}_i}{2b^3}$. s^p_{11} can now be solved from Eq. 4.40 as

$$s^p_{11} = \sigma^p_i\left[\frac{1}{9-\frac{4c}{3}}\right]^{\frac{1}{2}} \tag{4.41}$$

Substituting a value of $c = 0$ yields s^p_{11} for simple J_2 theory

$$s^p_{11} = \frac{\sigma^p_i}{3} \tag{4.42}$$

Equation 4.42 is, of course, identical to what is obtained from previous formulations and so this approach yields consistent results in the appropriate limits. Eq. 4.41 incorporates the effects of both simple and generalized J_2 plasticity through the parameter c. s^p_{22} and s^p_{33} can be calculated from the geometric symmetry relations provided in Eq. 4.32, namely $s^p_{11} = s^p_{22} = -\frac{1}{2}s^p_{33}$.

4.6 Residual Stresses After Unloading

With these results the residual stress field can be defined in the elastic and plastic regions from

$$\sigma^r_{ij} = \begin{cases} 0 & \text{for } \sigma^e_i < \sigma_s \\ s^p_{ij} - s^e_{ij} & \text{for } \sigma_s \leq \sigma^e_i \leq 2\sigma^p_e \end{cases} \tag{4.43}$$

Or in component form

$$\sigma^r_{11} = \sigma^r_{22} = -\frac{1}{2}\sigma^r_{33} = s^p_{11} - \frac{1}{3}\sigma^e_i \tag{4.44}$$

Equation 4.43 is based on the following assumptions: (1) the hydrostatic stresses have a negligible influence on the yield strength, (2) deformation is small and (3) unloading is purely elastic. When the equivalent elastic stress exceeds twice the equivalent stress

in the plastic deformation stage, $\sigma_i^e \geqslant 2\sigma_i^p$, the third assumption is discarded but Eq. 4.43 must be modified. For conditions of isotropic hardening, which is assumed here, reverse yielding will occur just after an amount of stress equal to $2\sigma_i^p$ unloads. The present analysis assumes conditions of reverse yielding must include the effects of the third invariant. Therefore, theses conditions must be expressed in terms of the elastic-plastic deviatoric stresses given by Eq. 4.41. The amount of stress that has not unloaded is

$$\Delta\sigma_i^e = \sigma_i^e - 6s_{11}^p \tag{4.45}$$

Unloading is no longer elastic after reverse yielding occurs. The equivalent elastic stress term, σ_i^e, in Eq. 4.44 must be replaced by the equivalent stress expression, $2\sigma_i^p + \Delta\sigma_i^p$, describing plastic deformation in the material, see Fig. 4.2. $2\sigma_i^p$ is the size of the new elastic domain and $\Delta\sigma_i^p$ is the amount of stress that unloads after the material has gone into reverse yielding. Rewriting the elastic-plastic deviatoric stress as $6s_{11}^p + \Delta\sigma_i^p$ gives the residual stress equations

$$\sigma_{11}^r = \sigma_{22}^r = -\frac{1}{2}\sigma_{33}^r = s_{11}^p - \frac{1}{3}(6s_{11}^p + \Delta\sigma_i^p) \tag{4.46}$$

We are again faced with the task of solving our unknown elastic-plastic quantities in terms of known, measurable elastic quantities. To solve the unknown, $\Delta\sigma_i^p$, in terms of elastic relations the following is used

$$\Delta\sigma_i^p = k_1\Delta\epsilon_i^p \tag{4.47}$$

which is defined in Fig. 4.2. The change in equivalent plastic strain is $\Delta\epsilon_i^p = \alpha\Delta\epsilon_i^e$ and from Hooke's law we know $\Delta\epsilon_i^e = \frac{\Delta\sigma_i^e}{E}$. Upon substituting Eqn. 4.45 into the latter equation the residual stress fields after reverse yielding are obtained. J.K. Li [12] refers to the residual stresses in Eqn. 4.44 and 4.46 as transresidual stresses because they are for a single impacting shot. The transresidual stresses must be modified to conform to conditions of 100% coverage. For 100% coverage the equilibrium equations

reduce to

$$\begin{aligned} \frac{\partial \sigma_{13}^r(x_3)}{\partial x_3} &= 0 \\ \frac{\partial \sigma_{23}^r(x_3)}{\partial x_3} &= 0 \\ \frac{\partial \sigma_{33}^r(x_3)}{\partial x_3} &= 0 \end{aligned} \tag{4.48}$$

Plane stress conditions exist at the surface $\sigma_{13}^r(0) = \sigma_{33}^r(0) = \sigma_{23}^r(0) = 0$ which allow the equilibrium equations to be solved giving the relation

$$\sigma_{13}^r(x_3) = \sigma_{33}^r(x_3) = \sigma_{23}^r(x_3) = 0 \tag{4.49}$$

Surface deformation is uniform and only occurs in the z direction acting to compress the surface, therefore

$$\epsilon_{11}^r(x_3) = \epsilon_{22}^r(x_3) = 0 \tag{4.50}$$

Therefore, the following conditions apply

$$\begin{aligned} \sigma_{11}^r &= \sigma_{22}^r = g_1(x_3) \\ \sigma_{33}^r &= 0 \\ \epsilon_{33}^r &= g_2(x_3) \\ \epsilon_{11}^r &= \epsilon_{22}^r = 0 \end{aligned} \tag{4.51}$$

The strains in Eqn. 4.51 are the inelastic strains. Unfortunately, the transresidual stresses and strains do not satisfy the conditions given in Eqn. 4.51. But the transresidual stresses can be relaxed by using Hooke's law

$$\sigma_{11}^{rel} = \sigma_{22}^{rel} = \frac{\nu}{1-\nu}\sigma_{33}^r \tag{4.52}$$

Subtracting these from the unrelaxed residual stresses yields the desired expression

$$\sigma_{11}^R = \sigma_{22}^R = \sigma_{11}^r - \frac{\nu}{1-\nu}\sigma_{33}^r = \frac{1+\nu}{1-\nu}\sigma_{11}^r \tag{4.53}$$

These residual stresses are for a semi infinite surface and are not self equilibrated.

4.7 Validation of Model

Fig. 4.3 provides multiple residual stress plots based on the $J_2 - J_3$ model. The shot diameter and velocity for the plots can be found in [37] and include $2R^* = 0.4\times10^{-3}$ m, and $V = 45$ m/s. The material peened was an Almen strip [96] made of spring steel (SAE 1070). The material properties are provided in Table 4.1. The shot velocity for the Almen strip was simulated [37] and measured to be 45m/s with an optical method. Fig. 4.3a gives the normalized residual stress (σ_{11}^R/σ_s), defined as the residual stress divided by the yield stress, for different values of c. Clearly, the theoretically predicted residual stress is strongly influenced by the parameter, c, and therefore the third invariant J_3. The magnitude of the residual stress is smallest for $c = -3.375$ but the depth of the residual stress is largest. However, for a value of $c = 2.25$ the magnitude of the residual stress is largest but the depth is smallest. In general, a larger c value increases the magnitude of the residual stress but decreases the depth. Also shown in Fig. 4.3b are residual stress predictions of measurements from an Almen strip [96]. The measurements from ref. [96] are corrected [37] because of material removal that alters the measured residual stress. Predictions based on the J2-J3 analysis of the Almen strip residual stress measurements are better than predictions based on J_2 theory. In each plot an edge is present when the residual stress begins to decrease sharply. At the edge a transition point occurs because Eqn.'s 4.44 and 4.46 along with Eqn. 4.53 are used to model elastic unloading and reverse yielding respectively.

Further verification of the J2-J3 model developed in section 3 is supported with published experimental residual stress data for Ti-6AL-4V alpha beta and Ti-6Al-4V STOA [34]. Material properties are provided in Table 1. The shot diameter used on the Ti-6Al-4V specimens is $2R^* = 0.4\times10^{-3}$. Shot velocities were not reported in [34] however the Ti-6Al-4V alpha-beta was shot peened at an intensity of 11A while Ti-6AL-4V STOA was shot peened with an intensity in the range 8A - 12A. The Almen intensity, A, is a standardized unit for the arc height of an A type Almen strip with

thickness 0.051 in. An approximate value for the shot velocity can be obtained from the intensity by using the relation provided in [37]. Based on the intensity levels, Ti-6Al-4V alpha beta and Ti-6Al-4V STOA were found to be peened at an approximate shot velocity of 60 m/s and 40 m/s respectively.

Predictions of the Ti-6AL-4V alpha beta and Ti-6Al-4V STOA residual stress measurements are given in Fig. 4.5. A value of $c = 2.25$ was used and held constant for this material. Again, improved predictions of the residual stress field is observed compared to using a value of $c = 0$, corresponding to simple J_2 plasticity theory. The J2-J3 model yields a value of the compressive stress at the surface approximately -600 MPa. The experimental value is also -600 MPa. Results based on Iliushin's theory alone yield a value a little larger than -750 MPa. In general, for this particular set of experimental data we see improved accuracy for the entire deformed layer from the surface to a depth of zero compressive stress. Even though the analysis for a single indenting shot has been modified for 100% coverage, improved prediction of the residual stress depth should not always be expected because it is dictated by the number of impacts and this model is for only a single impact. However, predictions of the maximum subsurface residual stresses are accurate and compare well with experimental data.

Residual stresses from shot peened 7075-T7351 [97] were also used to validate the J2-J3 model. Rectangular aluminum specimens with a thickness, width, and length of 8.1 mm, 25.4 mm, and 115 mm respectively were shot peened on all four sides to 100% coverage. Two different Almen intensities, 8A and 12A, were applied to the test specimens. The residual stresses were measured using an X-ray diffraction stress analyzer with an X-ray target, CrK, every 0.1 mm. A mixture of S 230 and S 280 cast steel shots were used to shot peen the samples. Property and parameter inputs for the model include $E = 70$ GPa, $\nu = 0.31$, $\sigma_s = 462$ MPa, $\sigma_b = 526$ MPa, and $2R^* = 0.584 \times 10^{-3}$ m. The velocities used, 40 and 60 m/s, are consistent with those used for the Ti-6Al-4V specimens, which had similar intensities. Both models

Table 4.1: Table of material properties.

Material	Modulus of Elasticity	Yield Stress	Ultimate Stress
Spring Steel (SAE 1070) [96]	200 GPa	1120 MPa	1270MPa
Aluminum 7075-T7351 [97]	70 GPa	462 MPa	526 MPa
Ti-6Al-4V alpha beta [34]	113.8 GPa	930 MPa	1000 MPa
Ti-6Al-4V STOA [34]	113.8 GPa	965 MPa	1034 MPa

fail to predict the residual stress at the surface with any reasonable accuracy but, in general, the J2-J3 model performs most adequately. However, the measured surface residual stress is questionable because the specimen that was peened at a 12A intensity produced an equivalent surface residual stress to the 8A intensity. The 12A intensity should produce a larger compressive stress at the surface. See appendix B for details of the computational calculations.

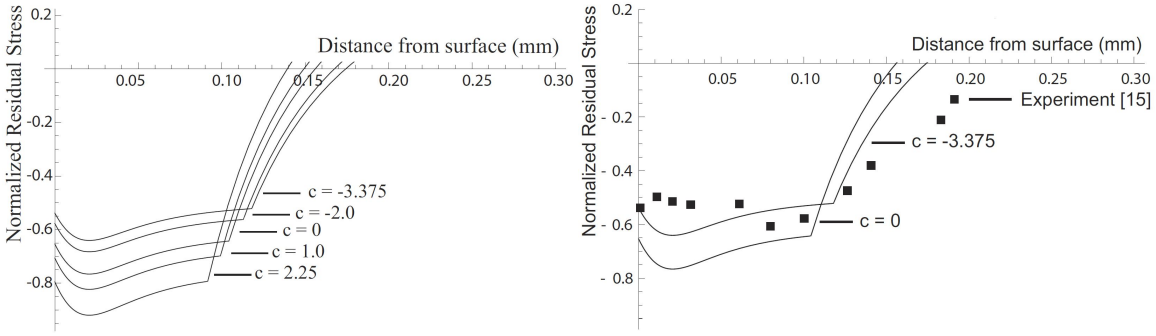

(a) (b)

Figure 4.3: (a) Plots of normalized residual stress for c = -3.375, 0 and 2.25 (b) Prediction of residual stresses in SAE 1070 spring steel [96]. c = 0 corresponds to results obtained by using Iliushin's theory and c = -3.375 was used in the current analysis

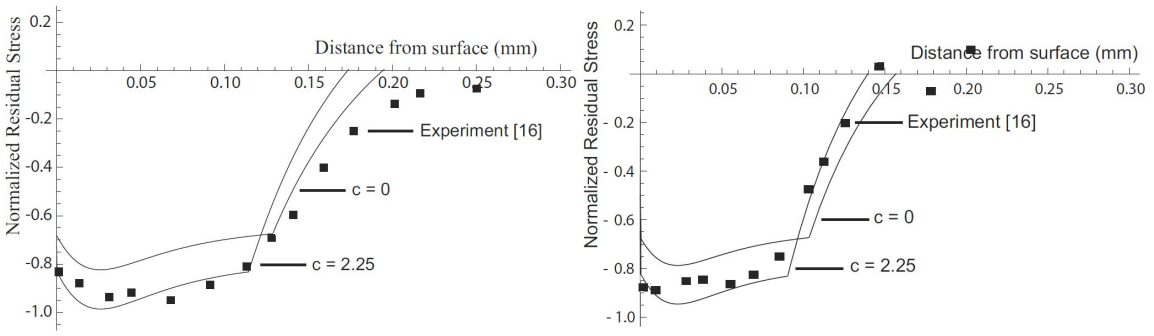

Figure 4.4: (a) Reproduction of experimental residual stress data of Ti-6Al-4V alpha beta (b) Reproduction of experimental residual stress data of Ti-6Al-4V STOA [34]. Predictions made with the J2 J3 model are more accurate than simple J2 theory

4.8 Conclusions

The elastic-plastic deviatoric stress of a generalized isotropic material has been systematically calculated using incremental plasticity. The complex stress state induced during the peening process makes prediction of yielding difficult. An attempt has been made to remedy this difficulty by incorporating a yield criterion into residual stress models that more accurately predicts the yielding behavior of structures during combined loading. Even though the full strength of incremental plasticity has not been completely exploited here, it has been utilized to relate the elastic-plastic deviatoric stress to the third invariant, J_3. The new approach to solve the elastic-plastic deviatoric stress is easily incorporated into previously existing residual stress models and may provide more accurate results. Results of cold rolled spring steel, Ti-6V-4Al and Al 7075 indicate the theoretical and experimental residual stresses are indeed influenced by J_3.

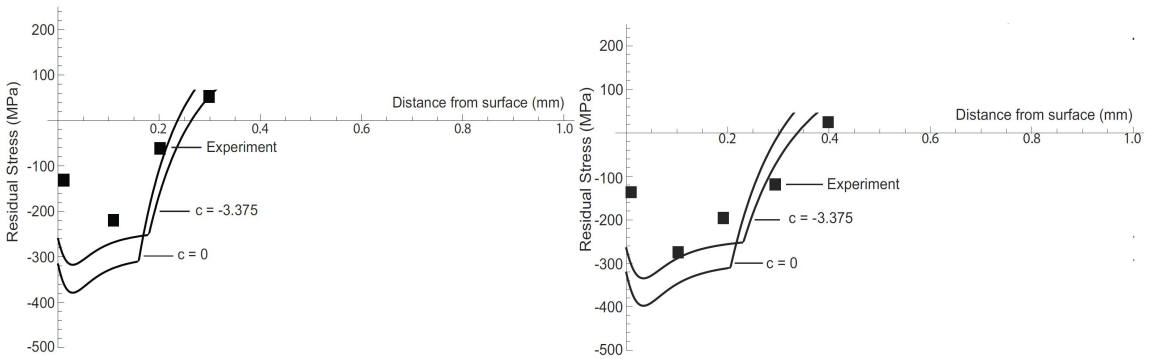

Figure 4.5: (a) Reproduction of experimental residual stress data of Ti-6Al-4V alpha beta (b) Reproduction of experimental residual stress data of Ti-6Al-4V STOA [34]. Predictions made with the J2 J3 model are more accurate than simple J2 theory

Chapter 5

A SEMI-ANALYTICAL MODEL OF TIME DEPENDENT PLASTIC STRAINS INDUCED DURING SHOT PEENING

5.1 Introduction

Shot peening is one of the most effective mechanical surface treatment processes for increasing the fatigue strength of structural components. With its important purpose and extensive use, a strong theoretical understanding is necessary to optimize the process and maximize benefits. The time dependent response of the material during the peening process is a largely overlooked and neglected research topic. Research of the time dependent plastic strains produced from shot peening has remained largely in the realm of numerical analysis. There is a scarcity of analytical research.

When a semi-infinite surface is shot peened the in-plane inelastic strains are zero because of compatibility. As a result, the in-plane residual stress and plastic strain are linearly related. These boundary conditions motivate a second order differential equation similar in mathematical form to a modified Kelvin solid model with a strain acceleration term. Solving the resulting equation gives a closed form expression for the plastic strain as a function of time. The plastic strain rate is solved by taking the derivative with respect to time. Comparisons with published finite element data show good agreement and are within 10% for most of the loading and unloading period.

For decades shot peening has been used in the aerospace, automotive, pressurized vessel, and medical industries to increase the fatigue strength of fatigue critical components. Its great benefits have been well documented. For example, shot peening has been shown to improve the fatigue strength of high strength aluminum alloys by

as much as 25-35%. The primary mechanism responsible for the increase in fatigue life is the compressive residual stress induced from the peening process. Shot peening can induce a compressive residual stress near 60% of the materials UTS Y. Oshida [98]. In general, analytical research of shot peening is limited but modeling of the time dependent behavior of plastic strains and strain rates is nonexistent. Only numerical models have shed light on the behavior of the plastic strain and strain rate time history. Finite element models developed by S.T.S. Al-Hassani [14] and S.A. Meguid [15] investigate the dynamic nature of the loading process of single impacting shots. The behavior predicted from each study is identical, the plastic strain increases sharply during loading reaching a constant strain during unloading. The time intervals of loading and unloading of the shot are extremely short, on the order of a microsecond. S.A. Meguid [16] used a 3D axisymmetric finite element analysis to model the time variation of the plastic strain rate for a position directly below the shot and close to the surface. Their results indicate that the plastic strain rate increase dramatically reaching values as high as $6 \times 10^5 \frac{1}{s}$ during loading but when the shot begins to rebound these values decrease drastically and decay to zero. The importance of plastic strain rates on the compressive residual stress is well documented through finite element simulations [14, 16]. Al-Hassani et al reported the effect of material strain rate dependency for repeated and progressive impacts of shots on the stress profile. However, the author cautions that the results are not experimentally verified. Meguid et al on the other hand, performed a dynamic elasto-plastic finite element analysis of the process using a rate sensitive material. They found that plastic strain rates contribute significantly to both the level and distribution of the residual stress field. A three dimensional elasto-plastic finite element model was developed by ElTobgy et al [49]. They concluded that a strain rate sensitive material should be used because of high plastic strain rates.

An attempt is made in this paper to develop a semi-analytical model of the time dependent plastic strains based on simple, intuitive mathematical relations. A second

order differential equation is derived that is a function of the strain acceleration, strain rate and strain which, when solved, predicts the time dependent plastic strain and strain rate. The differential equation is similar to an equation proposed by Kornilov [99] which takes into account the impulsive loading of structures by incorporating the strain acceleration, $\ddot{\epsilon}_p$. With some mathematical manipulations the proposed equation can accurately predict the behavior of the time history of the plastic strain and strain rate.

5.2 Theoretical Development

5.2.1 Equilibrium, Boundary Conditions and the Residual Stress and Plastic Strain Tensors

The surface is assumed to be semi-infinite with positive z direction pointing downward. The residual stresses in the radial and tangential directions, σ^r_{11} and σ^r_{22}, only vary through the thickness (in the z direction) not on any plane perpendicular. When 100% coverage is reached we have the condition, $\sigma^r_{11} = \sigma^r_{22} = \sigma^r$, because of loading symmetry. As a result, equilibrium in component form is

$$\begin{aligned} \frac{\partial \sigma^r(x_3)}{\partial x_1} + \frac{\partial \sigma^r_{12}(x_3)}{\partial x_2} + \frac{\partial \sigma^r_{23}(x_3)}{\partial x_3} = 0 \\ \frac{\partial \sigma^r(x_3)}{\partial x_1} + \frac{\partial \sigma^r_{21}(x_3)}{\partial x_2} + \frac{\partial \sigma^r_{13}(x_3)}{\partial x_3} = 0 \\ \frac{\partial \sigma^r_{33}(x_3)}{\partial x_3} + \frac{\partial \sigma^r_{23}(x_3)}{\partial x_2} + \frac{\partial \sigma^{x_2}_{13}(x_3)}{\partial x_1} = 0 \end{aligned} \tag{5.1}$$

There are two scenarios in which Eqn. 5.1 is valid. The first occurs for a single shot impact and the second is for multiple shot impacts. 100% coverage is considered equivalent to the case of multiple shot impacts. For a single impact, if the analysis is limited to the location directly below the shot, the residual stress tensor will be independent of x_1 and x_2. Thus, the principal stresses and therefore the residual stress are only functions of depth, z. Furthermore, deformation only occurs in the x_3 direction or identically z-direction. When 100% coverage occurs, the stresses in the

x_1 and x_2 direction do not change for a given depth. Therefore, all partial derivatives with respect to x_1 and x_2 go to zero. To better conceptualize these conditions, assume 100% coverage and choose various points on the surface or below, as long as the chosen points have identical depths, different values for the residual stress will not be found because the surface is uniformly deformed. Hence, the equilibrium relations for both these scenarios are

$$\begin{aligned} \frac{\partial \sigma^r_{13}(3)}{\partial x_3} &= 0 \\ \frac{\partial \sigma^r_{23}(x_3)}{\partial x_3} &= 0 \\ \frac{\partial \sigma^r_{33}(x_3)}{\partial x_3} &= 0 \end{aligned} \tag{5.2}$$

Plane stress conditions exist at the surface $\sigma^r_{13}(0) = \sigma^r_{33}(0) = \sigma^r_{23}(0) = 0$ because deformation of the shot peened layer is small compared to the thickness of the specimen. The equilibrium equations can be solved, yielding the more general relations

$$\sigma^r_{13}(x_3) = \sigma^r_{33}(x_3) = \sigma^r_{23}(x_3) = 0 \tag{5.3}$$

The residual stress tensor now has the simplified form

$$\underline{\sigma}^r(x_3) = \begin{pmatrix} \sigma^r(x_3) & 0 & 0 \\ 0 & \sigma^r(x_3) & 0 \\ 0 & 0 & 0 \end{pmatrix}$$

From incompressibility conditions and symmetry we have the plastic strain tensor

$$\underline{\epsilon}^p(x_3) = \begin{pmatrix} \epsilon^p(x_3) & 0 & 0 \\ 0 & \epsilon^p(x_3) & 0 \\ 0 & 0 & -2\epsilon^p(x_3) \end{pmatrix}$$

The total strain, which is time dependent during loading and unloading, is the superposition of an elastic and inelastic portion, namely

$$\underline{\epsilon}(x_3,t) = \underline{\epsilon}^{el}(x_3,t) + \underline{\epsilon}^{ine}(x_3,t) \tag{5.4}$$

The elastic strain in Eqn. 5.4 comes from the Hertzian stress that is generated during loading. When shots stop impacting the surface the elastic strain associated with the Hertzian stress disappears because deformation is reversible. Eqn. 5.4 may then be expressed as

$$\underline{\epsilon}(x_3) = \underline{\epsilon}^{ine}(x_3) \tag{5.5}$$

Eqn. 5.5 is valid only when shot peening stops. Returning to Eqn. 5.4, the inelastic strain, $\underline{\epsilon}^{ine}(x_3,t)$, is a superposition of the elastic strain resulting from the residual stress and the irreversible plastic strain. The elastic strain corresponding to the residual stress is governed by the laws of elasticity. Eqn. 5.4 can be written as

$$\underline{\epsilon}(x_3,t) = \underline{\epsilon}^{el}(x_3,t) + \underline{C\sigma}^{r}(x_3,t) + \underline{\epsilon}^{p}(x_3,t) \tag{5.6}$$

Where $\underline{C}$ is the compliance matrix. For modeling purposes, discard the stochastic condition of impacting so that *during* peening deformation is uniform and only acts to compress the surface. The inelastic strain tensor can now be solved for both impacting conditions from compatibility. Recall, the six strain compatibility equations (with respect to the principal axes for simplicity):

$$\begin{aligned}
\frac{\partial^2 \epsilon_{11}^{ine}}{\partial x_2 \partial x_3} - \frac{\partial}{\partial x_1}\left(-\frac{\partial \epsilon_{23}^{ine}}{\partial x_1} + \frac{\partial \epsilon_{31}^{ine}}{\partial x_2} + \frac{\partial \epsilon_{12}^{ine}}{\partial x_3}\right) &= 0 \\
\frac{\partial^2 \epsilon_{22}^{ine}}{\partial x_3 \partial x_1} - \frac{\partial}{\partial x_2}\left(-\frac{\partial \epsilon_{31}^{ine}}{\partial x_2} + \frac{\partial \epsilon_{12}^{ine}}{\partial x_3} + \frac{\partial \epsilon_{23}^{ine}}{\partial x_1}\right) &= 0 \\
\frac{\partial^2 \epsilon_{33}^{ine}}{\partial x_1 \partial x_2} - \frac{\partial}{\partial x_3}\left(-\frac{\partial \epsilon_{12}^{ine}}{\partial x_3} + \frac{\partial \epsilon_{23}^{ine}}{\partial x_1} + \frac{\partial \epsilon_{31}^{ine}}{\partial x_2}\right) &= 0 \\
\frac{\partial^2 \epsilon_{11}^{ine}}{\partial x_2^2} + \frac{\partial^2 \epsilon_{22}^{ine}}{\partial x_1^2} - 2\frac{\partial^2 \epsilon_{12}^{ine}}{\partial x_1 \partial x_2} &= 0 \\
\frac{\partial^2 \epsilon_{11}^{ine}}{\partial x_3^2} + \frac{\partial^2 \epsilon_{33}^{ine}}{\partial x_1^2} - 2\frac{\partial^2 \epsilon_{13}^{ine}}{\partial x_1 \partial x_3} &= 0 \\
\frac{\partial^2 \epsilon_{22}^{ine}}{\partial x_3^2} + \frac{\partial^2 \epsilon_{33}^{ine}}{\partial x_2^2} - 2\frac{\partial^2 \epsilon_{23}^{ine}}{\partial x_2 \partial x_3} &= 0
\end{aligned} \tag{5.7}$$

Where x_3 corresponds with z. The shear strains are zero and all strains are independent of all components with the exception of x_3 (or depth z). We are left with

$$\begin{aligned} \frac{\partial^2 \epsilon_{11}^{ine}}{\partial x_3^2} &= 0 \\ \frac{\partial^2 \epsilon_{22}^{ine}}{\partial x_3^2} &= 0 \end{aligned} \tag{5.8}$$

Eqn. 5.8 is satisfied when the strains, ϵ_{11}^{ine} and ϵ_{22}^{ine}, are linear in x_3 (z), i.e.

$$\epsilon_{11}^{ine} = \epsilon_{22}^{ine} = a_o x_3 + a_1 \tag{5.9}$$

The boundary conditions for a semi-infinite surface require a_o to be zero so the strain converges to zero at infinity. Identically, a_1 is zero to ensure a strain of zero at infinity because no strain is present in the structure far from the surface. These conditions are only true for a thin plastically deformed layer satisfying the equilibrium and compatibility conditions in Eqn.'s 5.2 and 5.8.

Assumptions

Some of the major assumptions of the model include:

1. In the formulation we neglect the affect of wave propagation and inertia effects
2. We assume a plastic strain acceleration, $\ddot{\epsilon}^p(x_3, t)$, exists given the dynamic and impulsive nature of the loading
3. Deformation from multiple shot impacts occurs uniformly
4. The compatibility conditions of Eqn. 5.9 are valid during loading and unloading
5. Two conditions of loading and unloading are considered. For the first case, the residual stress is constant. In the second, the residual stress maintains a constant *rate*.

Based on the fourth assumption, the in-plane inelastic strains are now

$$\epsilon_{11}^{ine}(x_3,t) = \epsilon_{22}^{ine}(x_3,t) = 0 \tag{5.10}$$

Eqn. 5.10 is equally valid for a single shot impact and for multiple impacts. Writing the inelastic strain in terms of the residual stress and plastic strain gives

$$\epsilon^p(x_3,t) + \left(\frac{1-\nu}{E}\right)\sigma^r(x_3,t) = 0 \tag{5.11}$$

After shot peening has stopped and deformation is time independent, Eqn. 5.10 simplifies to

$$\epsilon_{11}^{ine}(x_3) = \epsilon_{22}^{ine}(x_3) = \epsilon^p(x_3) + \left(\frac{1-\nu}{E}\right)\sigma^r(x_3) = 0 \tag{5.12}$$

The residual stress is related to the plastic strain via Hooke's law and behaves linear elastically.

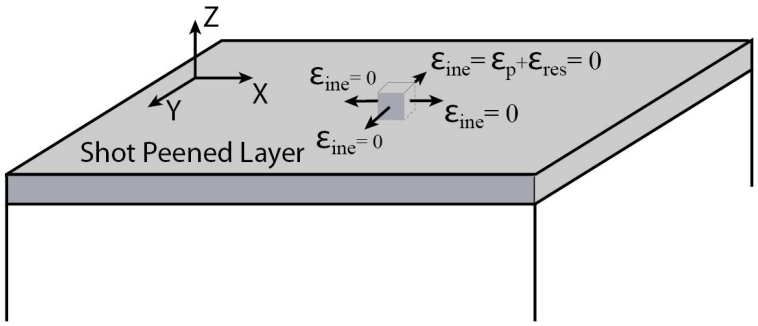

Figure 5.1: Idealized illustration of a thin uniformly shot peened layer. The in-plane inelastic strain, $\epsilon_{xx}^{ine} = \epsilon_{yy}^{ine} = 0$, is null because loading is perpendicular (parallel to z-axis) to the surface.

5.2.2 The Plastic Strain $\epsilon^p(z,t)$ and Residual Stress Field $\sigma^r(z,t)$

The inelastic strain in Eqn. 5.10 is a function of only depth and is therefore dependent on a single variable, z. As a result, consider the equation of motion for a simple mechanical system given as a 1 dimensional oscillator:

$$m\ddot{u_i}^r + b\dot{u_i}^r + ku_i^r = F_i \tag{5.13}$$

Relations similar to Eqn. 5.13 are not only common in system dynamics applications but are often used in the rheology of contact. In Eqn. 5.13, F_i is the contact force and u_i^r is the residual displacement. Eqn. 5.13 can be expressed in terms of stresses by taking the derivative of both sides with respect to area

$$m\frac{d\ddot{u_i}^r}{dA_j} + b\frac{d\dot{u_i}^r}{dA_j} + k\frac{du_i^r}{dA_j} = \frac{dF_i}{dA_j} \tag{5.14}$$

The right hand side is now defined as the stress on the surface. The force in the x_3 or equivalently z-direction is non-zero. However, the forces in the 11 and 22 direction are negligible because loading is strictly normal to the surface, therefore the traction is zero in these directions and the right side of Eqn. 5.14 is zero. Substitution of $dA_j = dz \times dx_j$ into Eqn. 5.14 gives

$$A\frac{d\ddot{u_i}^r}{dx_j} + B\frac{d\dot{u_i}^r}{dx_j} + C\frac{du_i^r}{dx_j} = 0 \tag{5.15}$$

Where $(i,j) \neq z$ and the units of A, B and C are respectively pressure-time^2, pressure-time and pressure. In the formulation, A, B, and C are constants independent of the velocity. The inelastic strain is defined in terms of the residual displacement as

$$\frac{1}{2}(u_{i,j}^r + u_{j,i}^r) = \epsilon_{ij}^{ine} \tag{5.16}$$

where the comma denotes differentiation. Note, the term on the left side goes to $\frac{du_i^r}{dx_i}$ (no sum on i) because the shear strains are negligible. Eqn. 5.15 can be expressed in terms of the inelastic strain by substituting Eqn. 5.16

$$A\ddot{\epsilon}^{ine} + B\dot{\epsilon}^{ine} + C\epsilon^{ine} = 0 \tag{5.17}$$

Where $\epsilon^{ine} = \epsilon_{11}^{ine} = \epsilon_{22}^{ine}$. The inelastic strain is equal to

$$\epsilon_{ij}^{ine} = \epsilon_{ij}^r + \epsilon_{ij}^p \tag{5.18}$$

Writing Eq. 5.17 in terms of the residual strain and plastic strain

$$A(\ddot{\epsilon}^r + \ddot{\epsilon}^p) + B(\dot{\epsilon}^r + \dot{\epsilon}^p) + C(\epsilon^r + \epsilon^p) = 0 \tag{5.19}$$

Eqn. 5.19 can be further simplified if the residual stress, $\sigma^r = C\epsilon^r$, maintains a constant value throughout loading so that $\dot{\epsilon}^r$ and $\ddot{\epsilon}^r$ go to zero

$$A\ddot{\epsilon}^p + B\dot{\epsilon}^p + C\epsilon^p = -C\epsilon^r = -\sigma^r \tag{5.20}$$

The derivation of Eqn. 5.20 is not completely applicable to the physical scenario we are trying to model. The residual stress does indeed vary with time during the loading and unloading process. Instead, return to Eqn. 5.17 but now consider the case in which the residual stress and therefore the residual strain, ϵ_{ij}^r maintains a constant stress and strain *rate*. Upon taking the derivative of Eqn. 5.17 gives the following third order ODE

$$A\dddot{\epsilon}^{ine} + B\ddot{\epsilon}^{ine} + C\dot{\epsilon}^{ine} = 0 \tag{5.21}$$

The reason for expressing Eqn. 5.17 in terms of the first, second and third derivatives will become apparent shortly. As was done previously, use the relation provided in Eqn. 5.18 to get

$$A(\dddot{\epsilon}^r + \dddot{\epsilon}^p) + B(\ddot{\epsilon}^r + \ddot{\epsilon}^p) + C(\dot{\epsilon}^r + \dot{\epsilon}^p) = 0 \tag{5.22}$$

Both the second and third derivative of the residual strain go to zero because the rate of change of the residual stress and strain is constant. Therefore, from $\dot{\sigma}^r = C\dot{\epsilon}^r$

$$A\dddot{\epsilon}^p(x_3,t) + B\ddot{\epsilon}^p(x_3,t) + C\dot{\epsilon}^p(x_3,t) = -\dot{\sigma}^r(x_3,t) \tag{5.23}$$

By taking the derivative of both sides of Eqn. 5.23, yields a solution that gives the desired behavior. Namely, an impulsive plastic strain rate. By introducing a time dependent residual strain and stress into Eqn. 5.23 accurately represents the physical process. *During contact of the shot, the residual stress is time dependent.* To model the impulsive behavior of the material during impacting, introduce the dirac delta function, $\delta(t-t_0)$, which has units of inverse time, $\frac{1}{t}$, to Eqn. 5.23. Equate the residual stress rate to a time independent residual stress multiplied by the delta function

$$\dot{\sigma}^r(x_3,t) = \sigma^r(x_3)\delta(t-t_0) \tag{5.24}$$

Inserting Eqn. 5.24 into Eqn. 5.23

$$A\dddot{\epsilon}^p(x_3,t) + B\ddot{\epsilon}^p(x_3,t) + C\dot{\epsilon}^p(x_3,t) = -\sigma^r(x_3)\delta(t-t_0) \tag{5.25}$$

Applying the method of Laplace transforms with initial conditions, $\epsilon^p(0) = \dot{\epsilon}^p(0) = \ddot{\epsilon}^p(0) = 0$, gives

$$\epsilon^p(x_3,t) = -\frac{\sigma^r(x_3)}{C} + \frac{\sigma^r(x_3)(-e^{(t-t_0)P}B + e^{(t-t_0)Q}B + e^{(t-t_0)P}T + e^{(t-t_0)Q}T)}{2CT} \tag{5.26}$$

where $T = \sqrt{B^2-4AC}$, $P = -\frac{B}{2A} - \frac{\sqrt{B^2-4AC}}{2A}$ and $Q = -\frac{B}{2A} + \frac{\sqrt{B^2-4AC}}{2A}$. Rewriting Eqn. 5.26 as

$$\epsilon^p(x_3,t) = -\frac{\sigma^r(x_3)}{C}\left(1 - \frac{(-e^{(t-t_0)P}B + e^{(t-t_0)Q}B + e^{(t-t_0)P}T + e^{(t-t_0)Q}T)}{2T}\right) \tag{5.27}$$

which can be further simplified to

$$\epsilon^p(x_3,t) = -\frac{\sigma^r(x_3)}{C}\lambda(t) \tag{5.28}$$

$\sigma^r(x_3)$ is the time independent residual stress and $\lambda(t) = 1 - \frac{(-e^{(t-t_0)P}B + e^{(t-t_0)Q}B + e^{(t-t_0)P}T + e^{(t-t_0)Q}T)}{2T}$. Taking $\sigma^r(x_3,t) = \sigma^r(x_3)\lambda(t)$ and $C = \frac{E}{1-\nu}$, we obtain

$$\epsilon^p(x_3,t) = -\frac{1-\nu}{E}\sigma^r(x_3,t) \tag{5.29}$$

Eq. 5.29 is identical to Eq. 5.11 of section 5.1. Notice that P and Q are always negative when $A > 0$ therefore $\lim_{t\to\infty}\lambda(t) = 1$ and the steady state response (as time goes to infinity) is

$$\lim_{t\to\infty}\epsilon^p(x_3,t) = -\lim_{t\to\infty}\frac{1-\nu}{E}\sigma^r(x_3)\lambda(t) = -\frac{1-\nu}{E}\sigma^r(x_3)\lim_{t\to\infty}\lambda(t) = -\frac{1-\nu}{E}\sigma^r(x_3)$$
$$\Rightarrow \epsilon^p(x_3) = -\frac{1-\nu}{E}\sigma^r(x_3)$$

Thus, the steady state response of the plastic strain given in Eqn. 5.28 is identical to the time independent plastic strain of Eqn. 5.12

An equation similar to Eqn. 5.20 has been proposed [99] that incorporates the influence of the plastic strain acceleration that occurs for impulsive loading. Traditionally, the equation provides a link between the effective stress and effective strain, effective strain rate and effective strain acceleration in the form

$$A\ddot{\epsilon}_i^{k^*} + B\dot{\epsilon}_i^{m^*} + C\epsilon_i^{n^*} = \sigma_i \tag{5.30}$$

The following modifications will be made based on the boundary conditions and results of the previous section:

1. Given the direct relation between the residual stress and plastic strain provided in Eq 5.11 we will cast Eq 5.30 alternately in terms of the time dependent plastic strain and residual stress.

2. The linear relation from Eq 5.11 between the plastic strain and residual stress will direct us to assume $k^* = m^* = n^* = 1$ in Eq 5.30.

After applying these modifications to the empirical relation of Eqn. 5.30 the following simple second order time dependent differential equation describes the dynamic behavior between the plastic strain and residual stress.

$$A\ddot{\epsilon}^p(x_3,t) + B\dot{\epsilon}^p(x_3,t) + C\epsilon^p(x_3,t) = \sigma^r(x_3,t) \tag{5.31}$$

Where the strain, strain rate and strain acceleration are represented as $\epsilon^p(x_3,t)$, $\dot{\epsilon}^p(x_3,t)$ and $\ddot{\epsilon}^p(x_3,t)$ respectively. Making reasonable modifications to Eqn. 5.30, proposed by Kornilov, yields an equation identical to Eqn. 6.8. Furthermore, the plastic strain rate is easily obtained by taking the derivative of Eqn. 5.28 with respect to time because it is a closed form time dependent solution of the plastic strain. Observe that when there is no strain acceleration, $\ddot{\epsilon}^p(x_3,t)$, Eqn. 5.31 simplifies to the Kelvin solid model of visco-elasticity. Clearly, the process is not visco-elastic. But the residual stress is governed by the laws of elasticity and is linearly related to the plastic strain because the in-plane inelastic strain is zero. These relations provide motivation to use similar tools of visco-elasticity.

5.3 Numerical Simulations

The coefficients in Eq. 5.31 may be related to the plastic flow behavior of the material during the high strain rate process. We have already shown that the parameter C is equivalent to a modulus. In order for the quantities $A\ddot{\epsilon}^p(x_3,t)$ and $B\dot{\epsilon}^p(x_3,t)$ to yield terms that are dimensionally consistent with the right hand side of the equation then A and B must have units of pressure-time and pressure-time^2 respectively or in SI units Pascal-sec and Pascal-sec^2. The parameter B has the same units as dynamic viscosity and may be interpreted as the materials resistance to flow during plastic deformation.

Research on the dynamic viscosity of metals undergoing plastic deformation from shock loading has been performed in [100–102]. Published values reported range between $3 \cdot 10$ - $4 \cdot 10^4$ Pa-sec for aluminum and 10^3 - 10^5 Pa-sec for steel [100]. These published values provide a starting point to identify B. A is assumed to be an empirical parameter.

A parametric simulation of Eqn. 5.26, provided in Fig.'s 5.2-4, shows the behavior of the plastic strain and strain rate during loading and unloading of the peened surface for variable A, B and C of Eq. 5.20. In Fig. 5.2, the plastic strain and strain rate is varied for A equal $1 \times 10^{-8}, 2 \times 10^{-8}$, and 4×10^{-8} kPa-sec^2. The difference between the strain is small but the max strain rate varies between a value of 6.21×10^5 and 5.27×10^5 strain per second. For values of A larger than 4×10^-8 kPa-sec^2 the solution yields a complex solution, perhaps valid for an alternate scenario, but is not valid for the proposed problem.

Fig. 5.3 shows how the strain and strain rate vary for B. B has a larger influence than A on both the strain and strain rate. Smaller values cause the plastic strain to converge to a steady state value faster. The strain rate is strongly influenced by the parameter B. The max strain rate varies from 4.8×10^5 to 7.0×10^5 strain per second. Parameter C is shown to heavily influence the strain and strain rate. C is

varied between 1000 and 4000 MPa, which changes the strain linearly from 0.1 to 0.4. Interestingly, the max value of the strain rate changes only slightly, but the time for the strain rate to converge to zero increases drastically as is observed in Fig. 5.4.

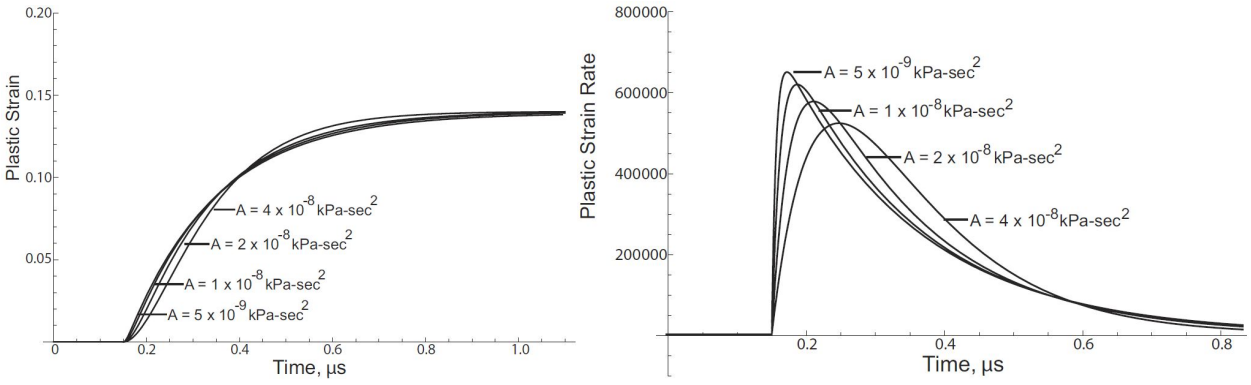

(a) (b)

Figure 5.2: a) Plastic strain and b) plastic strain rate versus time for variable A

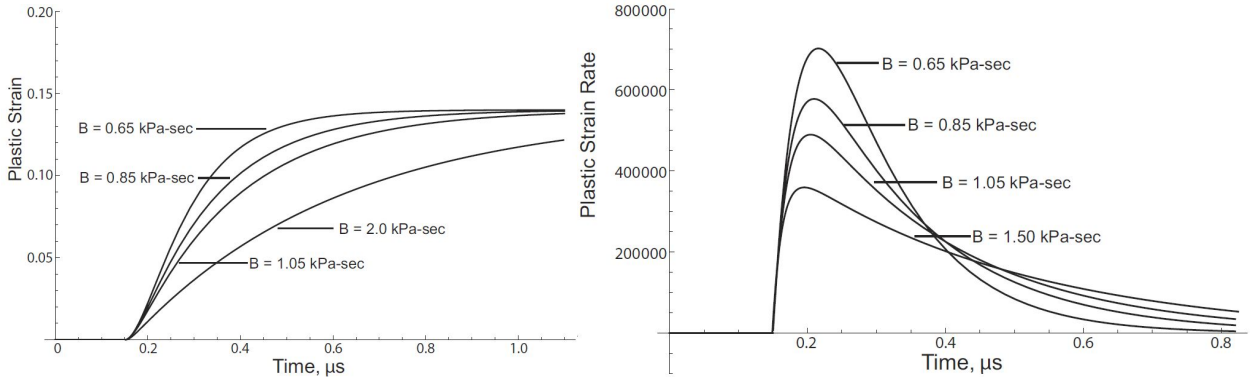

(a) (b)

Figure 5.3: a) Plastic strain and b) plastic strain rate versus time for variable B

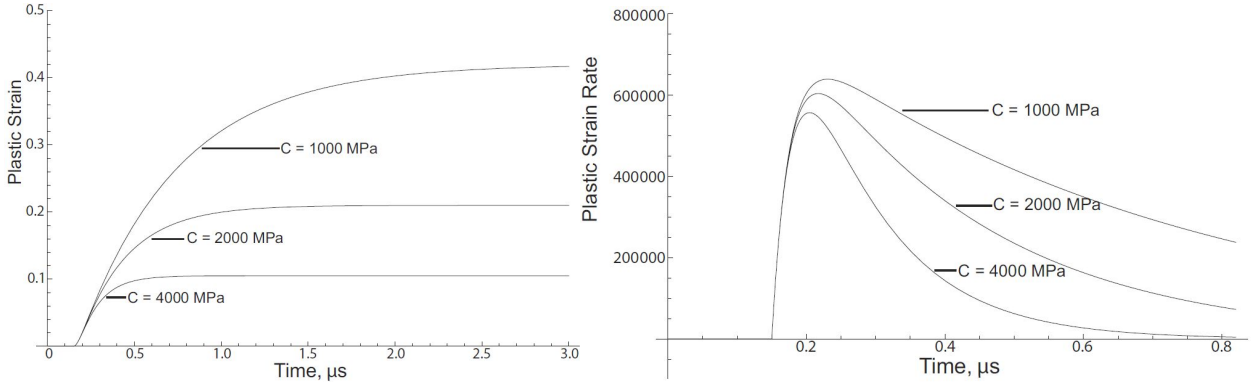

(a) (b)

Figure 5.4: a) Plastic strain and b) plastic strain rate versus time for variable C

5.4 Validation of Model

Figures 5.5 and 5.6 provide a plot of the plastic strain predicted from Eqn. 5.28 along with finite element simulations of Meguid et al. [15, 16, 42] for two different materials; a high strength stainless steel and AISI 4340. Material properties for the high strength stainless steel were acquired from published data and appropriate parametric values chosen based on the simulation include a hardening modulus of $E = 800MPa$, $\sigma^r(x_3 = 0) = 260MPa$, $B = .28kPa\text{-}sec$, $A = 8 \times 10^{-9} kPa\text{-}sec^2$, $\nu = 0.3$. The plot of the numerically predicted plastic strain in Fig. 5.5 is for a position directly below the shot on the surface. The value for the residual stress at the surface, $\sigma^r(x_3 = 0)$, used in the semi-analytical model is approximately half the yield strength of the material which is consistent with the analysis of Tirosh [13]. Experimental and theoretical values of post shot peened solids give a fractional value between $|\frac{1}{3}| - |\frac{1}{2}|$ of the yield strength for the residual stress at the surface. Unfortunately, if the elastic modulus is used in the model, the plastic strain is far too small. Hardening may be responsible for the discrepancy. The prediction is strikingly similar, aside from the irregularity that occurs during loading at a strain of approximately 0.14 in the finite

element simulations. The semi-analytical model gives a predicted plastic strain rate in Fig. 5.5b. Numerical results of the plastic strain rate were not provided in [15], the behavior is verified via numerical predictions provided in Fig. 5.6b. The numerical results indicate a strong resemblance of the plastic strain rate during loading and unloading of the shot to an impulse. There is a sudden large increase in strain rate because of loading and a slower decaying drop off during unloading. One can see the impact of the Dirac Delta function introduced to Eqn. 5.31; analytical results in Fig.'s 5.5 and 5.6 predict the behavior of the plastic strain rate to be impulsive too.

Fig. 5.6a provides a plot of plastic strain versus time for a point chosen $6.5\mu m$ from the surface. Again, numerical results of the plastic strain versus time are not provided but the time independent plastic strain is reported and has a value of approximately 0.16 for a strain rate sensitive target along the centerline on the surface. The yield stress approximated for AISI 4340 is $1600MPa$. Parameters and properties used are $E = 2700MPa$, $\sigma^r(x_3 = 0) = 600MPa$, $B = .85kPa\text{-}sec$, $A = 2 \times 10^{-8} kPa\text{-}sec^2$, $\nu = 0.3$. The hardening modulus was calculated from the stress strain curve and a residual stress, close to the surface, was approximated as 37.5% of $\sigma_y^0 \approx 1600MPa$. Eqn. 5.28 indeed predicts a steady state (time independent) plastic strain a little less than 0.16, almost identical to what Meguid et al. [16] obtained. Fig. 5.6b provides a plot of the plastic strain rate verified with numerical predictions. The plastic strain rate from the model and finite element analysis show very good agreement, within 10%, throughout most of the loading and unloading of the material. See appendix C for details of the computational calculations.

5.5 Conclusions

The mechanical behavior of a material undergoing shot peening is extremely complex. A multitude of phenomenon must be considered in order to investigate the plastic response of the material, for example strain hardening, shakedown and of course the dynamic behavior. In this work, the dynamic impulsive nature of the process was

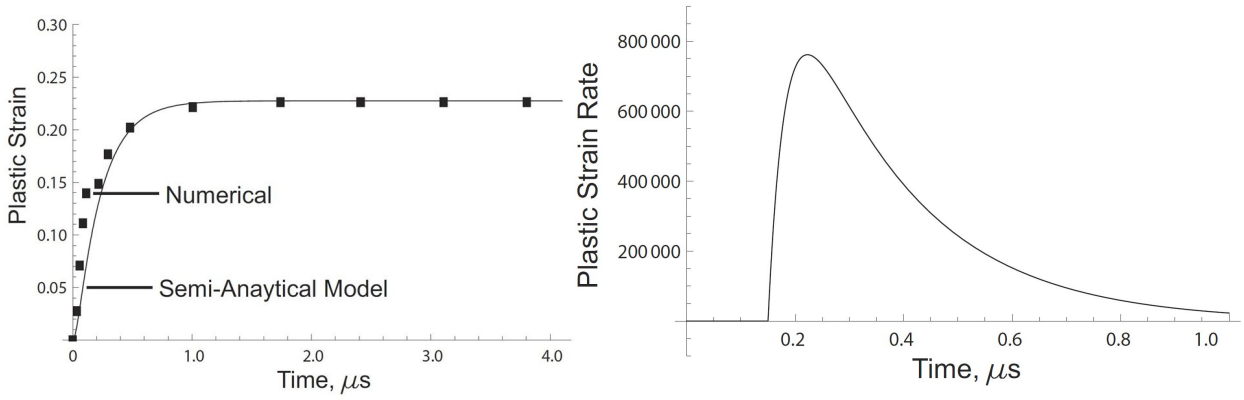

(a) (b)

Figure 5.5: a) Plastic strain, $\epsilon^p(t)$, versus time. Semi-analytical model is in good agreement with numerical results [15]. b) Plastic strain rate, $\dot{\epsilon}^p(t)$, versus time.

exploited to develop a simple model of the time dependent plastic strain and strain rate. Analytical work of the time dependent behavior during peening is severely limited because of the complexity. Though the model is semi-analytical, many of the parameters can be easily approximated from material properties and published data (i.e. yield strength, hardening modulus, dynamic viscosity). Even though verification of the model is limited, comparisons made with published finite element results show extremely good agreement and is well within 10% for a large duration of the loading and unloading process.

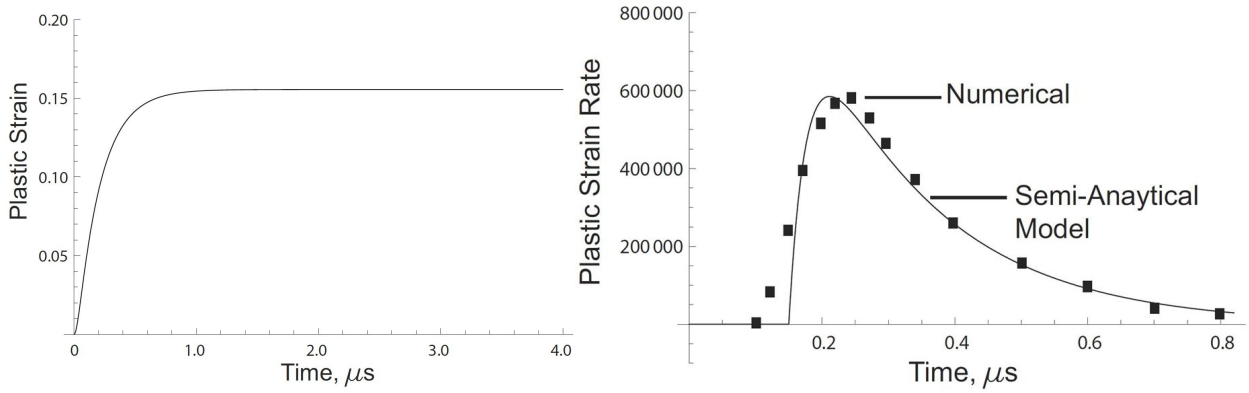

(a) (b)

Figure 5.6: a) Plastic strain, $\epsilon^p(t)$, versus time predicted by the semi-analytical model. The steady state plastic strain is 0.155 and results of the plastic strain reported in [16] are approximately 0.16. b) Prediction of the plastic strain rate, $\dot{\epsilon}^p(t)$, versus time. Comparison of model with finite element results are very good.

Chapter 6

STRAIN GRADIENT BASED SEMI-ANALYTICAL MODEL OF THE RESIDUAL STRESSES INDUCED BY SHOT PEENING

6.1 Introduction

Researchers [103–108] have established that strain gradients can play a role in describing material properties and behavior. For example, strain gradients have been used to explain indentation size effects. As the indentation size decreases the material hardness increases. Efforts made by Fleck et al [107] and Nix et al [108] attempted to explain the indentation size phenomenon with strain gradient based plasticity theories.

Couple stresses have also been linked to the strain gradient in elasticity. Couple stresses are responsible for a rotation of points in a continuum (as opposed to a stress which is responsible for a translation). A couple stress is often defined in the theory of elastic shells. Consider a shell that is divided into two parts by a curve. An action that acts on one part of the curve is represented by a line distribution of forces *and* couples along the dividing curve. Throughout the entirety of classical elasticity, the couple stresses are assumed to vanish. In classical elasticity a material point has only three degrees of freedom which corresponds to its position in Euclidean space. Couple stresses appear as a result of defining each point in a continuous media with the six degrees of freedom of a rigid body [103, 104]. Deformation behavior of materials in the micron scale has been experimentally shown to be size dependent. A couple stress based strain gradient theory provides a means of describing the size dependence.

Smyshlyaev et al [109] have used a strain gradient constitutive law to explain

the role of grain size behavior of polycrystals. The Hall-petch effect states that the strength of a metal increases with decreasing grain size [110]. Arguments posed by Smyshlyaev et al [109] suggest that a single crystals behavior is governed by a strain gradient constitutive law.

The approach developed here does not use the aforementioned strain gradient theories. However, the author believes that an investigation of strain gradient effects on the residual stress from peening, either from fine particle shot or laser, is an application with potential because indentation depths can be on the order of 1μm or less; well within the range of indentation size effects on hardness. The present chapter introduces a simple second order differential equation in plastic strain that empirically predicts the behavior of the residual stress. The equation however does not bring to light the physical influence of the strain gradient on the residual stress field. *The strain gradient merely provides a means of obtaining a closed form expression for the residual stress.* However, there exist strong similarities between the model developed in the present chapter and that of Mindlin [106].

Mindlin performed a rigorous analysis in which he derives equilibrium, boundary conditions and constitutive equations for a linear elastic material in the infinitesimal strain and its first and second gradients. The problem of separation of a solid along a plane was solved. Mindlin states that the second strain gradient has particular significance in regard to the cohesive force, which gives rise to the modulus of cohesion. The modulus of cohesion is directly related to surface tension, or equivalently the energy, per unit area, associated with the formation of a new surface. Surface tension clearly plays a significant role during shot peening because shots impact and increase the area of the target surface (this is why an Almen strip bows post-peening). The primary difference between the approach used here and that of Mindlin is the length scale considered. The plastically deformed peened layer is no less than a hundred micrometers but Mindlin considers interatomic distances in his models.

6.2 Theoretical Development

The same assumptions used to derive Eqn. 5.28 are equally applicable here. The surface is considered to be semi-infinite. Perfectly rigid shots impact normal to the surface.

$$m\ddot{u_i}^r + b\dot{u_i}^r + ku_i^r = F_i \tag{6.1}$$

Equations of this form are not only common in system dynamics applications but are often used in the rheology of contact. In Eqn. 6.1, F_i is the contact force and u_i^r is the residual displacement. Eqn. 6.1 can be expressed in terms of stresses by taking the derivative of both sides with respect to area

$$m\frac{d\ddot{u_i}^r}{dA_j} + b\frac{d\dot{u_i}^r}{dA_j} + k\frac{du_i^r}{dA_j} = \frac{dF_i}{dA_j} \tag{6.2}$$

The right hand side is now defined as the stress on the surface. The force in the z-direction is non-zero. However, the forces in the 11 and 22 direction are negligible because we assume loading is strictly normal to the surface, therefore the traction is zero in these directions and the right side of Eqn. 6.2 is zero. Substitution of $dA_j = dz \times dx_j$ into Eqn. 6.2 gives

$$A\frac{d\ddot{u_i}^r}{dx_j} + B\frac{d\dot{u_i}^r}{dx_j} + C\frac{du_i^r}{dx_j} = 0 \tag{6.3}$$

Where $(i,j) \neq z$ and the units of A, B and C are respectively $pressure{-}time^2$, $pressure{-}time$ and $pressure$. The inelastic strain is defined in terms of the residual displacement as

$$\frac{1}{2}(u_{i,j}^r + u_{j,i}^r) = \epsilon_{ij}^{ine} \tag{6.4}$$

where the comma denotes differentiation. Note, the term on the left side goes to $\frac{du_i^r}{dx_i}$ (no sum on i) because the shear strains are negligible for our particular physical scenario. Now, Eqn. 6.3 can be expressed in terms of the inelastic strain by substituting Eqn. 6.4

$$A\ddot{\epsilon}^{ine} + B\dot{\epsilon}^{ine} + C\epsilon^{ine} = 0 \tag{6.5}$$

Where $\epsilon^{ine} = \epsilon^{ine}_{xx} = \epsilon^{ine}_{yy}$. Now, the inelastic strain is equal to

$$\epsilon^{ine}_{ij} = \epsilon^{r}_{ij} + \epsilon^{p}_{ij} \tag{6.6}$$

Writing Eqn. 6.5 in terms of the residual strain and plastic strain

$$A(\ddot{\epsilon}^r + \ddot{\epsilon}^p) + B(\dot{\epsilon}^r + \dot{\epsilon}^p) + C(\epsilon^r + \epsilon^p) = 0 \tag{6.7}$$

Eqn. 6.7 can be further simplified by assuming the residual stress, $\sigma^r = C\epsilon^r$, is time independent so that $\dot{\epsilon}^r$ and $\ddot{\epsilon}^r$ go to zero

$$A\ddot{\epsilon}^p + B\dot{\epsilon}^p + C\epsilon^p = -C\epsilon^r = -\sigma^r \tag{6.8}$$

The next goal is to write Eqn. 6.8 in terms of spatial gradients of the plastic strain rather than time derivatives. One way to overcome the challenge is to introduce the notion of parametric derivatives. The line of thinking allows Eqn. 6.8 to be considered as a differential equation where derivatives are taken with respect to the parametric independent variable t. The equation is traditionally considered a function of two variables, both time t and depth z (or more generally x_j), but only temporal derivatives are present, so it remains an ordinary differential equation. Alternately, one may instead view the plastic strain and therefore Eqn. 6.8 as a function of a single variable say, depth z, that is parameterized with respect to an independent third variable t, considered as time in the present derivation. The plastic strain can be rewritten in the alternate form

$$\epsilon^{p}_{ij}(x_i(t)) = \frac{du^r_i(x_i(t))}{dx_j} \tag{6.9}$$

For the problem of material loading and unloading during impact, the position x_j and therefore the plastic strain, is parameterized according to the parameter t. No explicit parametric expression is defined for $x_j(t)$, but it is not necessary to have one for the present purpose. For the new parametric problem Eqn. 6.8 can be expressed

in terms of spatial gradients with the following transformation for $\dot{\epsilon}^p$ and $\ddot{\epsilon}^p$

$$\dot{\epsilon}^p(z(t)) \rightarrow \frac{d\epsilon^p(z(t))}{dz}\frac{dz}{dt}$$
$$\ddot{\epsilon}^p(z(t)) = \frac{d\dot{\epsilon}^p(z(t))}{dt} \rightarrow \frac{d}{dt}\left(\frac{d\epsilon^p(z(t))}{dz}\frac{dz}{dt}\right) = \frac{d}{dt}\left(\frac{d\epsilon^p(z(t))}{dz}\right)\frac{dz}{dt} + \frac{d\epsilon^p(z(t))}{dz}\frac{d^2z}{dt^2}$$
$$= \frac{d^2\epsilon^p(z(t))}{dz^2}\frac{dz}{dt}\frac{dz}{dt} + \frac{d\epsilon^p(z(t))}{dz}\frac{d^2z}{dt^2}$$
$$= \frac{d^2\epsilon^p(z(t))}{dz^2}\left(\frac{dz}{dt}\right)^2 + \frac{d\epsilon^p(z(t))}{dz}\frac{d^2z}{dt^2}$$

Where $\frac{d}{dt} = \frac{d}{dz}\frac{dz}{dt}$ and taking $\frac{dz}{dt} = v$ and $\frac{d^2z}{dt^2} = a$, as the velocity and acceleration respectively. The above parametric representation has been reduced to the one dimensional case, i.e. $x_j \rightarrow z$. At first glance, the transformation may look cumbersome. The first of these expressions is the strain rate, $\dot{\epsilon}^p$, and is a more general representation of the following familiar form upon substituting the true strain, $\epsilon = ln(z/z_o)$:

$$\dot{\epsilon} = \frac{d\epsilon}{dz}\frac{dz}{dt} = v\frac{d(ln(z) - ln(z_o))}{dz} = \frac{v}{z} \tag{6.10}$$

The last expression on the right of Eqn. 6.10, $\frac{v}{z}$ is the ratio of the velocity and length. For example, the length could represent the new distance at which two points on a specimen have been separated during a tensile test, v is the velocity at which separation occurs. Eqn. 6.10 is commonplace, and is a simple way of expressing the strain rate in many applications, for solving simpler mechanics problems. *The goal here is to keep the strain rate and strain acceleration as derivatives with respect to z because it provides the necessary form to describe the behavior of the residual stress as a function of depth*; as well as the correct solution for the necessary boundary conditions of the problem. The analysis is simplified by interpreting v and a as the shot velocity and acceleration respectively. The velocity and acceleration vary according to position below the shot, within the target material. However, the results should be order of magnitude accurate. The above expressions allow Eqn. 6.8 to be written in terms of z instead of t to obtain the desired equation. Substituting into Eqn. 6.8 yields a differential equation that relates the strain derivatives, up to second

order, to the residual stress.

$$v^2 A\frac{d^2\epsilon^p(z)}{dz^2} + aA\frac{d\epsilon^p(z)}{dz} + vB\frac{d\epsilon^p(z)}{dz} + C\epsilon^p(z) = \sigma^r(z) \tag{6.11}$$

Grouping like orders of the derivative in Eqn. 6.11 gives

$$v^2 A\frac{d^2\epsilon^p(z)}{dz^2} + (aA + vB)\frac{d\epsilon^p(z)}{dz} + C\epsilon^p(z) = \sigma^r(z) \tag{6.12}$$

Taking $A' \rightarrow v^2 A$, $B' \rightarrow aA + vB$, and $\sigma^r(z) \rightarrow \sigma_o^r \delta(z - z_o)$ yields a simpler form of Eqn. 6.12

$$A'\frac{d^2\epsilon^p(z)}{dz^2} + B'\frac{d\epsilon^p(z)}{dz} + C\epsilon^p(z) = \sigma_o^r \delta(z - z_o) \tag{6.13}$$

Equation 6.13 describes how the plastic strain varies in the z direction, directly below the impacting shot (i.e. x and y components equal to zero). By modifying the term, $\sigma^r(z)$, on the right hand side of Eqn. 6.13 further allows this equation to predict the behavior of the plastic strain. Namely, a value of the plastic strain that reaches a maximum just below the surface. Once the maximum value is attained, the strain quickly decays to zero exponentially. Prior to solving Eqn. 6.13, the assumptions of the boundary conditions are stated as follows:

1. The coordinate of the deformed surface is taken as $z' = z - z_o$, where z_o is a negative value representing the crater depth (alternately, with z_o negative, z' is equivalent to $z + z_o$)

2. The boundary conditions reference the original, undeformed, surface (i.e. the position of the surface before impacting begins) located at $z' = 0$, which is a distance z_o (the crater depth) from the deformed surface

3. Based on the first assumption the boundary conditions are $\epsilon^p(z' = z - z_o = 0) = 0$ and $\frac{d\epsilon^p(z'=z-z_o=0)}{dz} = 0$

The solution of Eqn. 6.13 based on the boundary conditions listed is now

$$\epsilon^p(z) = -\frac{\sigma_0^r \left(e^{(z-z_0)\left(-\frac{B'}{2A'}-\frac{\sqrt{B'^2-4A'C}}{2A'}\right)} - e^{(z-z_0)\left(-\frac{B'}{2A'}+\frac{\sqrt{B'^2-4A'C}}{2A'}\right)} \right)}{\sqrt{B'^2-4A'C}} \tag{6.14}$$

The heaviside function has been left out for convenience but acts to zero the residual stress for values of z' less than the crater depth, $|z_o|$. See appendix D for a derivation of Eqn. 6.14. The expression for the plastic strain in Eqn. 6.14 is related to the residual stress via Hooke's law

$$\sigma^r(z) = -C\frac{\sigma_0^r \left(e^{(z-z_0)\left(-\frac{B'}{2A'}-\frac{\sqrt{B'^2-4A'C}}{2A'}\right)} - e^{(z-z_0)\left(-\frac{B'}{2A'}+\frac{\sqrt{B'^2-4A'C}}{2A'}\right)} \right)}{\sqrt{B'^2-4A'C}} \tag{6.15}$$

Where $C = \frac{E}{1-\nu}$. The unknown stress quantity, σ_o^r, in Eqn. 6.15 is solved using the condition that the residual stress at the surface of the crater, $z = 0$ or equivalently $z' = |z_o|$, is approximately $\frac{1}{3}$ to 1 of the yield strength of the target material [13, 16]. Solving Eqn. 6.15 for $z = 0$ gives

$$\sigma^r(0) = C\frac{\sigma_0^r \left((e^{(-z_0)\left(-\frac{B'}{2A'}-\frac{\sqrt{B'^2-4A'C}}{2A'}\right)} - e^{(-z_0)\left(-\frac{B'}{2A'}+\frac{\sqrt{B'^2-4A'C}}{2A'}\right)} \right)}{\sqrt{B'^2-4A'C}} \tag{6.16}$$

Take $\lambda(0) = e^{(-z_0)\left(-\frac{B'}{2A'}-\frac{\sqrt{B'^2-4A'C}}{2A'}\right)} - e^{(-z_0)\left(-\frac{B'}{2A'}+\frac{\sqrt{B'^2-4A'C}}{2A'}\right)}$. Upon solving Eqn. 6.16 for σ_0^r provides the desired result

$$\sigma_0^r = \frac{\sigma^r(0)}{\lambda(0)}\frac{1-\nu}{C}\sqrt{B'^2-4A'C} \tag{6.17}$$

Substituting Eqn. 6.17 into Eqn. 6.16 yields

$$\sigma^r(z) = \frac{\sigma^r(0)}{\lambda(0)}\left(e^{(z-z_0)\left(-\frac{B'}{2A'}-\frac{\sqrt{B'^2-4A'C}}{2A'}\right)} - e^{(z-z_0)\left(-\frac{B'}{2A'}+\frac{\sqrt{B'^2-4A'C}}{2A'}\right)} \right) \tag{6.18}$$

or in more compact form

$$\sigma^r(z) = \sigma^r(0)\frac{\lambda(z)}{\lambda(0)} \tag{6.19}$$

The problem has effectively been reduced from finding the residual stress as a function of depth to simply finding the residual stress at the surface. This problem has been solved before, for example see Tirosh [13], and yields simple results. Tirosh uses an inclusion model and solves the in plane pressure acting on the inclusion to obtain the magnitude of the residual stress at the surface. Depending on plane stress or strain conditions he obtains values for the stress in the range

$$\frac{9}{32} \leq \left| \frac{\sigma^r(0)}{Y} \right| \leq \frac{3}{8} \tag{6.20}$$

or

$$\sigma^r(0) \approx -\frac{1}{3}Y \tag{6.21}$$

Y is the yield strength. The value is on the lower end of experimentally obtained values where $-\frac{1}{2}Y$ to $-\frac{4}{5}Y$ is found S. Shen [34]. S.A. Meguid [16] performed finite element studies on strain rate sensitive materials and showed that the residual stress at the surface can be larger than the yield strength of the material. Therefore from Eqn. 6.19

$$\sigma^r(z) = -hY\frac{\lambda(z)}{\lambda(0)} \tag{6.22}$$

Where h is chosen based on experimental or numerical results, and may reside between $\frac{1}{3}$ and 1. Eqn. 6.22 lacks a balancing tensile stress which indicates the solution is ideal for predicting the residual stress in a semi-infinite surface.

6.3 Validation of Model

Validation of Eqn. 6.22 is done using residual stress data from both experiment and finite element analysis. Experimental residual stress measurements from shot peened 7075-T7351 [97] were used to validate the strain gradient model. Rectangular aluminum specimens with a thickness, width, and length of 8.1 mm, 25.4 mm, and 115 mm respectively were shot peened on all four sides to 100% coverage. Two different Almen intensities, 8A and 12A, were applied to the test specimens. Shot velocities of

40 and 60 m/s are consistent with the range of Almen intensities used, as indicated in chapter 4. The residual stresses were measured using an X-ray diffraction stress analyzer with an X-ray target, CrK, every 0.1 mm. A mixture of S 230 and S 280 cast steel shots were used to shot peen the samples. Property and parameter inputs for the model include $\sigma^r(0) = 125$ MPa, $C = 1100$ MPa, and $R = 0.29 \times 10^{-3}$ m. The modulus parameter C was approximated from the stress strain curve provided in [111], for aluminum alloy 7050-T7452. The shot impact depth was not provided in [97] but a crater depth of 0.2mm was reported in [111] for a 50 m/s shot impact on 7050-T7451, a similar material, obtained from a finite element study. Therefore, d_o is set to 0.15mm and 0.20mm for the 40 m/s and 60 m/s impact respectively. A shot acceleration equal to $1 \times 10^6 \text{m/s}^2$ was used for both reproductions. The remaining parameters applied in the study include $B' = 3.5$ $kPa\text{-}sec$, $A' = 2.5 \times 10^{-6}$ $kPa\text{-}sec^2$. Fig. 6.1 provides comparisons of the model and measurements. The maximum subsurface residual stress predicted is within 10% of experiment but the location is underestimated by approximately $5\mu m$. In general, predictions are acceptable and within 10% for all experimental points, excluding the tensile region.

A Finite element study carried out by [111] provide residual stress results for 7050-T7451. Two different shot velocities, 22m/s and 50m/s, were considered and shot type S230 (R=0.29mm) for single and multiple shot impacts. Residual stress reproductions are compared with the 50m/s multiple shot impact simulation and 20m/s single shot speed. No substantial differences exist between single and multiple shot impact simulations aside from a deeper compressive layer caused by repeated impacting. Values for A', B', and C are identical with those used for predictions of the experimental results of Honda because aluminum alloys were used in each research study. An 8μm and 15μm crater depth for the 20m/s and 50m/s shot speeds were applied in the model. However, 5μm and 20μm depths were reported. The applied residual stress at the surface was 150 MPa for the 20m/s velocity and 281 Mpa for the 50m/s velocity, consistent with stresses reported at the surface in the

FEM. Comparisons made between the model and FEM are shown in Fig. 6.2. Again, the predicted maximum subsurface residual stress is consistent with FEM produced results but the location is approximately 25μm closer to the surface. Predictions of the residual stress depth are mixed. Single shot impact predictions over estimate the depth of the residual stress. But comparisons are more reliable for the multiple bombardment results indicating the model works best for repeated impacting. See appendix E for details of the computational calculations.

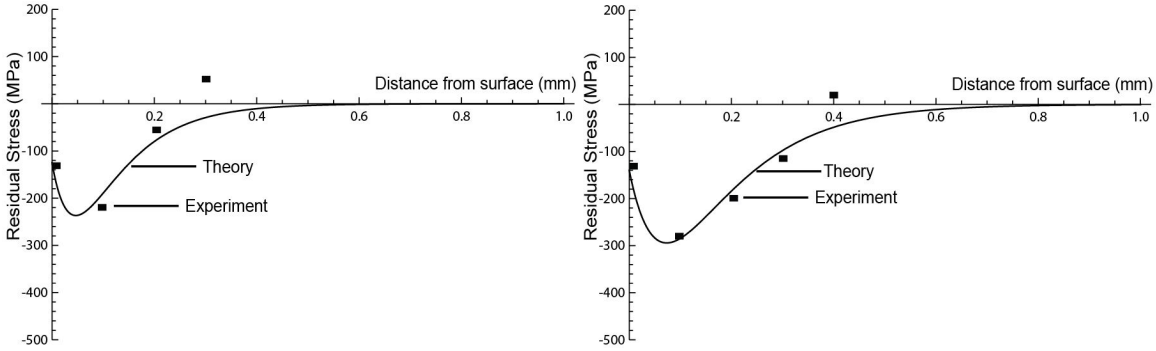

Figure 6.1: Comparison of residual stresses predicted from Eqn. 6.22 and measurements obtained from [97] for a) 40m/s and b) 60m/s shot speeds.

6.4 Conclusions

For shots impacting aluminum with a speed of 40 - 60m/s, the residual stress increases to a maximum of approximately 600 MPa at a depth of 50 - 100 μm and decreases to zero at a depth of approximately 150 to 200 μm's Bae [111]. Therefore, both the plastic strain and residual stress clearly exhibits large gradients. A semi analytical model based on the strain gradient behavior has been developed and validated for finite element simulations and experimental measurements of two aluminum alloys, 7075-T7351 and 7050-T7451, over the range of shot velocities 20, 40, 50, and 60m/s.

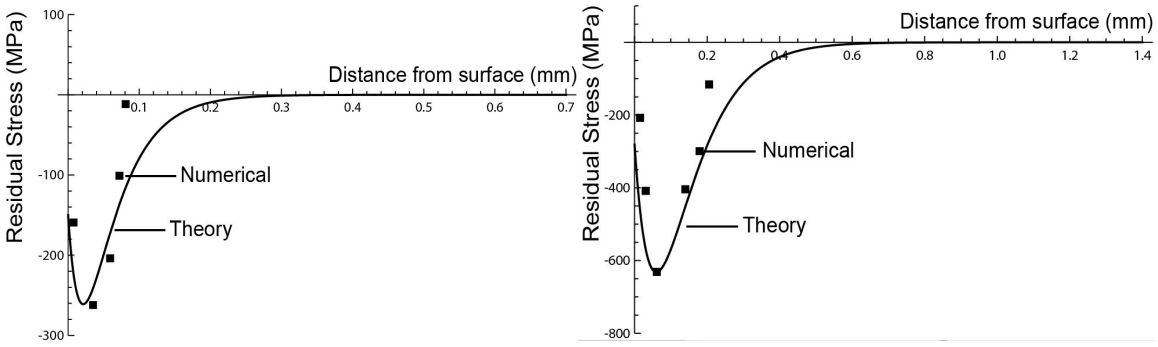

(a) (b)

Figure 6.2: Comparison of residual stresses predicted from Eqn. 6.22 and numerical simulations obtained from [111] for a) 20m/s and b) 50m/s shot speeds.

The results reveal that the model underestimates the depth of the maximum sub-surface compressive residual stress, and therefore compares most satisfactorily with residual stresses induced by multiple shot impacts. This conclusion is consistent for both numerical and experimental results. Though, the ad-hoc approach lacks the theoretical rigor of other strain gradient based theories [106]; *however its primary strength remains simplicity and relative accuracy.*

Chapter 7

SHAKEDOWN PREDICTION OF FATIGUE LIFE EXTENSION AFTER RESIDUAL STRESS RELAXATION VIA THE RECOVERY STRAIN

7.1 Introduction

The theory of shakedown is rooted in predicting material behavior that occurs during both low cycle fatigue and high cycle fatigue. Fatigue can be envisaged on the following three length scales [112]:

- The microscopic scale of dislocations
- The mesoscopic scale of grains
- The macroscopic scale of engineering structures

Fatigue is challenging because it can have similar or entirely contrasting physical behavior at each of these different length scales. Furthermore, the foundations of continuum mechanics begin to breakdown at the mesoscopic scale. Low cycle fatigue occurs when applied loads are large enough to induce irreversible deformation on a macroscopic scale. Plastic deformation therefore occurs throughout the bulk material. At the mesoscopic level, metal grains are subjected to homogenous irreversible deformation. In the low cycle fatigue region, there are three distinguishable domains of failure characterized by increasing load. These regions are alternating plasticity, also referred to as plastic shakedown, ratchetting (failure due to accumulation of plastic strains), and incremental collapse or failure from unrestricted plastic strains. During the initial cycles of low cycle fatigue plastic deformation occurs. Naturally, the plastic

deformation creates residual stresses which may prevent further accumulated plastic deformation (if shakedown occurs). The structure is said to plastically shakedown when the material will respond with closed cycles of plastic strain.

When plastic shakedown occurs, a given number of positive finite plastic strain cycles occur during the first half of the load cycle followed by equal magnitude negative strain the second half. The second half of the load cycle experiences no net gain in plastic strain. The structure shakes down to a steady state of non-cumulative cyclic plastic straining [113]. The structure will eventually fail over a finite number of load cycles

High cycle fatigue can also be divided into two distinct regions referred to as finite endurance limit and infinite endurance limit. Fatigue lives corresponding to a finite endurance limit are large, but definitely finite. Whereas fatigue lives are infinite for stress levels at the infinite endurance limit. On the macroscopic scale, there is no irreversible deformation, material behavior is purely elastic because all stresses are below the yield point of the material. However, on the mesoscopic scale, a certain number of grains experience an irreversible strain. In turn, a heterogenous plastic strain field is generated. Only misoriented crystals undergo plastic slip [112]. A residual stress will be generated from the heterogenous plastic strain field and shakedown may occur. Interestingly, in regard to the microstructure, the endurance limit and shakedown may be related [114].

7.2 Shakedown, Creep and the Recovery Process

7.2.1 A Brief Discussion of Classical Shakedown

A necessary, albeit approximate, criterion for shakedown to occur is for total plastic energy dissipated over any possible load path to be finite. Mathematically, finite plastic energy dissipation is expressed as

$$W_p = \int_0^t \sigma_{ij}\epsilon_{ij}^p dt < \infty \tag{7.1}$$

If the plastic energy dissipation does not satisfy Eqn. 7.1 then the structure will fail. For the criterion of Eqn. 7.1 to be satisfied, a residual stress field must be generated during loading. A time independent residual stress field guarantees that irreversible behavior has stopped and a purely elastic response is generated from loading. Thus, the necessary condition of shakedown is the existence of a time independent residual stress field. Therefore, the preceding description leads to the following

$$f[\sigma_{ij}^{e}(x,t) + \bar{\rho}_{ij}^{r}(x)] \leq \sigma_o \tag{7.2}$$

Where, $\sigma_{ij}^{e}(x,t)$ and $\bar{\rho}_{ij}^{r}(x)$ are the time varying elastic stress and steady state residual stress, respectively. The sum of the two stress distributions, the residual and elastic, should nowhere violate the yield criterion in the structure. The equality sign in Eqn. 7.2 produces the shakedown condition. Under certain circumstances a time dependent residual stress is a sufficient condition for shakedown. For example, in the presence of creep (and recovery), a constant residual stress is impossible. [115], instead, assumes the necessary condition for shakedown is the existence of a time dependent residual stress field, $\bar{\rho}_{ij}^{r}(x,t)$, which satisfies Eqn. 7.2.

7.2.2 A Brief Discussion of Creep and Shakedown

The material behavior of fatigue at elevated temperatures (temperatures more than $\frac{1}{2}$ the material melting point) are especially complex. Viscous strains become important and have a non-negligible impact on shakedown. Considerable effort has been devoted to identify under what circumstances shakedown will occur with creep strains present because of thermal loading, see for example Ponter [116].

Creep is a phenomenon that occurs under a wide variety of testing and environmental conditions. Creep can exist even at room temperature but is substantially more noticeable at elevated temperatures. Creep behavior can be classified as being limited or unlimited. Each of which occurs at different stress levels and operating conditions. Limited creep typically occurs in structural materials, such as metals,

at room temperature for stresses close to the yield point. Limited creep is usually irrecoverable after load removal [115]. Oftentimes, this behavior makes creep difficult to distinguish from plastic deformation. When both temperature and load increase creep becomes unlimited.

During repeated loading creep may increase indefinitely at loads less than the plastic shakedown limits (loads above which shakedown will not occur). Furthermore, the residual stress distribution which allows completely reversible behavior in plastic shakedown will relax away with time if creep is present. Creep has received considerable attention from researchers. But it should be pointed out that even creep behavior of materials under variable loading conditions is by no means well understood.

Martin and Hoff have pointed out that creep can be analyzed as a nonlinear elasticity problem. Therefore, approximate methods of elasticity may be used to solve problems involving creep Martin [117]. Creep strains have been analyzed assuming uniaxial behavior can be describe by a stress strain rate power law; which can be further generalized into a convex scalar function of the stress tensor, σ_{ij}. Klebenov, for example, uses the following form for the creep strain

$$\dot{\epsilon}^c_{ij} = \frac{\partial \Phi}{\partial \sigma_{ij}} \tag{7.3}$$

Where Φ is a convex homogeneous function characterizing the time-hardening creep behavior. Klebanov, examines the possibility of using Eqn. 7.3 to extend the classical results of Melan (1938) and Koiter(1956) to include unlimited creep.

7.2.3 A Brief Discussion of Recovery of a Shot Peened Residual Stress and Shakedown

At high temperatures researchers have suggested that the relaxation of a (shot peened) residual stress can be directly linked to a recovery strain. To be more precise, during purely thermal loading the recovery strain will increase and the elastic strain related

to the residual stress will decrease even though the plastic strain stays essentially constant. Relaxation occurs for multiple reasons. Thermal recovery and creep strains, both cause relaxation of the residual stress. Considerable work has been done verifying the occurrence of shakedown with creep and a similar approach is used here with the recovery strain.

The recovery strain is a macroscopic strain and appears during thermal recovery. Thermal recovery is caused by annihilation mechanisms of dislocations interacting with the crystalline vacancies. Recovery reorganizes the faults in the crystals, modifies the properties of the material and induces the relaxation of the residual stresses [118]. Therefore, thermal residual stress relaxation is a consequence of microplastic deformation processes thus converting elastic strains associated with residual stress into plastic ones J. Hoffman [119].

Several researchers including, W. Cao [120], have based their analysis of a relaxing residual stress on the following phenomenological expression of the recovery strain

$$\dot{\epsilon}_{ij}^{R} = A(1-\gamma(T))\dot{\rho}(T,t)\alpha_{ij} \tag{7.4}$$

Where A is a proportional coefficient, $\gamma(T)$ is the percentage of crystalline defects, and the tensorial quantity, α_{ij} is connected to the backstress of kinematic hardening. $\dot{\rho}$ is the variation of the mean density of defects and describes the kinetics of recovery. Eqn. 7.4 is a macroscopic tensorial parameter used to describe the microscopic changes of shot peened structures at elevated temperatures. I. Lillamand [121] points out that using a phenomenological approach has shortcomings. Eqn. 7.4 is not rigorous because the total strain tensors vary in the normal direction to the treated surface. Lillamand quantifies the strain changes, which are a state variable of the material, with mechanical equilibrium. He derives the following relation for the recovery strain

$$\underline{\epsilon}^{R} = \begin{pmatrix} \frac{1-\nu}{E}(\rho^{r}_{(g)} - \rho^{r}_{(r)}) & 0 & 0 \\ 0 & \frac{1-\nu}{E}(\rho^{r}_{(g)} - \rho^{r}_{(r)}) & 0 \\ 0 & 0 & -2\frac{1-\nu}{E}(\rho^{r}_{(g)} - \rho^{r}_{(r)}) \end{pmatrix}$$

Where $\rho^r_{(g)}$ and $\rho^r_{(r)}$ are the residual stress before and after recovery. The physical methodology of Lillamand determines that the recovery strain is a direct measure of the difference in the residual strain. The changes in the macroscopic strain distribution can be attributed to all the microstructural mechanisms that are activated during recovery. Namely, a release of previously pinned dislocations, created from shot peening, which leads to recovery. Dimensional changes in the shot peened structure are also linked to the recovery strain. Based on these results, the following conclusions are made and applicable in the present work:

- The recovery strain is closely comparable to the plastic strain
- The recovery strain will cause the residual stress to be time dependent
- Based on the first two items, shakedown is possible and the necessary condition is the existence of a safe time dependent residual stress

Thus, the work of Tirosh can be extended to include a shot peened structure that is subjected to fluctuating loads at elevated temperatures. Shakedown will provide accurate predictions of the improved fatigue limit (from shot peening) or alternatively, safe stress amplitudes, at elevated temperatures during residual stress relaxation. The diminishing benefits of shot peening can be quantified.

7.3 Lower Bound Shakedown in the Presence of a Recovery Strain

The first step we take here is deriving a lower bound shakedown theorem with a recovery strain present which induces relaxation at high temperatures. Melan was one of the first to develop a lower bound shakedown theorem. Decades later Koiter developed an upper bound theorem. Subsequent authors have derived lower and upper bound shakedown theorems with creep present. Classical shakedown analysis assumes that if a given elastic-plastic structure has already shaken down then the residual stress field will not vary anymore i.e. the residual stress developed throughout the

shakedown process is time independent. But if a recovery strain causes the residual stress to relax then it is not time independent. We must show that shakedown can still occur if a recovery strain exists. Therefore, we assume a necessary condition for shakedown is the existence of a safe time dependent residual stress field, $\bar{\rho}_{ij}$, which when taken together with the thermo-elastic stresses, is a stress field not violating the yield criterion at any point of a structure at any instant of time. The same technique has been employed by Klebanov for a static shakedown theorem of creep.

7.4 Lower Bound Shakedown

We begin the lower bound shakedown analysis and define the actual stress and strain in the body as

$$\sigma_{ij} = \sigma^e_{ij} + \rho^r_{ij} \tag{7.5}$$

$$\epsilon_{ij} = \epsilon^{(e)}_{ij} + \epsilon^{res}_{ij} + \epsilon^p_{ij} + \epsilon^\theta_{ij} + \epsilon^c_{ij} + \epsilon^R_{ij} \tag{7.6}$$

Where σ^e_{ij} and ρ^r_{ij} are the stresses that would exist in the body if it was perfectly elastic and the instantaneous residual stress field respectively. The superscript "r" is to denote the influence of the recovery process on the residual stress. The total strain is decomposed into all strain components present during the initial cycles of plastic deformation and thermal loading i.e. elastic strain ($\epsilon^{(e)}_{ij}$), elastic strain corresponding to the residual stress (ϵ^{res}_{ij}), plastic strain (ϵ^p_{ij}), thermal strain (ϵ^θ_{ij}), creep strain (ϵ^c_{ij}) and the newly included recovery strain or (ϵ^R_{ij}).

The residual stress can be written as $\rho^r_{ij} = C^{-1}_{ijkl}\epsilon^{res}_{kl}$. Creep is included to show how prior authors handled adding a viscous term. The same fundamental approach/techniqe is used to incorporate the recovery strain but of course with some slight differences because the physical mechanism responsible for residual stress relaxation and recovery are fundamentally different than creep. The strain rate, $\dot{\epsilon}_{ij}$, is easily found by taking the time derivative of Eqn. 7.6 above.

Now, define a safe stress distribution $\sigma_{ij}^{(s)}$ which is equal to the sum of a time dependent residual stress, $\bar{\rho}_{ij}^{r}$, and elastic stress, σ_{ij}^{e}, that nowhere violates the yield criteria

$$\sigma_{ij}^{(s)} = \sigma_{ij}^{e} + \bar{\rho}_{ij}^{r} \tag{7.7}$$

The other corresponding safe field variables are written as $\bar{\epsilon}_{ij}$, $\bar{\epsilon}_{ij}^{res}$, $\bar{\epsilon}_{ij}^{c}$, $\bar{\epsilon}_{ij}^{R}$, and by definition $\bar{\epsilon}_{ij}^{p} = 0$. Consider the non negative elastic complementary energy function

$$A(t) = \int_V \frac{1}{2} C_{ijkl}(\rho_{ij}^{r} - \bar{\rho}_{ij}^{r})(\rho_{kl}^{r} - \bar{\rho}_{kl}^{r})dV \geq 0 \tag{7.8}$$

The derivative of the elastic energy with respect to time is

$$\dot{A}(t) = \int_V C_{ijkl}(\rho_{ij}^{r} - \bar{\rho}_{ij}^{r})(\dot{\rho}_{kl}^{r} - \dot{\bar{\rho}}_{kl}^{r})dV \tag{7.9}$$

Eqn. 7.9 can be rewritten in terms of the safe field variables and strain variables by multiplying C_{ijkl} through

$$\dot{A}(t) = \int_V (\rho_{ij}^{r} - \bar{\rho}_{ij}^{r})(C_{ijkl}\dot{\rho}_{kl}^{r} - C_{ijkl}\dot{\bar{\rho}}_{kl}^{r})dV =$$
$$\int_V (\rho_{ij}^{r} - \bar{\rho}_{ij}^{r})([\dot{\epsilon}_{ij} - \dot{\epsilon}_{ij}^{p} - \dot{\epsilon}_{ij}^{c} - \dot{\epsilon}_{ij}^{R}] - [\dot{\bar{\epsilon}}_{ij} - \dot{\bar{\epsilon}}_{ij}^{p} - \dot{\bar{\epsilon}}_{ij}^{c} - \dot{\bar{\epsilon}}_{ij}^{R}])dV$$

We know from the principle of virtual work that

$$\int_V (\rho_{ij}^{r} - \bar{\rho}_{ij}^{r})(\dot{\epsilon}_{ij} - \dot{\bar{\epsilon}}_{ij})dV = 0 \tag{7.10}$$

which gives

$$\dot{W} = -\int_V (\rho_{ij}^{r} - \bar{\rho}_{ij}^{r})([\dot{\epsilon}_{ij}^{p} + \dot{\epsilon}_{ij}^{c} + \dot{\epsilon}_{ij}^{R}] - [\dot{\bar{\epsilon}}_{ij}^{c} + \dot{\bar{\epsilon}}_{ij}^{R}])dV =$$
$$-\int_V (\rho_{ij}^{r} - \bar{\rho}_{ij}^{r})([\dot{\epsilon}_{ij}^{p} + (\dot{\epsilon}_{ij}^{c} - \dot{\bar{\epsilon}}_{ij}^{c}) + (\dot{\epsilon}_{ij}^{R} - \dot{\bar{\epsilon}}_{ij}^{R})]dV$$

and after substituting Eqn. 7.5 and 7.7 we have

$$\dot{W} = -\int_V (\sigma_{ij} - \sigma_{ij}^{(s)})([\dot{\epsilon}_{ij}^{p} + (\dot{\epsilon}_{ij}^{c} - \dot{\bar{\epsilon}}_{ij}^{c}) + (\dot{\epsilon}_{ij}^{R} - \dot{\bar{\epsilon}}_{ij}^{R})]dV \tag{7.11}$$

The combination of three different concepts tells us that expression 7.11 is negative. First, break up the integral into three different quantities

$$\int_V (\sigma_{ij} - \sigma_{ij}^{(s)})\dot{\epsilon}_{ij}^{p} dV \tag{7.12}$$

$$\int_V (\sigma_{ij} - \sigma_{ij}^{(s)})(\dot{\epsilon}_{ij}^{c} - \dot{\bar{\epsilon}}_{ij}^{c}) dV \tag{7.13}$$

$$\int_V (\sigma_{ij} - \sigma_{ij}^{(s)})(\dot{\epsilon}_{ij}^{R} - \dot{\bar{\epsilon}}_{ij}^{R}) dV \tag{7.14}$$

We know $(\sigma_{ij} - \sigma_{ij}^{(s)})$ is positive because our safe stress field $\sigma_{ij}^{(s)}$ always lies inside the yield surface. Eqn. 7.12 is positive because the signs of the stress and strain rate are identical. During plastic deformation energy dissipation is positive, i.e. $\sigma\dot{\epsilon} \geq 0$; which is also known as Druckers Postulate. Eqn. 7.13 is also positive because the creep behavior is governed by a convex function [115]. Eqn. 7.14 is positive for the same reason as Eqn. 7.12. Recovery is a process of microplastic deformation converting elastic strains of the residual stress into plastic strains and is governed by Druckers Postulate as well. Therefore, Eqn. 7.11 is always negative. And because W is always nonnegative $\dot{W}$ must tend to zero and plastic deformation will not continue indefinitely. The structure will shakedown to a stabilized plastic strain field.

We have shown shakedown is still applicable with the presence of thermal recovery and a relaxing residual stress. The second part of this work will focus on implementing shakedown to predict fatigue-safe load amplitudes at high temperatures. Tirosh provides a technique to solve safe loading amplitudes for a stable residual stress field at room temperature. His approach can possibly be extended to predict safe fatigue scenarios for high temperature fatigue with residual stress relaxation present.

7.5 Application of Shakedown at Room Temperature to Shot Peened Ti-6Al-4V and Ti-5Al-5Mo-3Cr

The proof of Melan's lower bound shakedown theorem provided in section 7.4 is independent of the methodology utilized by Tirosh to calculate the infinite life fatigue

limit of a shot peened structure. However, the proof was necessary because shakedown has never been shown to be valid with a recovery strain present. Section 7.4 permits the use of Tirosh's model in the presence of a relaxing residual stress and recovery strain. The method devised by Tirosh is applied to fatigue data of Bae [111] for two titanium alloys, Ti 6Al-4V and Ti-5Al-5Mo-3Cr. Tirosh [13] uses shakedown to predict the infinite life ($N \geqslant 10^7$) fatigue limit for shot peened cylindrical specimens undergoing axial fatigue. Tirosh assumes (as is done here) that the residual stress throughout the shot peened layer is $-\frac{1}{3}\sigma_0$, where σ_0 is the yield strength. The stress ratio for the data utilized here is $R = 0.1$. From the data, a peak stress at infinite life (N=10^7) for an unpeened specimen is approximately 550 MPa and 600 MPa for Ti 6-4 and Ti 5553 respectively. Therefore, the mean stresses are $(550 + 55)/2 \approx 300MPa$ and $(600+60)/2 = 330MPa$ along with stress amplitudes of $(550-55)/2 \approx 250MPa$ and $(600 - 60)/2 = 270MPa$. The normalized mean stresses for each specimen are $\sigma_m/\sigma_0 = 300/1100 = 0.275$ and $\sigma_m/\sigma_0 = 330/1200 = 0.275$ for Ti 64 and Ti 5553 respectively. Now, the change in normalized mean stress can be calculated from the following

$$\Delta\sigma_m/\sigma_0 = 0.275 - \frac{2\sigma_r}{\sigma_0 3} = 0.275 - 0.22 = 0.055 \tag{7.15}$$

The change in normalized stress amplitude can be identified from Fig. 7.1 and is

$$\Delta\sigma_a/\sigma_{th} = 0.95 - 0.8 = 0.15 \tag{7.16}$$

Where σ_{th} is the threshold stress amplitude and is the stress amplitude at which the structure can survive at least $N_f \geq 10^7$ cycles under fully reverse cycles ($\sigma_m = 0$). The predicted increase in stress amplitude because of shot peening is $0.15 \times 250 = 37.5MPa$ and $0.15 \times 270 = 40.5MPa$ or approximately $40MPa$ for each material. The predicted stress amplitudes are now $250+40 = 290MPa$ and $270+40 = 310MPa$ for Ti 64 and Ti 5553 respectively. The corresponding peak stresses are $290 + 300 = 590MPa$ and $310 + 330 = 640MPa$. Extrapolating the fatigue data in [111] to $N = 10^7$ cycles gives an experimental fatigue limit of 600 and 635 MPa for Ti-64 and

Ti-5553 respectively, within 10% of theory.

7.6 Application of Shakedown at Elevated Temperatures to Shot Peened 403 Stainless Steel

Shakedown provides reasonable predictions of the increase in the infinite life fatigue strength at room temperature. Next, the shakedown principle is applied to high temperature fatigue, when the shot peening induced residual stress has relaxed partially due to an increase in the recovery strain. The fatigue life of the shot peened part has obviously diminished. The goal is to predict by how much the shot peening benefits have decreased. The proof in section 7.4 justifies using shakedown at high temperatures when a recovery strain is present. By extending the application of shakedown theory, a prediction of the infinite life fatigue strength can be obtained during relaxation of the residual stress. Degradation of the fatigue strength during high temperature, high cycle fatigue is of particular importance in the turbine industry. Childs [122] performed rotational beam fatigue experiments to determine the effect of elevated temperatures on the endurance limit of shot peened 403 stainless steel at room temperature, 260, and 400°C. The bar stock was shot peened at Almen intensities 8 - 10A. Prior to fatigue testing, the shot peened samples were stress relieved for 50 hrs at the testing temperature. Childs results showed that the endurance limit reduced from 460 MPa, at room temperature, to 400 MPa at 260 and 400°C. For an unpeened steel specimen, the endurance limit at 260°C is approximately 375 MPa. The calculation for both the room temperature and elevated temperature endurance limit is identical. For R = -1, the mean stress is zero, which gives a normalized mean stress of zero. The change in normalized mean stress is therefore calculated to be

$$\Delta\sigma_m/\sigma_0 = 0 - \frac{2\sigma_r}{3\sigma_0} \tag{7.17}$$

σ_r is the value of the relaxed residual stress measured from an Almen strip exposed to a temperature of 370°C, within the testing temperature range of the fatigue specimens.

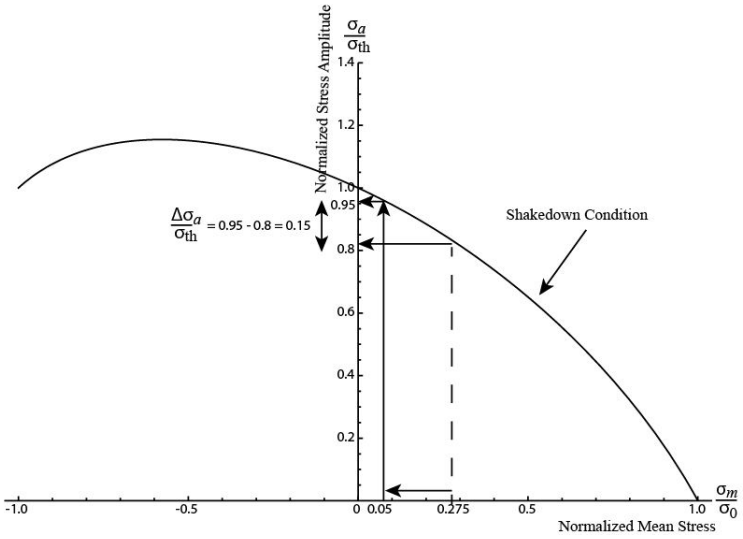

Figure 7.1: Procedure for calculating the infinite life fatigue limit of a shot peened fatigue specimen. The change in normalized stress amplitude is found from the change in normalized mean stress. The change in normalized

The Almen strip was also shot peened at the same intensity as the fatigue samples, 8 - 10A. Table 7.1 provides the experimental residual stress data. According to Fig. 7.1, the change in normalized stress amplitude is

$$\Delta\sigma_a/\sigma_{th} = 1.1 - 1.0 = 0.10 \tag{7.18}$$

Therefore, the predicted increase in stress amplitude is 375 + 37.5MPa=412.5MPa; which compares well with the experimental value of 403MPa. Fig. 7.2 provides results for the endurance limit calculated from the residual stress values in Table 7.1

7.7 Conclusion

We have shown that the lower bound shakedown theorem of Melan provides accurate predictions of the infinite life fatigue limit of shot peened specimens both at room temperature and after partial relaxation of the residual stress. However, limitations are present in the analysis. The residual stress applied in the model was measured

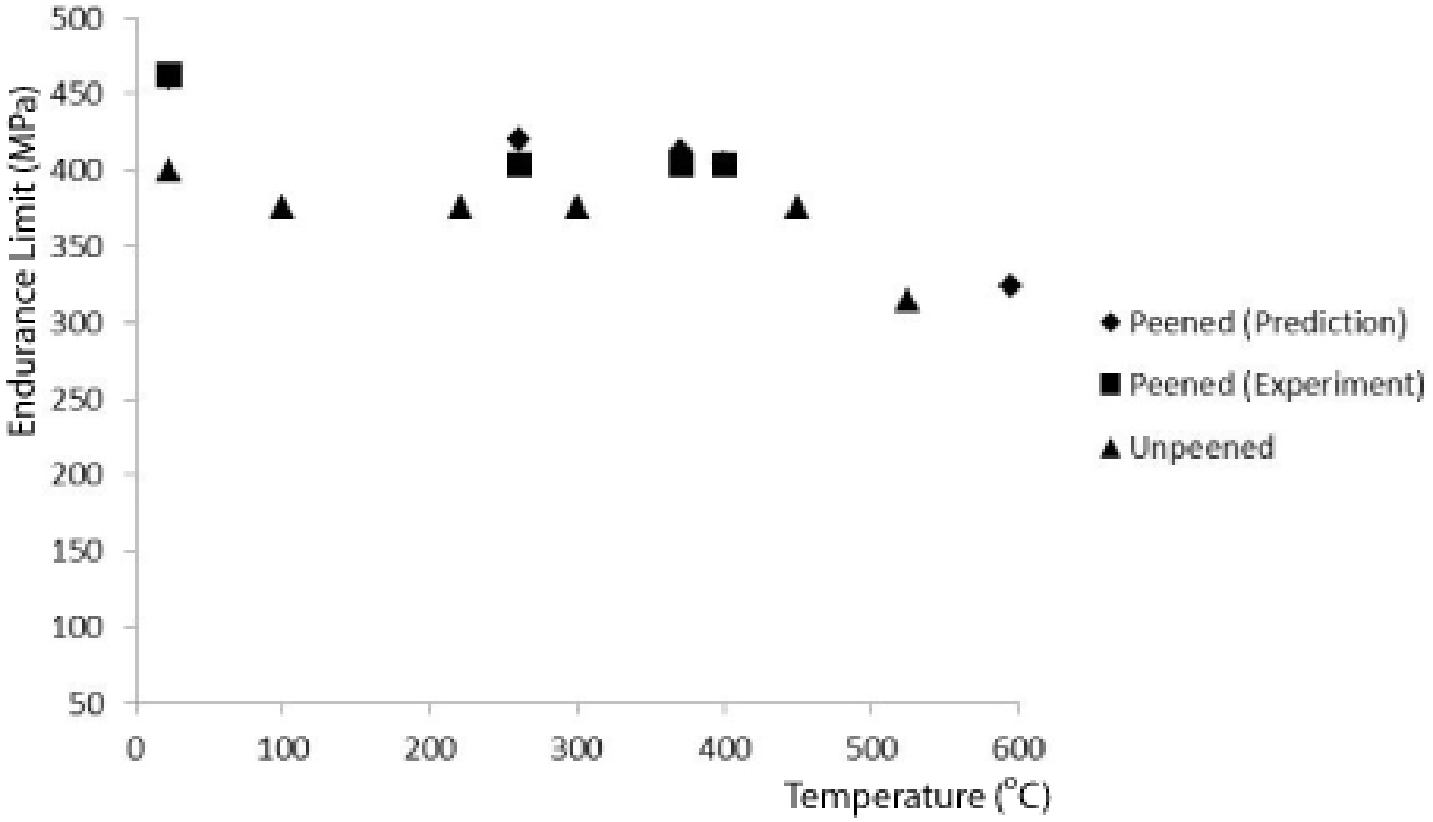

Figure 7.2: Plot comparing experimentally measured endurance limit (MPa) with analytically predicted endurance limit

from Almen strips *not* from the fatigue specimens. The Almen strips were shot peened with the same intensity but inevitably differences in the residual stress exist because of the different geometry. By using the residual stresses measured from the Almen strip, we do not need to be concerned with the theoretical complications associated with the viscous behavior of the material and its influence on the residual stress. Modeling of such phenomenon is not the focus of the present work.

Table 7.1: Summary of theoretical and experimental fatigue safe stress amplitudes (i.e. fatigue limit or fatigue threshold)

Temp./Mat	Res. Stress	Normalized Mean Stress	Change in Normalized Mean Stress	Fatigue/Endurance Limit ***Exp.***	Fatigue/Endurace Limit ***Theory***	Error
23/Steel	-515	0	-0.55	462 [122]	460	0.4%
260/Steel	-269	0	-0.28	403 [122]	420	-2.2%
370/Steel	-212	0	-0.25	403 [122]	412	-2.2%
400/Steel	-190	0	-0.20	403 [122]	405	-0.4%
23/Ti-6-4	-367	0.275	0.05	600 [111]	590	1.7%
23/Ti-5-5-5-3	-400	0.275	0.05	635 [111]	640	-0.8%

Chapter 8
SUMMARY AND CONCLUSION

8.1 Summary

A comprehensive theoretical investigation of the residual stress has been conducted. First, a mechanistic model, based on J3, was developed. Then, the time dependency of the plastic strain during loading and unloading was examined, followed by a strain gradient study of the residual stress. Finally, shakedown was used to predict the diminishing fatigue benefits resulting from a relaxing residual stress. Each model along with key aspects is summarized below.

The research compiled in the dissertation comprise 4 unique contributions to the field of shot peening. In chapter 4, incremental plasticity was used with a J3 dependent flow rule to calculate the plastic strain as a function of the third invariant, J3. The elasto-plastic deviatoric stress was then calculated from the J3 dependent plastic strain to provide a closed form solution of the J3-dependent residual stress. The first model is an extension of Li's work based on Iliushin's J2 deformation theory of plasticity. By incorporating the third invariant of the elasto-plastic deviatoric stress tensor, combined loading that occurs during shot peening is accounted for via the parameter c. For all experimental predictions, the J3 model is found to compare more satisfactorily than Li's model based on J2 alone.

The second model is based on the impulsive loading that occurs during shot peening and yields a closed form solution of the time dependent plastic strain. During impulse loading, a strain rate as well as a strain acceleration is produced from the energetic impact. Surface strikes can occur on time intervals shorter than 1μs. A second order differential equation of the plastic strain, in time, is derived from first

principles. From the strain compatibility conditions, the in-plane inelastic strain in the r and θ directions is zero for a semi-infinite structure. Based on equilibrium, the only non-zero components of the residual stress tensor are in the r and θ direction. These conditions provide the mathematical and physical basis to derive the following ODE

$$A\ddot{\epsilon}^p + B\dot{\epsilon}^p + C\epsilon^p = -C\epsilon^r = -\sigma^r \tag{8.1}$$

Eqn. 8.1 is similar to an empirical relation introduced in Kornilov [99]. Kornilov concludes that the stress-strain state of bodies subjected to impulsive loading depends on the strain acceleration. The desired solution must match the physical behavior, namely

- The strain must tend towards a constant value for large time
- The strain rate reaches a maximum value some time after the initial impact and tends to zero for large time

Therefore, Eqn. 8.1 is modified to the following form so the solution satisfies these requirements

$$A\dddot{\epsilon}^p(z,t) + B\ddot{\epsilon}^p(z,t) + C\dot{\epsilon}^p(z,t) = \sigma^r(z)\delta(t-t_0) \tag{8.2}$$

The solution to Eqn. 8.2 provides the exact behavior listed and the validity is compared against finite element predictions.

Eqn. 8.1 is also used to derive a semi-analytical model of the residual stress versus depth. In chapter 6, the plastic strain is parameterized with respect to time, i.e. $\epsilon^p_{ij}(x_i(t))$. Applying a simple transformation to Eqn. 8.1 permits a change of variable from t to z. Therefore, Eqn. 8.1 becomes a differential equation that is a function of depth, z, and the solution for the residual stress comes from the strain gradient equation

$$v^2 A\frac{d^2\epsilon^p(z)}{dz^2} + (aA + vB)\frac{d\epsilon^p(z)}{dz} + C\epsilon^p(z) = \sigma^r(z) \tag{8.3}$$

The solution to Eqn. 8.3, is exponential and decays to zero for depths greater than a few hundred micrometers. The same type of solution was obtained by Mindlin [106] for the residual strain, which also decays exponentially into the interior. Mindlin performed a rigorous analysis in which he derives equilibrium, boundary conditions and constitutive equations for a linear elastic material in the infinitesimal strain and its first and second gradients. Mindlin states that the second strain gradient has particular significance in regard to the cohesive force, which gives rise to the modulus of cohesion. The modulus of cohesion is directly related to surface tension, or equivalently the energy, per unit area, associated with the formation of a new surface. Surface tension clearly plays a significant role during shot peening because shots impact and increase the surface area of the target (this is why an Almen strip bows post-peening). *The primary difference between the results here and that of Mindlin is the length scale considered.* The plastically deformed peened layer is no less than a hundred micrometers but Mindlin considers interatomic distances in his models. The two models, developed entirely independent of each other, use fundamentally different approaches; however the strong similarities between the two solutions for the strain behavior is intriguing.

The fourth and final model is an application of the shakedown principle to approximate the infinite life fatigue limit of shot peened structures undergoing fatigue at elevated temperatures. The technique of using shakedown is adopted from Tirosh [13]. Shakedown will only occur under certain circumstances so verification, usually in the form of a proof using energy principles, is necessary. For example, if energy dissipation continues indefinitely because of creep strains, then shakedown will not occur. At elevated temperatures (+300 C) the residual stress will decrease in magnitude in response to a recovery strain. Therefore, a proof is provided in chapter 7 verifying the use of shakedown for a relaxing residual stress when a recovery strain is present. Verification of shakedown is followed by predictions of the room temperature infinite life fatigue strength of two titanium alloys, Ti-6Al-4V and Ti-5Al-5Mo-3Cr.

The infinite life fatigue strength at elevated temperatures is predicted and compared against experimental data of shot peened stainless steel.

8.2 Conclusions

The analytical work of chapter 4 is a contribution to the shot peening literature, as well as the field of solid mechanics for several reasons. To this author's knowledge, the thesis presents the first work determining the influence of the third invariant on a residual stress induced during shot peening. One of the goals of this thesis was to answer the question of how the third invariant influences the residual stress. The parameter c, introduced by the J3 dependent flow rule, is a material parameter and was found to influence the residual stress considerably. Conclusions of chapter 4 are highlighted:

- Predictions of two titanium alloys indicate that a value of c = -3.375 is more accurate than c =0, or equivalently, no influence of J3.

- Predictions of a steel alloy indicate that a value of c=2.25, provides better comparisons than J2 theory.

- Fig. 4.3 shows that c can change the normalized residual stress from approximately -0.55 to -0.8 for c=-3.375 and c=2.25 respectively. The normalized stress for c=0 is -0.65, therefore a maximum difference of 23% is present between J2 and J2-J3 theory.

A solution for the time dependent plastic strain is obtained in chapter 5 by deriving a rheological model that contains the strain acceleration. Motivation for the model is based on the impulsive nature of loading. Strain rates can be as large as $10^5 - 10^6 \frac{1}{s}$, implying the strain acceleration is a non-negligible aspect of the time dependent mechanical behavior. The analytically derived plastic strain and strain rate exactly describe material behavior predicted from finite element models. Indicating that the

strain acceleration was required in the mathematical framework. Conclusions that can be made based on the work from chapter 5 is as follows:

- Material behavior during impulse loading is dependent on the strain acceleration.
- Results of the theoretical model are within 10% of finite element simulation.

The time dependent plastic strain equation is modified with a transformation that converts the plastic strain rate and plastic strain acceleration to first and second order plastic strain gradients. Comparisons with experimental measurements and finite element studies for two aluminum alloys, show a strong correlation with the model. However, one limitation of the model is an under prediction of the depth at which the maximum residual stress occurs. The following conclusions are made:

- The error between experiment and numerical results is within 10%.
- Comparisons are more accurate for multiple shot impacts than a single shot.

Research indicates that the recovery strain is responsible for the relaxation of a shot peened residual stress at elevated temperatures. In the past, the lower bound shakedown theorem has been verified for plastic strains, thermal strains, and even creep strains; however no research exists with a recovery strain present. Therefore, a lower bound shakedown theorem with a recovery strain has been verified in chapter 7. Recovery is a microplastic deformation process converting elastic strains of the residual stress into plastic strains. Thus, the recovery strain is governed by Drucker's postulate, like the plastic strain, ϵ_{ij}^{p}, and shakedown will occur. The theory of shakedown predicts the infinite life fatigue strength of shot peened stainless steel at room temperature to be 460 MPa, identical with experiment. At 260 degrees C, the experimental fatigue strength is 400 MPa, whereas theory provides 420 MPa. Finally,

at 400 C both the model and theory give values of 400 MPa. Thus, we arrive at the following

- Melans lower bound shakedown theorem adequately predicts the extended life fatigue limit of a shot peened structure at room and elevated temperatures.

- All predictions of the infinite life fatigue limit at elevated temperatures are accurate to within 10% of experimental measurements.

8.3 Future Research Directions and Recommendations

The J2-J3 model can be extended to unconstrained plastic flow. When the plastic zone under the spherical indenter is no longer confined by the surrounding elastic continua, plastic flow becomes unconstrained. This causes plastic flow to bulge up from the original surface rather than sinking-in. The resolved stresses (to be used in J3) can then be taken from the pioneering work on incremental-plasticity under spherical indentation to elasto-plastic solids [by R. Hill,et al, 1989, Proceedings of the Royal Society of London] without relying anymore on Herzian's solutions. The incremental strain analysis used throughout chapter 4 remains applicable, however the environment needs to be redefined and a residual stress analysis based on a single indentation should be the focus instead of shot peening. At 100% coverage, the sinking in and bulging up behavior that defines constrained and unconstrained plastic flow is masked because of overlapping impacts. The complex process makes solving problems based on unconstrained flow less clear, but the approach remains a valid research subject. Furthermore, the influence of the third invariant on a residual stress, not necessarily produced by shot peening, is also a research area with potential.

The plastic strain and residual stress analysis of chapters 5 and 6 provide a starting point for a new way of studying impulsive loading of structures. Future work should be directed to finite element studies to better characterize the parameters A, B, and C. Experiments are encouraged as well, but because of the extremely short duration of

loading, this may result in substantial difficulty. An in depth finite element study will give some insight into the interpretation of these parameters and answer some lasting questions. For example, is B the dynamic viscosity and how can we interpret C? If the work is to be viewed as more than a semi-analytical model, these questions need to be answered. Two further research areas can be explored. There are many impulsive processes that the strain gradient based model can potentially be applied. Machining, for example, is another process where strain accelerations influences the mechanical process. Other surface treatment processes, like roller burnishing, that are similar in nature to shot peening may also benefit from the same analytical treatment. The solution to Eqn. 8.1 permits complex solutions, which is traditionally used to describe wave propagation. Elastic and plastic wave propagation, though not discussed here because it has a negligible affect on the residual stress, is another major topic of research in the theoretical and applied mechanics community. The author cannot definitively say whether, elastic or plastic wave propagation is applicable or not but, we have seen Eqn. 8.1 provides much flexibility when solving challenging mechanics problems.

The key requirements in the derivation of Eqn. 8.1 are

- A semi-infinite structure
- Axisymmetric geometry
- A zero state of shear stress

This list of boundary conditions are required for Eqn. 8.1 to be valid. The conditions are equally applicable for different colliding objects, for example, a rigid flat punch. Future work can verify the model for any impulsive collision that satisfies the list of requirements.

BIBLIOGRAPHY

[1] P.E. Cary. History of shot peening. *International Conference on Shot Peening 1*, 1981.

[2] H. Herts. Misc. papers (translated by jones and schott). *London: Macmillan*, 1896.

[3] L. Johnson. Contact mechanics. *Cambridge University Press*, 1985.

[4] B. Leroy. Collision between two balls accompanied by deformation: A qualitative approach to hertz's theory. *Am. J. Phys.*, 53(4):346–349, 1985.

[5] R. C. McClung. A literature survey on the stability and significance of residual stresses during fatigue. *Fatigue and Fracture of Engineering Materials and Structures*, 30(3):173–205, 2006.

[6] J. C. Campbell. Shot peening for improved fatigue properties and stress corrosion resistance. *Battelle Columbus Labs, MCIC Rep. 71-02*, 1972.

[7] H. Kakishima M. Matsui. Improvement of tribological performance of steel by solid lubrican shot peening in dry rolling/sliding contact wear tests. *Wear*, 260 (6):669–673, 2005.

[8] K. Tsuchiya M. Umemoto, Y. Todaka. Formation of nanocrystalline structure in steels by air blast shot peening. *Mater. Trans*, 44(7):1488–1493, 2003.

[9] A. Nikulari J. F. Flavenot. La mesure des contraintes residuelles, methode de la fleche, methode de la source de contraintes. *Les memories, Technique due*, 1977.

[10] S.T.S. Al-Hassani. Mechanical aspects of residual stress development in shot peening. *ICSP-1*, 1981.

[11] J. Frelat G. Inglebert Guechichi, L. Castex. Predicting the residual stresses due to shot peening. *Impact Surface Treatment*, 1986.

[12] W. Duo J.K. Li, Y. Mei. Mechanical approach to the residual stress field induced by shot peening. *Materials Science and Engineering*, 147(2):167–173, 1991.

[13] J. Tirosh. Extended fatigue life by shot peening process via shakedown analysis. *Journal of Applied Mechanics*, 75(1):11005–11012, 2008.

[14] D.C. Webb S.T.S. Al-Hassani, K. Kormi. Numerical simulation of multiple shot impact. *Internation Conference on Shot Peening 7*, 1999.

[15] J.C. Stranart S.A. Meguid, G. Shagal. Finite element modelling of shot peening residual stresses. *Journal of Materials Processing Technology*, 92(93):401–404, 1999.

[16] J.C. Stranart S.A. Meguid, G. Shagal. 3d fe analysis of peening of strain rate sensitive materials using multiple impingement model. *International Journal of Impact Engineering*, 27(2):119–134, 2002.

[17] M. Tokuda Y. Ohashi. The precise measurements of plastic behavior of mild steel tubular specimens subjected to combined torsion and axial force. *Journal of the Mechanics and Physics of Solids*, 21(4):241–244, 1973.

[18] E.W. Milburn. X-ray diffraction applied to shot peened surfaces. *Met. Treat.*, 1945.

[19] H.K.D.H Bhadeshia P.J. Withers. Residual stress. part 1 - measurement techniques. *Materials Science and Technology*, 17(4):355–365, 2001.

[20] A.A. Biggs. Analysis of factors affecting almen strip arc height after shot peening. *Masters Thesis*, 1999.

[21] M. Avrami. Kinetics of phase change. i general theory. *J. Chem. Phys.*, 7(12): 1103–1112, 1939.

[22] D. Kirk. Coverage: Development, measurement, control and significance. *The Shot Peener*, 2002.

[23] J.L. Davis. Analytical modeling of shot peening coverage and predictions of manually peened surfaces. *Masters Thesis*, 2009.

[24] D. Kirk. Shot peening. *Aircraft Engineering and Aerospace Technology: An International Journal*, 71(4):349–361, 1999.

[25] J.O. Almen. Shot peening intensity measurement. *The Shot Peener*, 1992.

[26] Y.F. Al-Obaid. Shot peening mechanics: experimental and theoretical analysis. *Mechanics of Materials*, 19(2-3):251–260, 1995.

[27] G. Inglebert M.T. Khabou, L. Castex. The effect of material behaviour law on the theoretical shot peening results. *European Journal of Mechanics A/Solids*, 9(6):537–549, 1990.

[28] G. Inglebert N. Point S. Slim, T. Harm. Prediction of residual stresses due to shot peening using modelling of the material behavior. *Materials and Manufacturing Processes*, 10(3):579–588, 1995.

[29] J. Casier J. Zarka. Elastic plastic response of a structure to cyclic loading: practical rules. *Mechanics Today*, 6:93–198, 1979.

[30] J.M. Proix G. Inglebert, J. Frelat. Structures under cyclic loading. *Arch. Mech.*, 37(4-5):365.

[31] J. Frelat G. Inglebert. Quick analysis of inelastic structures using a simplified method. *Num. Engng. Design*, 116(3):281–291, 1989.

[32] L. Castex R. Fathallah, G. Inglebert. Prediction of plastic deformation and residual stresses induced in metallic parts by shot peening. *Materials Science and Technology*, 14(7):631–639, 1996.

[33] A.A. Iliushin. Plasticity. *National Press of Technical and Theoretical Literature*, 1948.

[34] S.N. Atluri S. Shen. An analytical model for shot peening induced residual stresses. *Computers, Materials and Continua*, 4(2):75–85, 2006.

[35] S.T.S. Al-Hassani. An engineering approach to shot peening mechanics. *ICSP-2*, 1984.

[36] B. Maffeo O. Prakash B. Bhuvaraghan, S.M. Srinivasan. Analytical solution for single and multiple impacts with strain rate effects for shot peening. *CMES*, 57 (2):137–158, 2010.

[37] C. Perron M. Levesque H.Y. Miao, S. Larose. An analytical approach to relate shot peening parameters to almen intensity. *Surface and Coatings Technology*, 205(7):2055–2066, 2010.

[38] N.L. Muskhelishvili. *Some basic problems of the mathematical theory of elasticity.* P. Noordhoff Ltd., 1963.

[39] N. Matsuoka K. Mori, K. Osakada. Finite element analysis of peening process with plastically deforming shot. *Journal of Materials Processing Technology*, 45:607–612, 1994.

[40] C. Drost gen. Helling K. Schiffner. Simulation of residual stresses by shot peening. *Computers and Structures*, 72(1-3):329–340, 1999.

[41] K. Mori J. Edberg, L. Lindgren. Shot peening simulated by two different finite element formulations. *Simulations of Materials Processing: Theory, Methods and Applications*, 1995.

[42] J.C. Stranart J. Daly S.A. Meguid, G. Shagal. Three dimensional dynamic finite element analysis of shot peening induced residual stresses. *Finite Elements in Analysis and Design*, 31(3):179–191, 1999.

[43] D.C. Webb S.T.S. Al-Hassani, K. Kormi. Numerical simulation of multiple shot impact. *Internation Conference on Shot Peening 7*, 1999.

[44] O. Vohringer J. Schwarzer, V. Schulze. Evaluation of the influence of shot parameters on residual stress profiles using element simulation. *Materials Science Forum*, 2003.

[45] M.S. Klair S.A. Meguid. Finite element studies into incomplete coverage in shot peening. *International Conference on Shot Peening 2*, 1984.

[46] M.S. Klair S.A. Meguid. Elastoplastic coindentation analysis of a bounded solid using finite element method. *International Journal of Mechanical Sciences*, 27 (3):157–168, 1985.

[47] J.C. Stranart S.A. Meguid, G. Shagal. Development and validation of novel fe models for 3d analysis of peening of strain rate sensitive materials. *Journal of Engineering Materials and Technology*, 129:271–283, 2007.

[48] Y.F. Al-Obaid. Three dimensional dynamic finite element analysis for shot peening mechanics. *Computers and Structures*, 36(4):681–689, 1990.

[49] M.A. Elbestawi M.S. EITobgy, E. Ng. Three dimensional elastoplastic finite element model for residual stresses in the shot peening process. *Proc. Instn Mech. Engrs*, 218(11):1471–1481, 2004.

[50] C. Perron M. Levesque H.Y. Miao, S. Larose. On the potential applications of a 3d random finite element model for the simulation of shot peening. *Advances in Engineering Software*, 40(10):1023–1038, 2009.

[51] E. G. Herbert. The work hardening of steel by abrasion. *Engineering*, pages 470–472, 1927.

[52] J. O. Almen. Peened surfaces improve endurance of machined parts. *Metal Progress*, 43:209–215, 1943.

[53] J. O. Almen. Shot blasting to increase fatigue resistance. *SAE Transactions*, 51:248–268, 1943.

[54] Y. Murakami S. Taira. On the changes in residual stresses due to repeated stressing. *Proceedings of the 3rd Japan Congress on Testing Materials*, 1960.

[55] K. Tosha. Papers on shot peening published in the world for the last thirteen years. *International Conference on Shot Peening 7*, 1999.

[56] M. T. Milan G. Hammersley E. R. de los Rios, A. Walley. Fatigue crack initiation and propagation on shot-peened surfaces in a316 stainless steel. *International Journal of Fatigue*, 17(7):493–499, 1995.

[57] O. Vohringer K. Lang, V. Schulze. Shot peening and fatigue strength of steels. *International Conference on Shot Peening 8*, 2002.

[58] Dr.Ing I. Altenberger. Thesis, universitat gh kassel, forschungsberichte des instituts fur werkstoffkunde - metallische werkstoffe der universitat gh kassel. *Verlag Universitatsbibliothek Kassel*, 2000.

[59] B. Moran J. Lamer, J. B. Cohen. The effects of residual macrostresses on fatigue crack initiation. *Materials Science and Engineering A*, 284(1-2):268–279, 2000.

[60] L. Weber H. Berns. *in: Residual Stresses in Science and Technology.*, 1987.

[61] L. Weber H. Berns. Fatigue progress in shot-peened surface layers. *International Conference on Shot Peening 3*, 1987.

[62] E. Macherauch P. Starker, H. Wohlfahrt. Subsurface crack initiation during fatigue as a result of residual stresses. *Fatigue of Engineering Materials and Structures*, 1(3):319–327, 1979.

[63] M. Yao R. Wang S. Wang, Y. Li. Fatigue limit of shot peened metal. *Journal of Materials Processing Technology*, 73:57–63, 1998.

[64] Y. Hirose K. Iida. The residual stress distribution in shot peened carburized steel under fatigue. *International Conference on Shot Peening 7*, 1999.

[65] R. Prabhakaran J. C. Newman Jr. M. J. Dubberly R. A. Everett. Jr., W. T. Matthews. The effects of shot and laser peening on fatigue life and crack growth in 2024 aluminum alloy and 4340 steel. *In: USAF Structural Integrity Program Conference, San Antonio, Texas.*, 2000.

[66] S. Tekeli. Enhancement of fatigue strength of sae 9245 steel by shot peening. *Materials Letters*, 57(3):604–608, 2002.

[67] A. Bignonnet. Fatigue strength of shot peened grade 35 ncd 16 steel. variation of residual stresses by shot peening according to type of loading. *International Conference on Shot Peening 3*, 1987.

[68] T. E. Arnold J. T. Cammett, C. A. Sauer. Observations on shot peening residual stresses in 17 cr – 7 ni austenitic stainless steel and their redistribution via mechanical loading. *International Conference on Shot Peening 5*, 1993.

[69] R. M. Pelloux G. S. Was. The effect of shot peening on the fatigue behavior of alloy 7075-t6. *Metallurgical and Materials Transactions A*, 10(5):656–658, 1979.

[70] W. J. D. Shaw X. Y. Zhu. Correlation of fatigue crack growth behaviour with crack closure in peened specimens. *Fatigue & Fracture of Engineering Materials & Structures*, 18(7-8):811–820, 1995.

[71] A. S. Kobayashi T. Honda, M. Ramulu. Effect of shot peening on fatigue crack growth in 7075-t7351. *Journal of ASTM International*, 2(6):1–14, 2005.

[72] A. Levers E. R. de los Rios, M. Trooll. Improving the fatigue crack resistance of 2024-t351 aluminum alloy by shot peening. *Proceedings Ceas Forum: Life Extension– Aerospace Technology Opportunities*, 1999.

[73] L. Wagner. Mechanical surface treatments on titanium, aluminum and magnesium alloys. *Metarials and Science Engineering A*, 263(2):210–216, 1999.

[74] S. A. Meguid D. W. Hammond. Fatigue fracture and residual stress relaxation in shot peened components. *Surface Engineering*, 1990.

[75] C. Mueller L. Wagner. Effect of shot peening on fatigue behavior in al-alloys. *Metarials and Manufacturing Processes*, 7(3):423–440, 1992.

[76] F.L. Seppi. Relief of shot-peened compressive layer by fatigue loading. *Proceedings of a Workshop on Nondestructive Evaluation of Residual Stress*, 1975.

[77] J.L. Lebrun G. Maeder C. Bathias, J.P. Bonnafe. X-ray diffraction and acoustic emission study of fatigue damage in aluminum alloys. *ASTM STP 1004*, pages 25–36, 1988.

[78] B. Scholtes W. Zinn. Mechanical surface treatments of lightweight materials–effects on fatigue strength and near surface microstructure. *J. Mater.*, 8(2): 145–151, 1999.

[79] W. Rosellini P. Scardi V. Fontanari, F. Frendo. Analysis of residual stress distribution in shot peened al 6082 t5 alloy subjected to fatigue loading. *Sur-*

face Treatment 5, Proceedings of the 5th International Conference on Computer Methods and Experimental Measurements for Surface Treatment Effects, 2001.

[80] R.A. Millard J.M. Potter. The effect of temperature and load cycling on the relaxation of residual stresses. *Proceedings of the 25th Conference on Application of X-Ray Analysis*, 1976.

[81] G. Lutjering L. Wagner. Influence of a shot peening treatment on the fatigue limit of ti-6al-4v. *International Conference on Shot Peening 2*, 1984.

[82] G. Lutjering L. Wagner. Influence of shot peening on the fatigue beahvior of titanium alloys. *International Conference on Shot Peening 1*, 1981.

[83] L. Wagner H. Boeckels. Effect of prior cold work on fatigue performance of shot peened ti-2.5cu. *International Conference on Shot Peening 9*, 2005.

[84] L. Wagner A. Drechsler, J. Kiese. Effects of shot peening and roller burnishing on fatigue performance of various titanium alloys. *International Conference on Shot Peening 7*, 1999.

[85] L. Wagner T. Ludian. Mechanical surface treatments for improving fatigue behavior in titanium alloys. *Advances in Materials Science*, 8(2):44–52, 2008.

[86] J. A. Viens E. C. Reed. The influence of surface residual stress on fatigue limit of titanium. *J. Engng. Ind.*, 82(1):76–78.

[87] L. Wagner T. Dorr. Fatigue response of various titanium alloys to shot peening. *Surface Treatment IV: Computer Methods and Experimental Measurements, Proceeding of the 4th International Conference on Computer Methods and Experimental Measurements for Surface Treatment Effects*, 1999.

[88] K. A. Padmanabhan B. R. Sridhar, K. Ramachandra. Effect of shot peening on

the fatigue and fracture behaviour of two titanium alloys. *Journal of Materials Science*, 31(22):5953–5960, 1996.

[89] A. Yuen S. W. Hopkins G. R. Leverant, B. S. Langer. Surface residual stresses, surface topography and the fatigue behavior of ti-6al-4v. *Metall. Trans.*, 10: 251–257, 1979.

[90] E. Macherauch O. Vohringer, Hirsch. Relaxation of shot peening induced residual stresses of ti-6al-4v by annealing or mechanical treatment. *Proceedings of the 5th International Conference on Titanium*, 1984.

[91] L. Zhang W. Cheong, W. Zhuang. Study of residual stress relaxation using x-ray diffraction. *Key Engng. Mater.*, 274-276:871–876, 2004.

[92] W.N. Findley M.J. Michno. An historical perspective of yield surface investigation for metals. *Int. J. Non-Linear Mechanics*, 11(1):59–82, 1976.

[93] D.C. Drucker F. Edelman. Some extensions of the elementary plasticity theory. *Journal of the Franklin Institute-Engineering and Applied Mathematics*, 251(6): 581–605, 1951.

[94] D.J. Han W.F. Chen. *Plasticity for Strucural Engineers*. Springer-Verlag, New York, 1988.

[95] J. Lubliner. *Plasticity Theory*. Macmillan, New York, 1990.

[96] L. Castex W. Cao, R. Fathallah. Correlation of almen arc height with residual stress in shot peening process. *Mater. Sci. Technol.*, 11(9):967–973, 1995.

[97] A.S. Kobayashi T. Honda, M. Ramulu. Fatigue of shot peened 7075-t7351 senb specimen- a 3-d analysis. *Fatigue Fract Engng Mater Struct*, 29:416–424, 2006.

[98] J. Daly Y. Oshida. Fatigue damage evaluation of shot peened high strength aluminum alloy. *Second International Conference in Impact Surface Treatment*, 1986.

[99] T.L. Kornilov. Method for accounting for the effect of strain acceleration on the stress strain state of structural elements. *Kharkov Aviation Institute, Translated from Problemy Prochnosti*, 1986.

[100] Yu.I. Meshcheryakov G.G. Savenkov. Structural viscosity of solids. *Combustion, Explosion, and Shock Waves*, 38(3):352–357, 2002.

[101] G.G. Savenkov. Dynamic viscosity and material relaxation time during shock loading. *Journal of Applied Mechanics and Technical Physics*, 51(2):148–154, 2010.

[102] V.N. Mineev and A.V. Mineev. Viscosity of metals under shock-loading conditions. *J. Phys. IV France*, 7(C3):C3–583 – C3–585, 1997.

[103] R.A. Toupin. Elastic materials with couple stresses. *Archive of Rational Mechanics and Analysis*, 11(1):385–414, 1962.

[104] R.A. Toupin. Theories of elasticity with couple stresses. *Archive of Rational Mechanics and Analysis*, 17(2):85–112, 1964.

[105] R.D. Mindlin. Micro-structure in linear elasticity. *Archive of Rational Mechanics and Analysis*, 16(1):51–78, 1964.

[106] R.D. Mindlin. Second gradient of strain and surface-tension in linear elasticity. *Int. J. Solids Structures*, 1(4):417–438, 1965.

[107] M.F. Ashby J.W. Hutchinson N.A. Fleck, G.M. Muller. Strain gradient plasticity: theory and experiment. *Acta metall. mater.*, 42(2):475–487, 1994.

[108] H. Gao W.D. Nix. Indentation size effects in crystalline materials: a law for strain gradient plasticity. *J. Mech. Phys. Solids*, 46(3):411–425, 1998.

[109] N.A. Fleck V.P. Smyshlyaev. The role of strain gradients in the grain size effect for polycrystals. *J. Mech. Phys. Solids*, 46(3):411–425, 1996.

[110] E.O. Hall. The deformation and aging of mild steel. *Proc. Phys. Soc.*, 64(9): 747–753, 1951.

[111] H. Bae. *Experimental study of shot peening process and its effects on high cycle fatigue in aero space materials*. Phd. Thesis, University of Washington, 2011.

[112] A. Constantinescu. A unified approach for high and low cycle fatigue based on shakedown concepts. *Fatigue Fract. Engng. Mater. Struct.*, 26(6):561–568, 2003.

[113] M. Abdel-Karim. Shakedown of complex structures according to various hardening rules. *International Journal of Pressure Vessels and Piping*, 82(6):427–458, 2005.

[114] D.C. Drucker. On the macroscopic theory of inelastic stress-strain-time-temperature behaviour. *Advances in Materials Research in the NATO Nations*, 1963.

[115] J.T. Boyle J.M. Klebanov. Shakedown of creeping structures. *Int. J. Solids Structures*, 35(23):3121–3133, 1998.

[116] A.R.S. Ponter. On the relationship between plastic shakedown and the repeated loading of creeping structures. *Trans. ASME, ser. E, J. Appl. Mech*, 38(2):437–441, 1971.

[117] J.B. Martin. A displacement bound technique for elastic continua subjected to a certain class of dynamic loading. *J. Mech. Phys. Solids*, 12(3):165–175, 1964.

[118] B. Brenier J.Y. Guedou L. Castex W. Cao, M. Khadhraoui. Thermomechanical relaxation of residual stresses in shot peened nickel base superalloy. *Materials Science and Technology*, 10(11):947–954, 1994.

[119] O. Vohringer E. Macherauch J. Hoffman, B. Scholtes. Thermal relaxation of shot peening residual stresses in the differently heat treated carbon steel ck 45. *ICSP-3*, 1987.

[120] B. Brenier J.Y. Guedou L. Castex W. Cao, M. Khadhraoui. Experimental investigations and modeling of relaxation behavior of shot peening residual stresses at high temperature for nickel base superalloys. *Materials Science and Technology*, 13(4):360–367, 1995.

[121] J.M. Sprauel R. Chiron I. Lillamand, L. Barrallier. Macroscopic and microscopic evolutions of a shot peened layer during isothermal recovery. *Metallurgical and Materials Transactions A*, 31(1):213–224, 2000.

[122] W.H. Childs. *The effect of elevated temperature on shot peened 403 stainless steel.* Analytical and Experimental Methods for Residual Stress Effects in Fatigue, ASTM STP 1004, 21-24, 1986.

Curriculum Vitae
Julio Lawrence Davis

EDUCATION

PhD, December 2012

Mechanical Engineering, University of Washington, Seattle, Wa.

Dissertation: *Analytical Modeling and Applications of Residual Stresses Induced by Shot Peening*

MSME, 2009

Mechanical Engineering, University of Washington, Seattle, Wa.

Thesis: *Development of an Analytical Shot Peening Coverage Model for the Verification of a Manually Peened Surface: Theory and Experiment*

BS, 2005

Physics, University of Washington, Seattle, Wa.

PROFESSIONAL EXPERIENCE

Research

Manufacturing Science and Technology Laboratory Dept. of Mechanical Engineering, UW April, 2007 - December 2012

Doctoral research is focused on the mathematical modeling of residual stresses induced from surface treatment processes.

Past research conducted includes an analytical model predicting what fraction of area a part was shot peened after a given amount of time with respect to critical input parameters and material properties. Verified using experimental results from manual peening experiments.

Cryogenics Lab, UW September, 2003 - June, 2004 Position: Research Assistant

Developed a DC calorimeter system that is used to conduct research on a very small carbon nanotube sample. Specifically did work on wiring, circuitry, interfacing experiment with laboratory hardware and software for temperature sensors.

Condensed Matter Physics Lab, UW September, 2004- June, 2005 Position: Research Assistant

Conducted research with carbon nanotubes on a DC calorimeter system that I helped develop. Gained experience in data analysis and data interpretation. Research conducted will help pave the way to a better understanding of nanostructures and nanotechnology.

Teaching

September, 2007 - April, 2009 Teaching Assistant, Department of Physics, UW

- Physics 121/114: Course includes selected topics from Newtonian mechanics. Duties include lab instructor, grading exams, and assisting in lecture.
- Physics 122/118/115: Course includes selected topics from electricity and oscillatory motion, circuits, and basic thermodynamics. Duties include lab instructor, grading exams and assisting in lecture
- Physics 116: Course topics include sound, light, and modern physics. Duties include grading exams and assisting in lecture.

Teaching Assistant, Department of Mechanical Engineering, UW September, 2009 - Winter, 2011

- Mechanical Engineering 354 (2 quarters): Mechanical behavior of materials laboratory class. Course covers mechanics of materials at an intermediate

level. Topics include classical beam theory, structures, photoelasticity, failure theories, fracture mechanics, tensile testing, impact testing, buckling, etc.

- Mechanical Engineering 541: Fatigue; selected topics in fatigue including stress based fatigue, fracture mechanics and strain based fatigue.

- Mechanical Engineering 559: Fracture Mechanics; Applications of LEFM to failure analysis.

- Mechanical Engineering 450: Composite Materials and Design; Stress and strain analysis of continuous fiber composite materials. Orthotropic elasticity, lamination theory, failure criterion, and design philosophies, as applied to structural polymeric composites.

Tutoring

Tutor, North Seattle Community College, September, 2003 - June, 2006

- Tutor for North Seattle Community College and high school students taking courses in mathematics and science. Courses include advanced algebra, precalculus, calculus, classical mechanics and electricity and magnetism.

- Exhibit patience and strong written and verbal communication skills to tutor foreign exchange students. Proofread papers and essays.

Tutor, Physics Department, University of Washington, Fall, 2007 - Spring, 2009

- Tutor for UW physics study center. Assist students with homework questions taking the introductory physics sequences.

Employment History

Stress Analyst 787-9 MTE/Spoilers, The Boeing Co., September, 2011 - December, 2012

Conducted stress analysis and authored stress notes for 787-9 spoiler 5 composite part, as well as two metallic fittings using Nastran/Patran and CATIA finite element codes.

Stress Analyst 787-8 fuselage, The Boeing Co., December, 2012 - Present
Conducted stress analysis using Nastran/Patran finite element code on the 787-8 section 48 fuselage structure.

HONORS AND AWARDS

- Louis and Katherine Marsh Fellowship; University of Washington College of Engineering fellowship in the amount of $12,156.
- Kaiser Aluminum Fellowship; University of Washington College of Engineering fellowship in the amount of $11,000.
- Donald C. Whitworth Fellowship; College of Engineering fellowship in the amount of $16,000.
- NASA Space Grant Graduate Fellow; fellowship based on academic record and research interest. Provides tuition assistance plus $5000 for a single quarter
- Received Louis V Uranga Scholarship for $1500
- Received Deans list several quarters

PROFESSIONAL AFFILIATIONS AND SOCIETIES

- Member, ASME
- Member, American Physical Society
- Member, Society of Physics Students

PUBLICATIONS

1. J. Davis and M Ramulu, "A Semi-Analytical Model of Time Dependent Plastic Strains Induced During Shot Peening", submitted to International Journal of Applied Mechanics.

2. J. Davis and M Ramulu, "Analytical Modeling of Shot Peening Residual Stresses by Evaluating the Elastic-Plastic Deviatoric Stresses Using J2-J3 Plasticity", submitted to Meccanica.

3. J. Davis, H. Bae, M Ramulu, "Analytical Modeling of Shot Peening Coverage and Verification of Manually Peened Surfaces", South Bend, IN., ICSP 2011.

4. J. Davis and M. Ramulu., "Theoretical analysis of Material Removal Mechanism in Abrasive Jet Machining of Si3N4, to be submitted to Journal of Materials Processing Technology.

5. J. Davis and M. Ramulu, "A Generalized J2 Theory for the Analytical Modeling of Residual Stresses Induced by Shot Peening", South Bend, IN., ICSP 2011.

6. J. Davis and M. Ramulu, "A Coverage Model for the Verification of a Manually Peened Surface" PNW AIAA Tech Symposium, at Boeing 2-22 Auditorium October 25, 2008.

Appendix A

EQUIVALENT ELASTO-PLASTIC STRESSES

Starting from Eqn. 4.24 and the Von Mises yield function

$$de_{ij}^{p} = \bar{G}\partial f \frac{\partial f}{\partial \sigma_{ij}} = \bar{G} s_{ij}^{p} dJ_2 \tag{A.1}$$

We follow the same procedure outlined in textbook [94] to obtain an expression of $\bar{G}$ in terms of s_{ij}^{p}. Begin by taking the product of Eqn. A.1 with itself

$$de_{ij}^{p} de_{ij}^{p} = \bar{G}^2 2 J_2 dJ_2^2 \tag{A.2}$$

By taking the root of both sides we have

$$d\epsilon_{i}^{p} = \frac{2}{3}\bar{G}\sigma_{i}^{p} dJ_2 = \frac{4}{9}\bar{G}\sigma_{i}^{p2} d\sigma_{i}^{p} \tag{A.3}$$

Solving for $\bar{G}$ yields

$$\bar{G} = \frac{9}{4}\frac{1}{H_p \sigma_{i}^{p2}} = \frac{3}{4 H_p J_2} \tag{A.4}$$

Upon substituting Eqn. A.4 into Eq. A.1 gives

$$de_{ij}^{p} = s_{ij}^{p}\bar{G} dJ_2 = s_{ij}^{p}\frac{3a(2n+1)}{4b}\left(\frac{3}{b^2}\right)^{n} J_2^{n-1} dJ_2 \tag{A.5}$$

Where an $H_p = \frac{b}{a(2n+1)}\left(\frac{b^2}{3J_2}\right)^{n}$ has been used. Find the first principal plastic strain of Eqn. A.5 and write the equation in terms of the stress components with $J_2 = \frac{1}{2}s_{ij}^{p}s_{ij}^{p} = 3s_{11}^{p2}$ and $dJ_2 = s_{ij}^{p} ds_{ij}^{p} = 6 s_{11}^{p} ds_{11}^{p}$

$$de_{11}^{p} = \frac{3a(2n+1)}{4b}\left(\frac{3}{b^2}\right)^{n}(3s_{11}^{p2})^{n-1} 6 s_{11}^{p2} ds_{11}^{p} = \frac{6a(2n+1)}{4b}\left(\frac{3}{b^2}\right)^{n}(3s_{11}^{p})^{2n} ds_{11}^{p} \tag{A.6}$$

Integrating this result gives e_{11}^{p}

$$e_{11}^{p} = \frac{6a}{4b}\left(\frac{3}{b}\right)^{2n}(s_{11}^{p})^{2n+1} \tag{A.7}$$

By making use of Eqn. 4.11, $e_{11}^p = \frac{1}{3}(1+\nu)\epsilon_i^p = \frac{a\sigma_i^{p3}}{2b^3}$, we have the following

$$\frac{1}{3}(1+\nu)\epsilon_i^p = \frac{1}{3}(1+\nu)\left[a\left(\frac{\sigma_i^p}{b}\right)^{2n+1}\right] = \frac{6a}{4b}\left(\frac{3}{b}\right)^{2n}(s_{11}^p)^{2n+1} \tag{A.8}$$

Now, by solving for s_{11}^p in terms of σ_i^p, the desired result is obtained

$$s_{11}^p = \left[\frac{4b}{6a}\left(\frac{b}{3}\right)^{2n}\frac{1}{3}(1+\nu)a\left(\frac{\sigma_i^p}{b}\right)^{2n+1}\right]^{\frac{1}{2n+1}} = \frac{1}{3}\sigma_i^p \tag{A.9}$$

Appendix B

MATHEMATICA INPUT AND OUTPUT FOR CHAPTER 4

All raw data is given in this section for the analytical predictions in chapter 4. The mathematica input and output used to produce Fig.'s 4.3-4.5 is in Fig.'s B.1-B.10. Note, in Fig.'s 4.3-4.5 only portions of the plot that are physically correct for the problem are shown. The remaining parts of the curve have not been shown.

```
In[149]:= νs = .31
          νt = .31
          Es = 210 × 10^3 × 10^6
          Et = 200 × 10^3 × 10^6
          ρ = 7800
          θ = Pi / 2
          k = .8
          Dm = .4 × 10^-3
          R = Dm / 2
          v = 45
          Eh = ((1 - νs^2) / Es + (1 - νt^2) / Et) ^-1
          ae = Dm / 2 (5 / 4 Pi k ρ (v Sin[θ]) ^2 / Eh ) ^ (1 / 5)
          p0 = 1 / Pi (40 Pi k ρ Eh^4 (v Sin[θ]) ^2) ^ (1 / 5)
          σs = 1120 × 10^6
          ϵs = σs / Et
          Sb = 1270 × 10^6
          ϵb = .082
          A = (1 + (z / ae) ^2) ^ (-1)
          B = 1 - z / ae ArcTan[ae / z]
          ap = R (8 ρ (v Sin[θ]) ^2 / (9 σs)) ^ (1 / 4)
          α = ap / ae
          k1 = (Sb - σs) / (ϵb - ϵs)
          k2 = 0
          σxe = -p0 (-.5 A + (1 + νt) B)
          σye = -p0 (-.5 A + (1 + νt) B)
          σze = -p0 A
          c = 0
```

(a)

```
J2 = 1 / 6 ((σxe - σye) ^2 + (σye - σze) ^2 + (σze - σxe) ^2)

J3 = Det[( σxe - σem   0          0
           0           σye - σem  0
           0           0          σze - σem )]

σie = (3 J2) ^ .5
σem = -2 / 3 p0 (1 + νt) B
sex = 1 / 3 p0 (1.5 A - (1 + νt) B)
sey = 1 / 3 p0 (1.5 A - (1 + νt) B)
sez = -2 sex
ϵie = σie / Et
ϵxe = - (1 + νt) / Et p0 (-.5 A + (1 + νt) B)
ϵye = - (1 + νt) / Et p0 (-.5 A + (1 + νt) B)
ϵze = - (1 + νt) / Et p0 ( A - 2 νt B)
exe = 1 / 3 (1 + νt) ϵie
eye = 1 / 3 (1 + νt) ϵie
eze = -2 / 3 (1 + νt) ϵie
ϵip = ϵs + α (ϵie - ϵs)
σip1 = σs + k1 (ϵip - ϵs)
σip2 = Sb + k2 (ϵip - ϵb)
epx = 1 / 3 (1 + νt) ϵip
epy = 1 / 3 (1 + νt) ϵip
epz = -2 epx
spx1 = σip1 (3^.5 / ((3 - 4 c / 9) ^.5 (27 - 4 c))) ^ (1 / 3)
spx2 = 1 / 3 σip2
spy1 = spx1
spy2 = 1 / 3 σip2
spz1 = -2 spx1
spz2 = -2 spx2
σxr1 = spx1 - 1 / 3 (σie)
```

(b)

```
σyr1 = spx1 - 1 / 3 (σie)
σzr1 = -2 σxr1
σxr2 = 1 / 3 (σip2 - σie)
σyr2 = 1 / 3 (σip2 - σie)
σzr2 = -2 σxr2
δσie = σie - 2 × 3 spx1
δϵie = δσie / Et
δϵip = α δϵie
δσip1 = k1 δϵip
σxr11 = spx1 - 2 spx1 - 1 / 3 (δσip1)
δσie2 = σie - 2 σip2
δϵie2 = δσie2 / Et
δϵip2 = α δϵie2
δσip2 = k2 δϵip2
σxr22 = 1 / 3 (-σip2 - δσip2)
σxR11 = σxr11 (1 + νt) / (1 - νt) / (1120 × 10^6)
σxR1 = σxr1 (1 + νt) / (1 - νt) / (1120 × 10^6)
Plot[{σxr1, σxr11, σie, σip1} , {z, 0, .05}, PlotRange → {-1000, 4000}]
Plot[{σxr1, σxr11}, {z, 0, 1.2 × 10^-3},
 PlotRange → {-1200 10^6 / (1120 × 10^6), 250 × 10^6 / (1120 × 10^6)},
 PlotStyle → {Black, Black}]
Plot[{σxR1, σxR11}, {z, 0, .3 × 10^-3},
 PlotRange → {-1200 10^6 / (1120 × 10^6), 250 × 10^6 / (1120 × 10^6)},
 PlotStyle → {Black, Black}]
```

(c)

Figure B.1: Mathematica Input for Fig.'s 4.3a and 4.3b. The only input parameter varied was c, which was set to -3.375, -2.0, 0, 1.0, and 2.25.

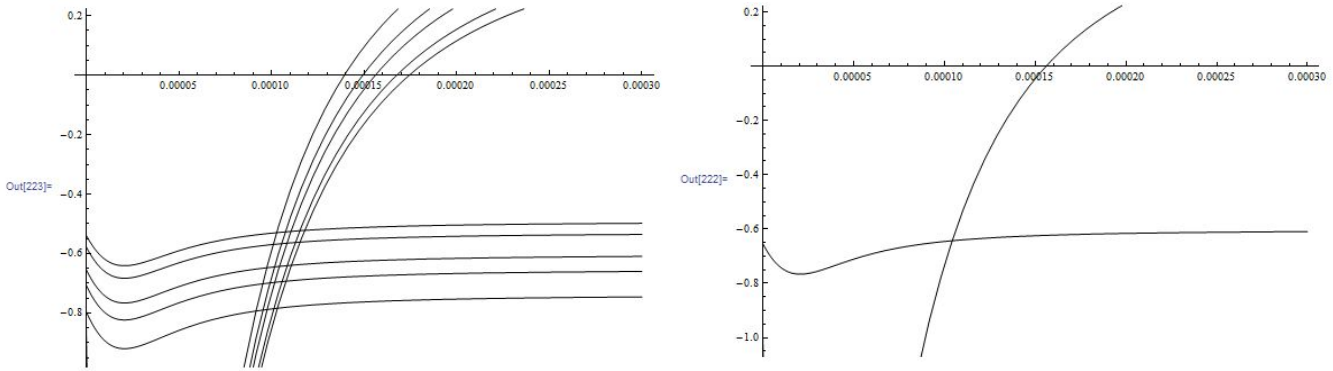

(a) (b)

Figure B.2: Mathematica Output for Fig.'s 4.3a and 4.3b, corresponding to the input provided in Fig. B.1.

```
In[371]:= νs = .31
          νt = .33
          Es = 210 × 10^3 × 10^6
          Et = 113. × 10^3 × 10^6
          ρ = 7800
          θ = Pi / 2
          k = .8
          Dm = .432 × 10^-3
          R = Dm / 2
          v = 55
          Eh = ((1 - νs^2) / Es + (1 - νt^2) / Et) ^-1
          ae = Dm / 2 (5 / 4 Pi k ρ (v Sin[θ]) ^2 / Eh ) ^ (1 / 5)
          p0 = 1 / Pi (40 Pi k ρ Eh^4 (v Sin[θ]) ^2) ^ (1 / 5)
          σs = 930 × 10^6
          ϵs = σs / Et
          Sb = 1000 × 10^6
          ϵb = .062
          A = (1 + (z / ae) ^2) ^ (-1)
          B = 1 - z / ae ArcTan[ae / z]
          ap = R (8 ρ (v Sin[θ]) ^2 / (9 σs)) ^ (1 / 4)
          α = ap / ae
          k1 = (Sb - σs) / (ϵb - ϵs)
          k2 = 0
          σxe = -p0 (-.5 A + (1 + νt) B)
          σye = -p0 (-.5 A + (1 + νt) B)
          σze = -p0 A
          c = 2.25
          J2 = 1 / 6 ((σxe - σye) ^2 + (σye - σze) ^2 + (σze - σxe) ^2)
          J3 = Det[{{σxe - σem, 0, 0}, {0, σye - σem, 0}, {0, 0, σze - σem}}]
          σie = (3 J2) ^.5
```

(a)

```
          σem = -2 / 3 p0 (1 + νt) B
          sex = 1 / 3 p0 (1.5 A - (1 + νt) B)
          sey = 1 / 3 p0 (1.5 A - (1 + νt) B)
          sez = -2 sex
          ϵie = σie / Et
          ϵxe = - (1 + νt) / Et p0 (-.5 A + (1 + νt) B)
          ϵye = - (1 + νt) / Et p0 (-.5 A + (1 + νt) B)
          ϵze = - (1 + νt) / Et p0 ( A - 2 νt B)
          exe = 1 / 3 (1 + νt) ϵie
          eye = 1 / 3 (1 + νt) ϵie
          eze = -2 / 3 (1 + νt) ϵie
          ϵip = ϵs + α (ϵie - ϵs)
          σip1 = σs + k1 (ϵip - ϵs)
          σip2 = Sb + k2 (ϵip - ϵb)
          epx = 1 / 3 (1 + νt) ϵip
          epy = 1 / 3 (1 + νt) ϵip
          epz = -2 epx
          spx1 = σip1 (3^.5 (3 - 4 c / 9) ^-.5 / ((27 - 4 c))) ^ (1 / 3)
          spx2 = 1 / 3 σip2
          spy1 = spx1
          spy2 = 1 / 3 σip2
          spz1 = -2 spx1
          spz2 = -2 spx2
          σxr1 = spx1 - 1 / 3 (σie)
          σyr1 = spx1 - 1 / 3 (σie)
          σzr1 = -2 σxr1
          σxr2 = 1 / 3 (σip2 - σie)
          σyr2 = 1 / 3 (σip2 - σie)
          σzr2 = -2 σxr2
          δσie = σie - 2 × 3 spx1
          δϵie = δσie / Et
          δϵip = α δϵie
```

(b)

```
          δσip1 = k1 δϵip
          σxr11 = spx1 - 2 spx1 - 1 / 3 (δσip1)
          δσie2 = σie - 2 σip2
          δϵie2 = δσie2 / Et
          δϵip2 = α δϵie2
          δσip2 = k2 δϵip2
          σxr22 = 1 / 3 (-σip2 - δσip2)
          σxR11 = σxr11 (1 + νt) / (1 - νt) / (930 × 10^6)
          σxR1 = σxr1 (1 + νt) / (1 - νt) / (930 × 10^6)
          Plot[{σxr1, σxr11, σie, σip1} , {z, 0, .05}, PlotRange → {-1000, 4000}]
          Plot[{σxr1, σxr11}, {z, 0, 1.2 × 10^-3}, PlotRange → {-900 10^6, 250 × 10^6}]
          Plot[{σxR11, σxR1}, {z, 0, .3 × 10^-3},
           PlotRange → {-1000 10^6 / (930 × 10^6) , 250 × 10^6 / (930 × 10^6)},
           PlotStyle → {Black, Black}]
```

(c)

Figure B.3: Mathematica Input for Fig. 4.4a

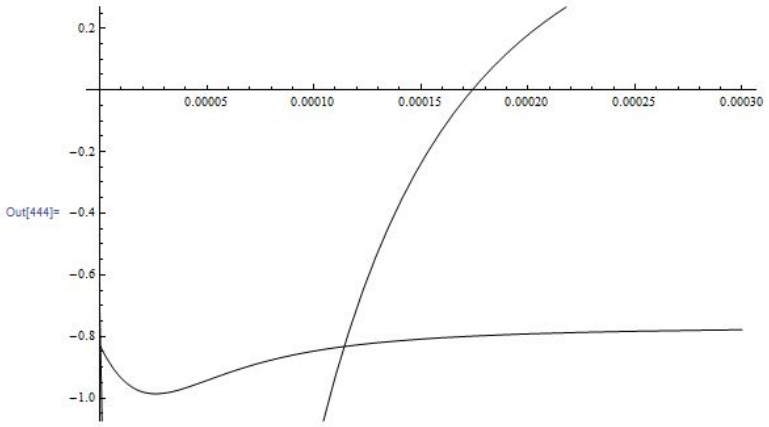

Figure B.4: Mathematica Output for Fig. 4.4a, corresponding to the input provided in Fig. B.3.

```
In[519]:= vs = .31
          vt = .33
          Es = 210 × 10^3 × 10^6
          Et = 113 × 10^3 × 10^6
          ρ = 7800
          θ = Pi / 2
          k = .8
          Dm = .432 × 10^-3
          R = Dm / 2
          v = 40
          Eh = ((1 - vs^2) / Es + (1 - vt^2) / Et) ^ -1
          ae = Dm / 2 (5 / 4 Pi k ρ (v Sin[θ]) ^2 / Eh ) ^ (1 / 5)
          p0 = 1 / Pi (40 Pi k ρ Eh^4 (v Sin[θ]) ^2) ^ (1 / 5)
          σs = 965 × 10^6
          ϵs = σs / Et
          Sb = 1034 × 10^6
          ϵb = .062
          A = (1 + (z / ae) ^2) ^ (-1)
          B = 1 - z / ae ArcTan[ae / z]
          ap = R (8 ρ (v Sin[θ]) ^2 / (9 σs)) ^ (1 / 4)
          α = ap / ae
          k1 = (Sb - σs) / (ϵb - ϵs)
          k2 = 0
          σxe = -p0 (-.5 A + (1 + vt) B)
          σye = -p0 (-.5 A + (1 + vt) B)
          σze = -p0 A
          c = 2.25
          J2 = 1 / 6 ((σxe - σye) ^2 + (σye - σze) ^2 + (σze - σxe) ^2)
          J3 = Det[{{σxe - σem, 0, 0}, {0, σye - σem, 0}, {0, 0, σze - σem}}]
          σie = (3 J2) ^ .5
```

(a)

```
          σem = -2 / 3 p0 (1 + vt) B
          sex = 1 / 3 p0 (1.5 A - (1 + vt) B)
          sey = 1 / 3 p0 (1.5 A - (1 + vt) B)
          sez = -2 sex
          ϵie = σie / Et
          ϵxe = - (1 + vt) / Et p0 (-.5 A + (1 + vt) B)
          ϵye = - (1 + vt) / Et p0 (-.5 A + (1 + vt) B)
          ϵze = - (1 + vt) / Et p0 ( A - 2 vt B)
          exe = 1 / 3 (1 + vt) ϵie
          eye = 1 / 3 (1 + vt) ϵie
          eze = -2 / 3 (1 + vt) ϵie
          ϵip = ϵs + α (ϵie - ϵs)
          σip1 = σs + k1 (ϵip - ϵs)
          σip2 = Sb + k2 (ϵip - ϵb)
          epx = 1 / 3 (1 + vt) ϵip
          epy = 1 / 3 (1 + vt) ϵip
          epz = -2 epx
          spx1 = σip1 (3^.5 (3 - 4 c / 9) ^-.5 / ((27 - 4 c))) ^ (1 / 3)
          spx2 = 1 / 3 σip2
          spy1 = spx1
          spy2 = 1 / 3 σip2
          spz1 = -2 spx1
          spz2 = -2 spx2
          σxr1 = spx1 - 1 / 3 (σie)
          σyr1 = spx1 - 1 / 3 (σie)
          σzr1 = -2 σxr1
          σxr2 = 1 / 3 (σip2 - σie)
          σyr2 = 1 / 3 (σip2 - σie)
          σzr2 = -2 σxr2
          δσie = σie - 2 × 3 spx1
          δϵie = δσie / Et
          δϵip = α δϵie
```

(b)

```
          δσip1 = k1 δϵip
          σxr11 = spx1 - 2 spx1 - 1 / 3 (δσip1)
          δσie2 = σie - 2 σip2
          δϵie2 = δσie2 / Et
          δϵip2 = α δϵie2
          δσip2 = k2 δϵip2
          σxr22 = 1 / 3 (-σip2 - δσip2)
          σxR11 = σxr11 (1 + vt) / (1 - vt) / (965 × 10^6)
          σxR1 = σxr1 (1 + vt) / (1 - vt) / (965 × 10^6)
          Plot[{σxr1, σxr11, σie, σip1} , {z, 0, .05}, PlotRange → {-1000, 4000}]
          Plot[{σxr1, σxr11}, {z, 0, 1.2 × 10^-3}, PlotRange → {-900 10^6, 250 × 10^6}]
          Plot[{σxR11, σxR1}, {z, 0, .3 × 10^-3},
           PlotRange → {-1000 10^6 / (965 × 10^6) , 250 × 10^6 / (965 × 10^6)},
           PlotStyle → {Black, Black}]
```

(c)

Figure B.5: Mathematica Input for Fig. 4.4b

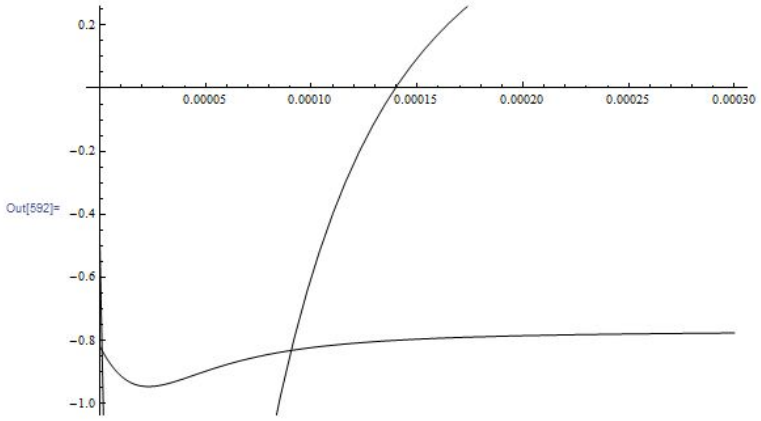

Figure B.6: Mathematica Output for Fig. 4.4b, corresponding to the input provided in Fig. B.5.

```
vs = .31
vt = .33
Es = 210 × 10^3 × 10^6
Et = 70 × 10^3 × 10^6
ρ = 7800
θ = Pi / 4
k = .8
Dm = .584 × 10^-3
R = Dm / 2
v = 40
Eh = ((1 - vs^2) / Es + (1 - vt^2) / Et) ^ -1
ae = Dm / 2 (5 / 4 Pi k ρ (v Sin[θ]) ^2 / Eh ) ^ (1 / 5)
p0 = 1 / Pi (40 Pi k ρ Eh^4 (v Sin[θ]) ^2) ^ (1 / 5)
σs = 462 × 10^6
ϵs = σs / Et
Sb = 526 × 10^6
ϵb = .11
A = (1 + (z / ae) ^2) ^ (-1)
B = 1 - z / ae ArcTan[ae / z]
ap = R (8 ρ (v Sin[θ]) ^2 / (9 σs)) ^ (1 / 4)
α = ap / ae
k1 = (Sb - σs) / (ϵb - ϵs)
k2 = 0
σxe = -p0 (-.5 A + (1 + vt) B)
σye = -p0 (-.5 A + (1 + vt) B)
σze = -p0 A
c = -3.375
J2 = 1 / 6 ((σxe - σye) ^2 + (σye - σze) ^2 + (σze - σxe) ^2)
J3 = Det[{{σxe - σem, 0, 0}, {0, σye - σem, 0}, {0, 0, σze - σem}}]
σie = (3 J2) ^ .5
```

(a)

```
σem = -2 / 3 p0 (1 + vt) B
sex = 1 / 3 p0 (1.5 A - (1 + vt) B)
sey = 1 / 3 p0 (1.5 A - (1 + vt) B)
sez = -2 sex
ϵie = σie / Et
ϵxe = - (1 + vt) / Et p0 (-.5 A + (1 + vt) B)
ϵye = - (1 + vt) / Et p0 (-.5 A + (1 + vt) B)
ϵze = - (1 + vt) / Et p0 ( A - 2 vt B)
exe = 1 / 3 (1 + vt) ϵie
eye = 1 / 3 (1 + vt) ϵie
eze = -2 / 3 (1 + vt) ϵie
ϵip = ϵs + α (ϵie - ϵs)
σip1 = σs + k1 (ϵip - ϵs)
σip2 = Sb + k2 (ϵip - ϵb)
epx = 1 / 3 (1 + vt) ϵip
epy = 1 / 3 (1 + vt) ϵip
epz = -2 epx
spx1 = σip1 (3^.5 (3 - 4 c / 9) ^-.5 / ((27 - 4 c))) ^ (1 / 3)
spx2 = 1 / 3 σip2
spy1 = spx1
spy2 = 1 / 3 σip2
spz1 = -2 spx1
spz2 = -2 spx2
σxr1 = spx1 - 1 / 3 (σie)
σyr1 = spx1 - 1 / 3 (σie)
σzr1 = -2 σxr1
σxr2 = 1 / 3 (σip2 - σie)
σyr2 = 1 / 3 (σip2 - σie)
σzr2 = -2 σxr2
δσie = σie - 2 × 3 spx1
δϵie = δσie / Et
δϵip = α δϵie
```

(b)

```
δϵip = α δϵie
δσip1 = k1 δϵip
σxr11 = spx1 - 2 spx1 - 1 / 3 (δσip1)
δσie2 = σie - 2 σip2
δϵie2 = δσie2 / Et
δϵip2 = α δϵie2
δσip2 = k2 δϵip2
σxr22 = 1 / 3 (-σip2 - δσip2)
σxR11 = σxr11 (1 + vt) / (1 - vt) / (1)
σxR1 = σxr1 (1 + vt) / (1 - vt) / (1)
Plot[{σxr1, σxr11, σie, σip1} , {z, 0, .05}, PlotRange → {-1000, 4000}]
Plot[{σxr1, σxr11}, {z, 0, 1.2 × 10^-3}, PlotRange → {-900 10^6, 250 × 10^6}]
Plot[{σxR11, σxR1}, {z, 0, 1 × 10^-3},
 PlotRange → {-500 10^6 / (1), 250 × 10^6 / (1)}, PlotStyle → {Black, Black}]
```

(c)

Figure B.7: Mathematica Input for Fig. 4.5a

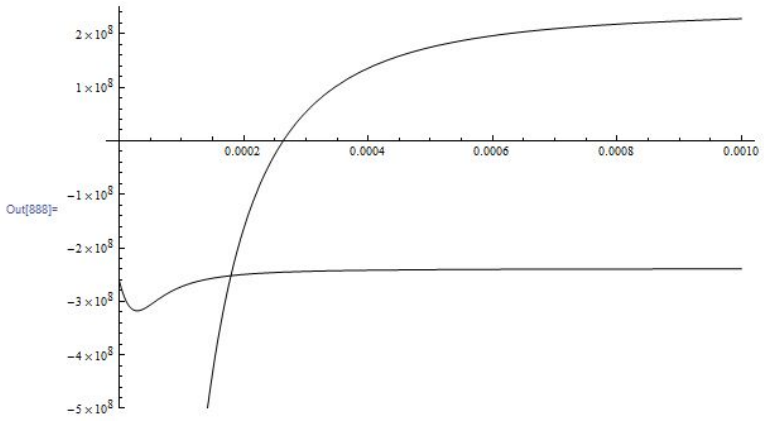

Figure B.8: Mathematica Output for Fig. 4.5a, corresponding to the input provided in Fig. B.7.

```
In[963]:= νs = .31
          νt = .33
          Es = 210 × 10^3 × 10^6
          Et = 70 × 10^3 × 10^6
          ρ = 7800
          θ = Pi / 4
          k = .8
          Dm = .584 × 10^-3
          R = Dm / 2
          v = 60
          Eh = ((1 - νs^2) / Es + (1 - νt^2) / Et) ^-1
          ae = Dm / 2 (5 / 4 Pi k ρ (v Sin[θ]) ^2 / Eh ) ^ (1 / 5)
          p0 = 1 / Pi (40 Pi k ρ Eh^4 (v Sin[θ]) ^2) ^ (1 / 5)
          σs = 462 × 10^6
          εs = σs / Et
          Sb = 526 × 10^6
          εb = .11
          A = (1 + (z / ae) ^2) ^ (-1)
          B = 1 - z / ae ArcTan[ae / z]
          ap = R (8 ρ (v Sin[θ]) ^2 / (9 σs)) ^ (1 / 4)
          α = ap / ae
          k1 = (Sb - σs) / (εb - εs)
          k2 = 0
          σxe = -p0 (-.5 A + (1 + νt) B)
          σye = -p0 (-.5 A + (1 + νt) B)
          σze = -p0 A
          c = -3.375
          J2 = 1 / 6 ((σxe - σye) ^2 + (σye - σze) ^2 + (σze - σxe) ^2)
          J3 = Det[{{σxe - σem, 0, 0}, {0, σye - σem, 0}, {0, 0, σze - σem}}]
          σie = (3 J2) ^ .5
```

(a)

```
          σem = -2 / 3 p0 (1 + νt) B
          sex = 1 / 3 p0 (1.5 A - (1 + νt) B)
          sey = 1 / 3 p0 (1.5 A - (1 + νt) B)
          sez = -2 sex
          εie = σie / Et
          εxe = - (1 + νt) / Et p0 (-.5 A + (1 + νt) B)
          εye = - (1 + νt) / Et p0 (-.5 A + (1 + νt) B)
          εze = - (1 + νt) / Et p0 ( A - 2 νt B)
          exe = 1 / 3 (1 + νt) εie
          eye = 1 / 3 (1 + νt) εie
          eze = -2 / 3 (1 + νt) εie
          εip = εs + α (εie - εs)
          σip1 = σs + k1 (εip - εs)
          σip2 = Sb + k2 (εip - εb)
          epx = 1 / 3 (1 + νt) εip
          epy = 1 / 3 (1 + νt) εip
          epz = -2 epx
          spx1 = σip1  (3^.5 (3 - 4 c / 9) ^-.5 / ((27 - 4 c))) ^ (1 / 3)
          spx2 = 1 / 3 σip2
          spy1 = spx1
          spy2 = 1 / 3 σip2
          spz1 = -2 spx1
          spz2 = -2 spx2
          σxr1 = spx1 - 1 / 3 (σie)
          σyr1 = spx1 - 1 / 3 (σie)
          σzr1 = -2 σxr1
          σxr2 = 1 / 3 (σip2 - σie)
          σyr2 = 1 / 3 (σip2 - σie)
          σzr2 = -2 σxr2
```

(b)

```
          δσie = σie - 2 × 3 spx1
          δεie = δσie / Et
          δεip = α δεie
          δσip1 = k1 δεip
          σxr11 = spx1 - 2 spx1 - 1 / 3 (δσip1)
          δσie2 = σie - 2 σip2
          δεie2 = δσie2 / Et
          δεip2 = α δεie2
          δσip2 = k2 δεip2
          σxr22 = 1 / 3 (-σip2 - δσip2)
          σxR11 = σxr11 (1 + νt) / (1 - νt) / (1)
          σxR1 = σxr1 (1 + νt) / (1 - νt) / (1)
          Plot[{σxr1, σxr11, σie, σip1}, {z, 0, .05}, PlotRange → {-1000, 4000}]
          Plot[{σxr1, σxr11}, {z, 0, 1.2 × 10^-3}, PlotRange → {-900 10^6, 250 × 10^6}]
          Plot[{σxR11, σxR1}, {z, 0, 1 × 10^-3}, PlotRange → {-500 10^6 / (1), 250 × 10^6 / (1)}, PlotStyle → {Blac
```

(c)

Figure B.9: Mathematica Input for Fig. 4.5b

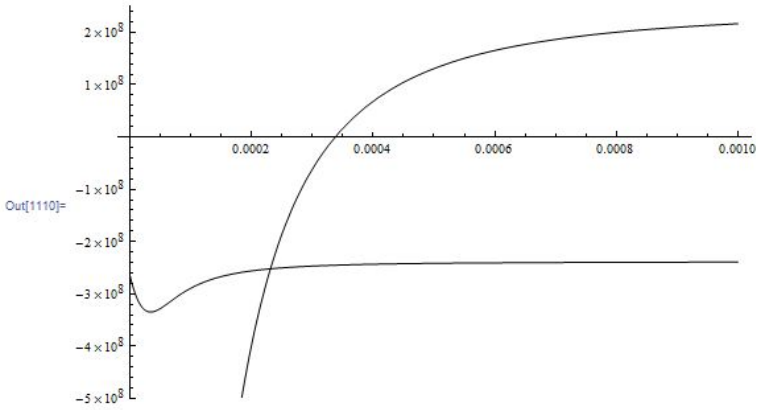

Figure B.10: Mathematica Output for Fig. 4.5b, corresponding to the input provided in Fig. B.10.

Appendix C

MATHEMATICA INPUT AND OUTPUT FOR CHAPTER 5

Appendix C provides all raw data for the analytical predictions in chapter 5. The mathematica input and output used to produce Fig.'s 5.5 and 5.6 are in Fig.'s C.1 and C.2. The parameters in Fig. C.1 have the following values: A=2.5×10^{-9}kPa-sec^2, B=0.28 kPa-sec, C=$\frac{8\times10^5}{1-.3}$kPa, σ=260000kPa. The parameters in Fig. C.2 have the following values: A=8×10^{-9}kPa-sec^2, B=0.28 kPa-sec, C=$\frac{2.7\times10^6}{1-.3}$kPa, σ=600000kPa. Substitution of these parameters into the Eqn. 5.27 gives the plot in Fig. C.2(a), i.e.

$$\epsilon^p(t) = 0.156 - 0.121(-0.21e^{-3.73\times10^7 t} + 1.493e^{-5.17\times10^6 t}) \tag{C.1}$$

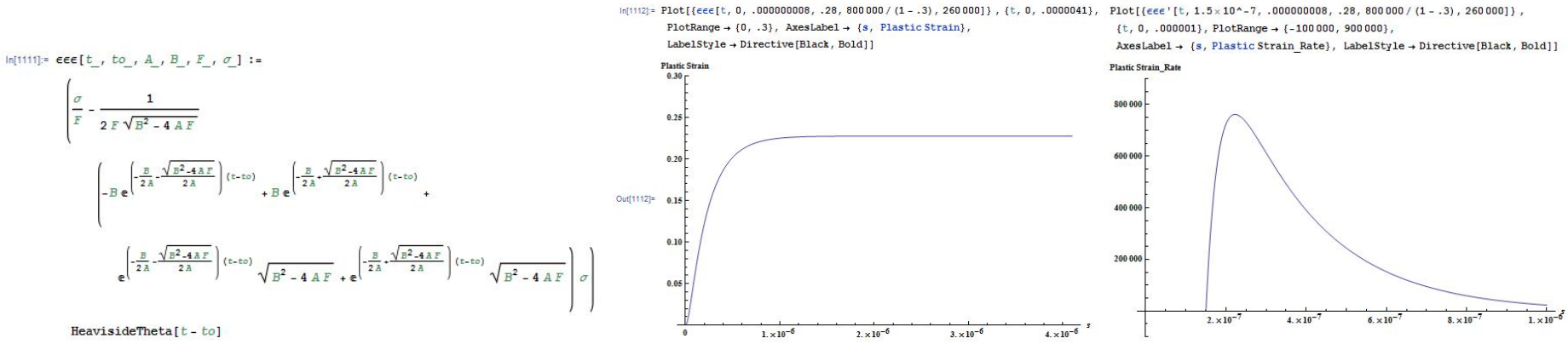

(a) (b) (c)

Figure C.1: Mathematica Input and output for Fig. 5.5. Units are in kPa, kPa-sec, and kPa-sec^2

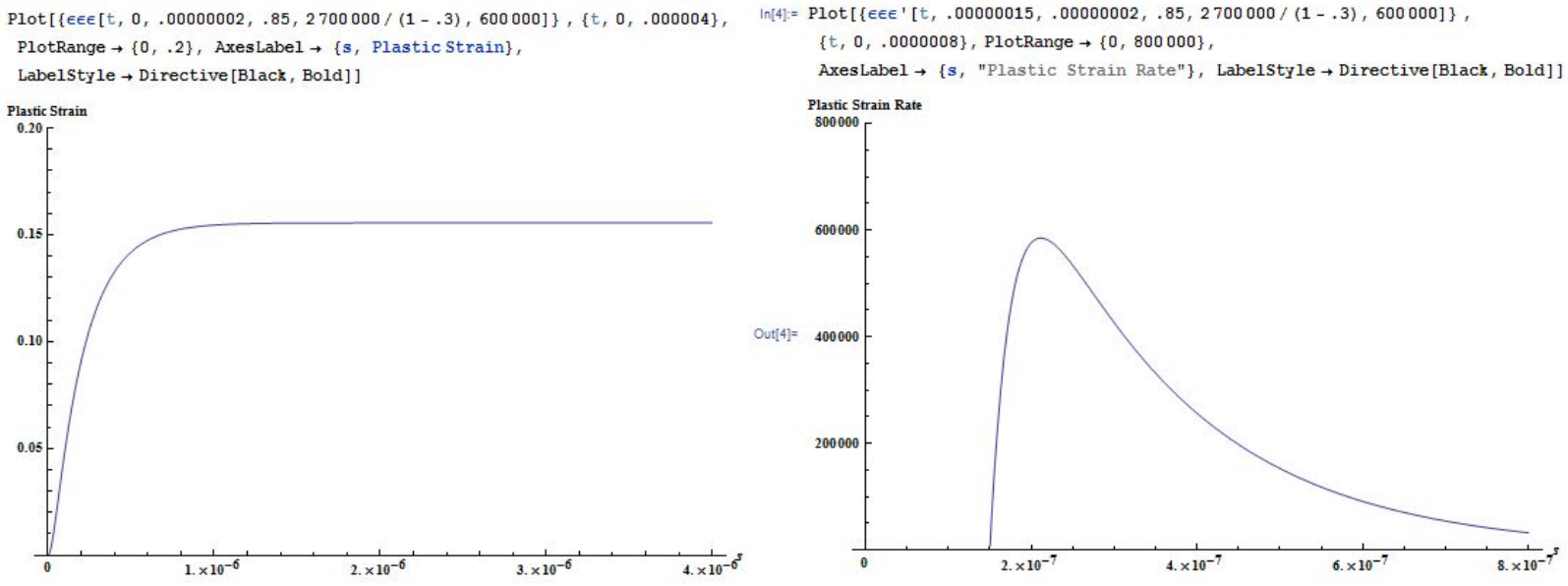

(a) (b)

Figure C.2: Mathematica output for Fig. 5.6

Appendix D

DERIVATION OF THE PLASTIC STRAIN AS A FUNCTION OF DEPTH

Equation 6.14 is derived here by using the method of Laplace transforms on Eqn. 6.15. Recall Eqn. 6.15

$$A'\frac{d^2\epsilon^p(z)}{dz^2} + B'\frac{d\epsilon^p(z)}{dz} + C\epsilon^p(z) = \sigma_o^r\delta(z - z_o) \tag{D.1}$$

Taking the Laplace transform of both sides of this equation yields

$$A's^2\Sigma(s) - s\epsilon^p(0) - \epsilon'^p(0) + B'(s\Sigma(s) - \epsilon^p(0)) + C\Sigma(s) = \sigma_o^r e^{-z_o s} \tag{D.2}$$

Where the prime denotes differentiation with respect to depth, z. *The boundary conditions outlined in the sixth chapter give* $\epsilon'^p(0) = \epsilon^p(0) = 0$. Therefore, Eqn. D.2 becomes

$$A's^2\Sigma(s) + B's\Sigma(s) + C\Sigma(s) = \sigma_o^r e^{-z_o s} \tag{D.3}$$

Solving, Eqn. D.3 for $\Sigma(s)$ now gives

$$\Sigma(s) = \frac{\sigma_o^r e^{-z_o s}}{A's^2 + B's + C} \tag{D.4}$$

The solution of Eqn. D.1 can be obtained by taking the inverse Laplace transform of Eqn. D.4; yielding the desired result

$$\epsilon^p(z) = -\frac{\sigma_0^r\left(e^{(z-z_0)\left(-\frac{B'}{2A'}-\frac{\sqrt{B'^2-4A'C}}{2A'}\right)} - e^{(z-z_0)\left(-\frac{B'}{2A'}+\frac{\sqrt{B'^2-4A'C}}{2A'}\right)}\right)}{\sqrt{B'^2 - 4A'C}} \tag{D.5}$$

Appendix E

MATHEMATICA INPUT AND OUTPUT FOR CHAPTER 6

All raw data for the analytical predictions in chapter 6 is given in this section. The mathematica input and output used to produce Fig.'s 6.1 and 6.2 are in Fig.'s E.1 and E.2. The parameters in Fig.'s E.1 and E.2 have the following values: z_o=-0.00015m and -0.00020m, A=2.5×10^{-6}kPa-sec^2, v=40 m\s and 60 m\s, B=3.75 kPa-sec, a=-5×10^6 m\s^2 and -1×10^7, C=10^6kPa, σ=125000kPa and 140000kPa. The parameters in Fig. E.2 have the following values: z_o=-0.00008m and -0.00015m, A=2.5×10^{-6}kPa-sec^2, v=20 m\s and 50 m\s, B=3.75 kPa-sec, a=-1×10^6 m\s^2 and -8×10^6 m\s^2, C=10^6kPa, σ=150000kPa and 281400kPa. Substitution of these parameters into the Eqn. 6.22 gives the plot in Fig. D.1(b), i.e.

$$\sigma^r(z) = -798.8(e^{-23926.2(z+0.000015)} - e^{-10448.8(0.000015+z)}) \tag{E.1}$$

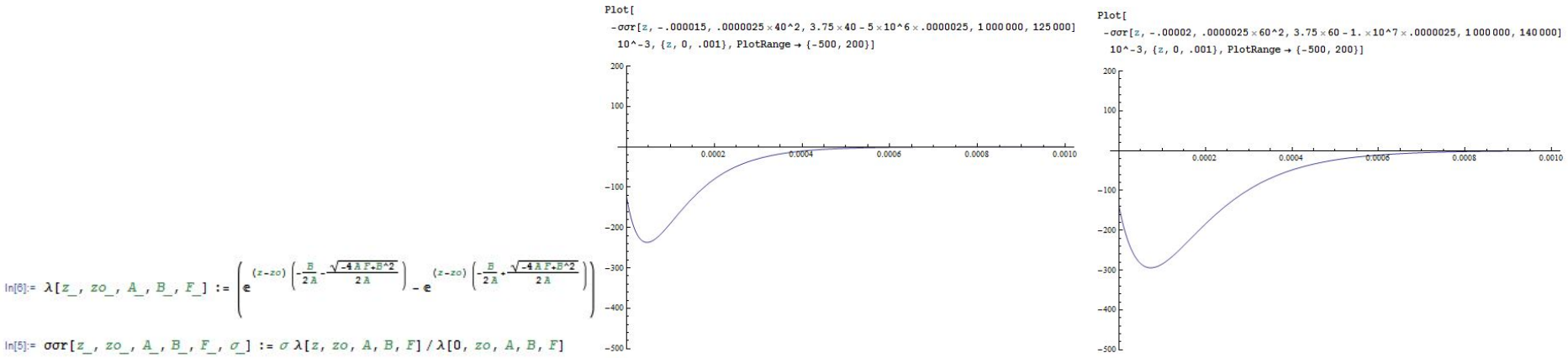

(a) (b) (c)

Figure E.1: Mathematica Input and output for Fig. 6.1.

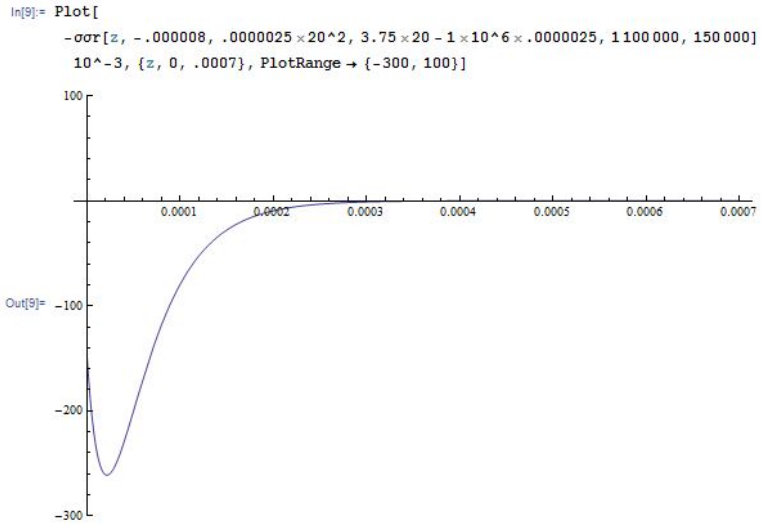

(a)

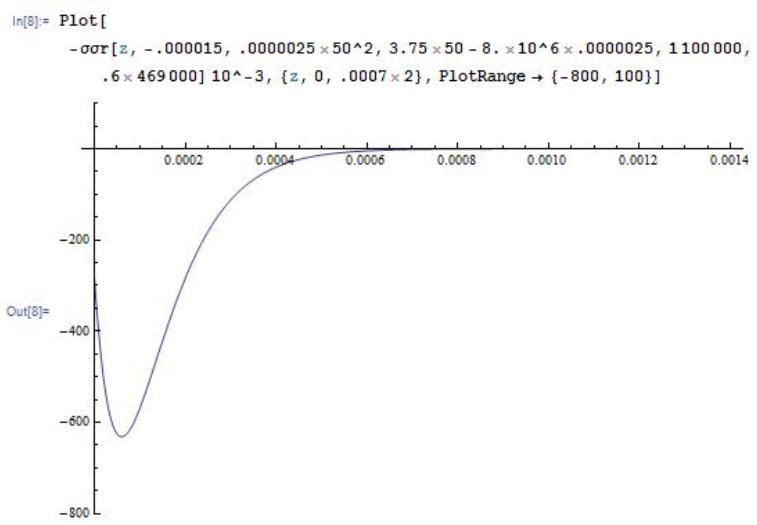

(b)

Figure E.2: Mathematica output for Fig. 6.2